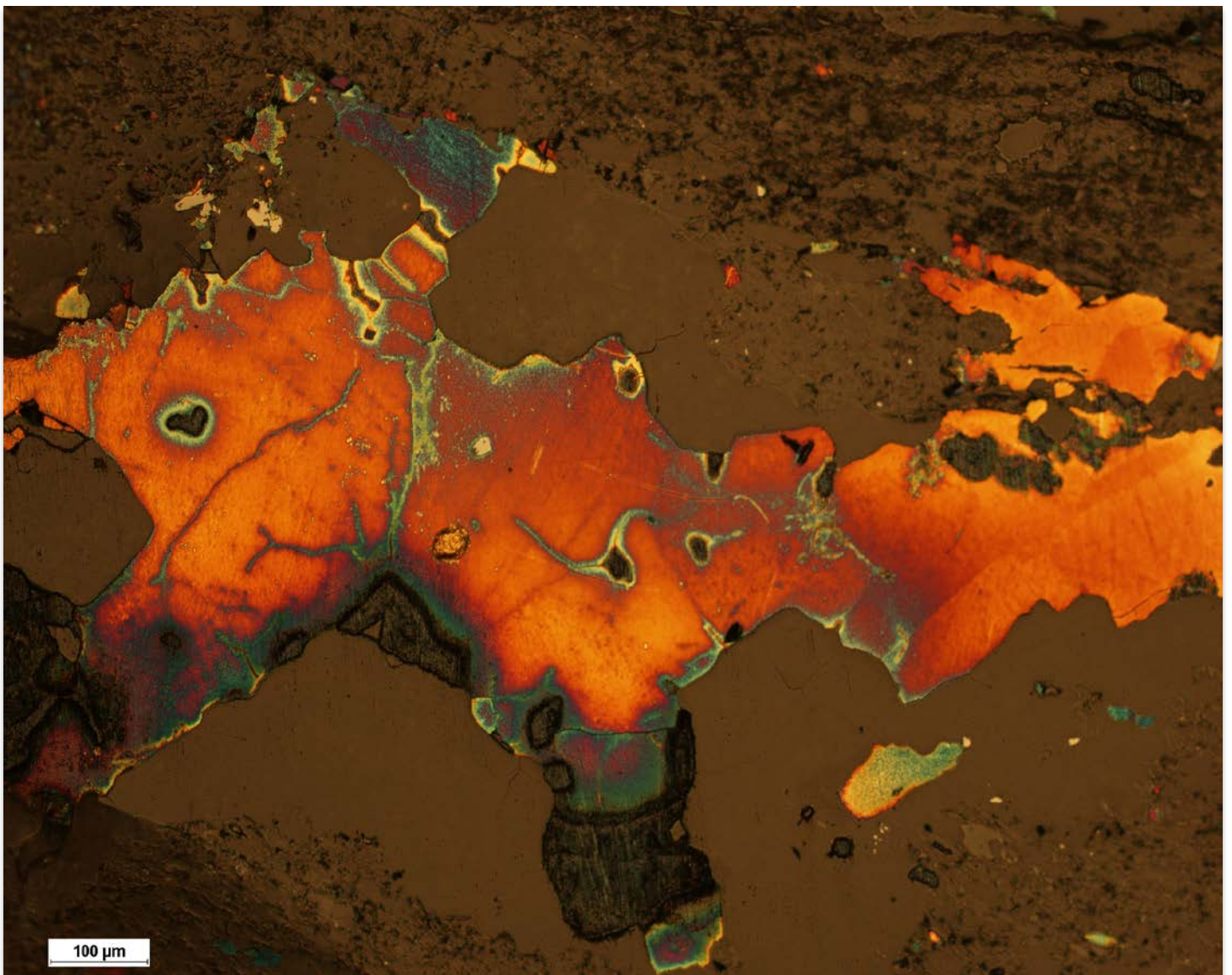


Geochemistry of sediment-hosted copper deposits and their environmental impact:

*A case study from the Nussir and Ulveryggen deposits, Repparfjord
Tectonic Window, Northern Norway*

—
Yulia Mun

A dissertation for the degree of Philosophiae Doctor – August 2019



Dissertation for the degree of Philosophiae Doctor

Geochemistry of sediment-hosted copper deposits and their environmental impact:

A case study from the Nussir and Ulveryggen deposits, Repparfjord Tectonic Window, Northern Norway

Yulia Mun



UiT - The Arctic University of Norway
Faculty of Sciences and Technology
Department of Geosciences
August 2019

Supervisors:

Dr. Sabina Strmić Palinkaš

Department of Geosciences
UiT The Arctic University of Norway
Tromsø, Norway

Dr. Kåre Kullerud

Norsk Bergverksmuseum,
Kongsberg, Norway

Preface

This doctoral thesis presented herein was conducted from late November 2013 until August 2019, with a break due to a maternity leave from June 2016 till September 2017, at the Department of Geosciences, UiT – The Arctic University of Norway. The research was funded by the Troms Fylkeskommune, SINTEF, and UiT via research grant No. A31596. The thesis was co-supervised by Kåre Kullerud (Norsk Bergverksmuseum) and Sabina Strmić Palinkaš (UiT), with Kåre Kullerud as the main supervisor until March 2018, and Sabina Strmić Palinkaš as the main supervisor in the final stage of the project.

The PhD program included 25% of work dedicated to assigned duty work that included teaching and assistance in preparation of lectures, exercises, tutorial at BSc level courses in mineralogy and general geology. I have assisted and later was a leader of various field courses in general geology and structural geology for BSc and MSc students from Norway, Russia, Finland, and Uzbekistan. I was also involved into the organization of the UArctic workshop at the UiT, and for some time I was a member of a Faculty Board and editorial board of the Department's Newsletter. The UiT provided a scholarship for three months at the University of California Riverside via "Staying abroad" scheme in order to establish the collaboration with UCR researchers and have a work experience at foreign Institute. The visit to UCR resulted in establishing an environmental laboratory at the UiT. Throughout the PhD courses I have learned a lot about the geology of Northern Norway, mineral deposits and the environmental consequences of mining activities. I have applied various analytical analyses and techniques to study rocks formed more than 2 Ga ago as well as to study recent materials and chemical reactions. As a part of my PhD, field works to the Røros mining area and Repparfjord Tectonic Window were organized. In 2015 I participated in a research cruise with RV Helmer Hansen to Repparfjorden. The

laboratory work for this research was conducted at the UiT – The Arctic University of Norway, University of Oslo, University of Bergen, and University of California Riverside. Microprobe analyses have been performed in collaborative partner, the Institute of Geology and Geophysics of the Republic of Uzbekistan.

The results of this research have been presented both in oral and poster forms at international and national conferences, including 12th International Congress for Applied Mineralogy (ICAM 2015, Istanbul, Turkey), UArctic workshop (2018, UiT), NYKOS meeting (2018, UiT), Bergen Vinterkonferansen (2019, Bergen, Norway), European Geosciences Union (EGU) General Assembly (2019, Vienna, Austria). As a part of the Arctic Marine Geology and Geophysics School (AMGG), I participated in various activities including seminars, workshops, and conferences.

Acknowledgements

I would firstly like to thank Troms Fylkeskommune, SINTEF in particular Gorm Breimo, and UiT The Arctic University of Norway for funding this PhD project and giving me the opportunity to study this interesting and complex topic and work in a nice, friendly, and highly professional environment.

I would like to express my deep gratitude to my supervisors Sabina Strmić Palinkaš and Kåre Kullerud, thank you for giving me an opportunity to try and test new ideas, make mistakes, and then fix them, learn how to be flexible and creative if something does not go according to a plan. Dear Kåre, thank you so much for believing in me and granting this PhD project to me, I have always appreciated this, it was a great though not an easy journey.

Dear Sabina, I do not know how to thank you for not having fear and taking me as a new student at the beginning of your career at the UiT. You are the one who saved this project by stepping in and showing the direction where we can go. Thank you for all our scientific and not so scientific discussions and small talks, your fast responses even in the middle of the night or a week-end, your support, your kindness and infinite understanding.

I would also like to thank Dr. Andrey Bekker, associate professor at the University of California Riverside. Dear Andrey, thank you for your enormous help with the first manuscript, your perpetual patience and advice while I was developing my scientific writing skills, thank you for your enthusiasm and interest in discussion. I would also like to thank Andrey's family, Roza Livovna, Anna and Lev for making my stay in Riverside nice and warm as being with my own family.

My deep gratitude goes to our laboratory ladies Trine, Karina, and Ingvild. Tusen takk kjære jenter for deres hjelp med alt som trengs, deres gode humør hele tida og light chat i løpet av dagen. Takk Edel for din hjelp og tips med prøvene og analyser.

I would like to thank Ronny Setså, a journalist from Geoforskning.no, who made this work known to the broad audience both geologists and not, people in Norway who care about Mother Nature.

I would like to thank former and present staff, colleagues and friends at the Department of Geosciences for creating a nice and friendly working atmosphere. I would especially like to thank our Head of Department, Matthias Forwick, for keeping this warm atmosphere trying to find solutions to all problems, resolve conflicts, and promoting the department around the world. Thank you, André Pedersen, Cecilie Helen Rikstad, Ann Kirsti Pettersen for all your help with endless invoices and paper work.

Я бы хотела также поблагодарить моих первых учителей по различным областям геологии: Рустама Исмаиловича, Халбая Джангировича, Турабека Нугмановича, Нину Алексеевну, Рашида Нигматовича, Ачила Кушмурадовича, Владимира Деньтьевича, Элеонору Ашотовну и многих других преподавателей факультета «Геологии» Национального Университета Узбекистана за фундаментальные знания в области геологических наук, за привитую любовь к геологии. Саша и Рустам, спасибо вам за прекрасные, веселые, плодотворные полевые сезоны и конечно же за прекрасную атмосферу взаимоподдержки и дружбы на нашем рабочем месте, кабине №217.

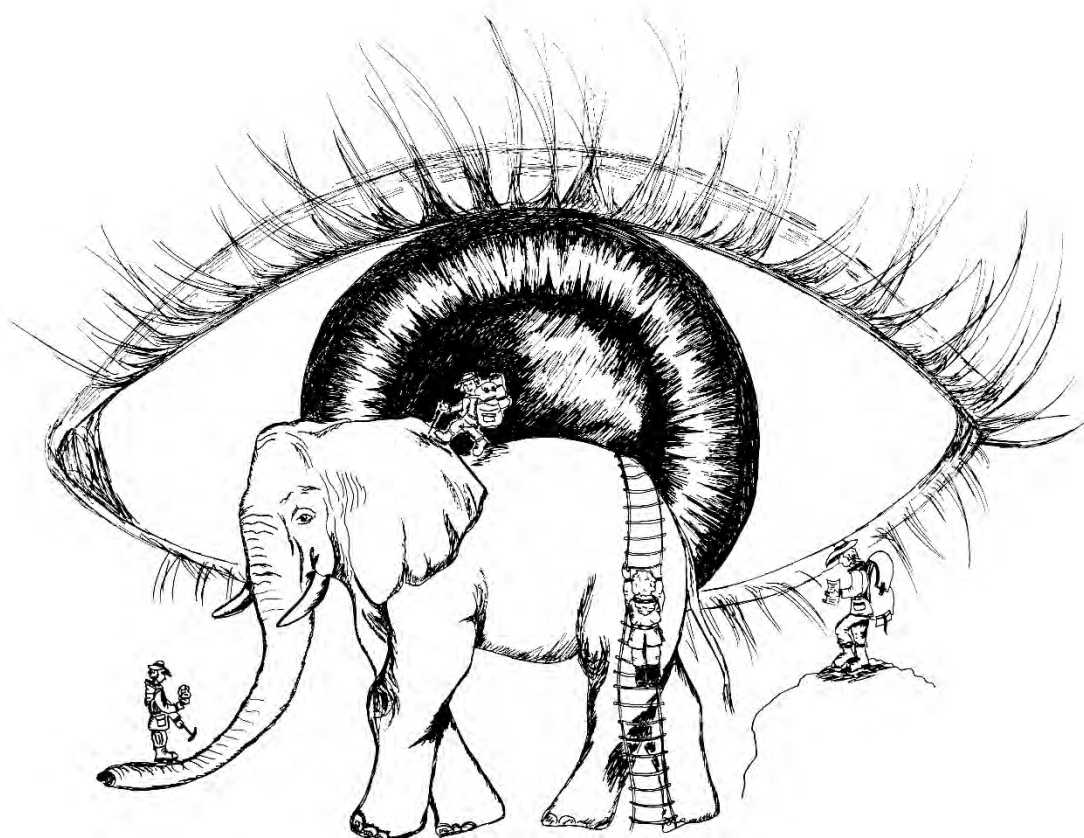
I would also like to thank all of my friends, Anna and Alexey, Alexey and Daria, Mariana and Calvin, Sunil, Friederike, Monica, Kasia, Noortje, Diane, Eythor, Marianne, Nicole, Andrea, Andreia, Emmelie and David, Kamila, Jack and many others. Thank you for making this period also full of fun that was a mixture between great loud parties and calm relaxing knitting evenings, or dinners. Dear Emmelie, thank you for our nice discussion

that gave me a great insight for the second manuscript. Hanne and Kai, you became really my “sister and brother in crime”, thank you so much for our chats, great discussions, constructive critics, nice dinners, help in everything starting from computer software’s and finishing with snow shovelling.

My dear Polina Safronova and Vera Iversen, thank you for being there whenever it was necessary, our phone calls are always a great moment to share achievements and falls, thank you for cheering me in hard and tough moments.

The last but not least I would like to thank my Russian and Italian families. Mio caro Giuseppe, grazie per tutto il tuo amore e supporto durante questi anni del mio dottorato. So che non era facile neanche per te ma ti ringrazio del cuore per essere sempre accanto pronto per aiutarmi e sopportarmi, grazie per la tua pazienza e credenza in me e in che ciò faccio. Grazie Sabino, Elvira e Rita per tutto il vostro aiuto con Alessio, per creare la possibilità per me di poter lavorare o riposare.

Моя дорогая семья, папа, мама, Катюша, кока Тома, Ариаша благодарю вас за то, что вы всегда верили в меня, поддерживали меня несмотря ни на что, вы наверное верили больше в то, что я смогу дойти до конца, чем я сама, спасибо вам за огромную помощь и поддержку. Люблю вас безмерно. Анжелочка, ты хоть и не член моей семьи, но по духу уж точно, благодарю тебя за наши разговоры, после которых всё казалось возможным и доступным к исполнению, за твою уверенность в то, что всё получится. Мой дорогой сыночек, Алессио, тебя я тоже благодарю за то, что ты просто есть, люблю тебя безусловно.



Trying to look at the task from various points of view...

Illustration: ©Ekaterina Anpleeva (Mun). *All rights reserved.*

Contents

Preface	I
Acknowledgements	III
List of papers	2
Introduction	3
Scientific background	4
Ore potential of the Repparfjord Tectonic Window	4
VMS type of deposits. Røros mining area in Central Norway.....	7
Mine tailings and AMD: synthesis	9
Tools to predict AMD.....	14
Remediation of AMD	15
Materials	19
Methods and techniques	21
Petrography and mineralogy of host rocks and ore mineralization	21
Lithogeochemistry.....	22
Stable isotopes.....	23
Fluid inclusions study.....	24
X-ray Powder Diffraction (XRD)	25
Grain-size analysis.....	26
TOC.....	27
Thermodynamical modelling.....	27
Sequential extraction.....	27
Raman spectrometry	28
Synopsis of research	29
Paper 1 – Evolution of metal-bearing fluids at the Nussir and Ulveryggen sediment-hosted Cu deposits, Repparfjord Tectonic Window, Northern Norway	29
Paper 2 – Stability of Cu-sulphides in submarine tailing disposals: A case study from Repparfjorden, northern Norway	30
Paper 3 – The role of ore-forming processes and tailing disposal site conditions on a contrasting environmental impact of Cu-sulphide deposits in Norway.	31
Conclusion	32
References	34

List of papers

Paper 1

Mun Y., Strmić Palinkaš S., Kullerud K., Nilsen K.S., Neufeld K., Bekker A. Evolution of metal-bearing fluids at the Nussir and Ulveryggen sediment-hosted Cu deposits, Repparfjord Tectonic Window, Northern Norway, *submitted to Norwegian Journal of Geology*.

Paper 2

Mun Y., Strmić Palinkaš S., Forwick M., Junttila J., Pedersen K.B., Sternal B., Neufeld K., Tibljaš D., Kullerud K. Stability of Cu-sulphides in submarine tailing disposals: A case study from Repparfjorden, northern Norway, *to be submitted to a special issue of Minerals "Environmental Geochemistry of Mineral Deposits", deadline for manuscript submissions: 30 November 2019*.

Paper 3

Mun Y., Strmić Palinkaš S., Kullerud K. The role of ore-forming processes and tailing disposal site conditions on a contrasting environmental impact of Cu-sulphide deposits in Norway, *to be submitted to Journal of Geochemical Exploration*

Introduction

Growing world technology, fast changing electronic gadgets, electric cars, solar batteries, windmills etc. require a huge quantity of metals and metalloids, including Cu. Therefore, a sustainable mining is an essential component in the modern global economy. In addition, at more local scale, the mining sector creates working places and develops infrastructure. However, the sustainable mining should be predated by fundamental geological studies. The wider knowledge on the genetic model of an mineral deposit contributes to the estimation of resources, increase probability for finding of new ore bodies, and overall contribution to the general knowledge on ore forming processes. The knowledge of petrography, mineralogy, litho geochemistry, and mineral chemistry creates also a solid background for prediction of environmental impacts of mineral deposits and associated waste and tailing disposal sites. Poorly controlled mining and insufficiently well-planned closure of the production site can lead to drastic consequences for the environment including the formation of acid mine drainage (AMD).

The main aim of this thesis is to contribute to better understanding of origin of the Cu-mineralization in Paleoproterozoic sediment hosted deposits as well as to estimate their environmental impact. Two sediment-hosted Cu deposits, Nussir and Ulveryggen, located in Northern Norway, were chosen for case studies. A particular focus has been given to environmental aspects of the submarine tailing site in Repparfjorden that contains the mine waste material from historical mining activities in 1970s. To get a better insight into the role of ore-forming processes on a contrasting environmental impact of Cu-sulphide deposits in Norway, in addition to the Nussir and Ulveryggen sediment hosted deposits, samples from the Røros volcanogenic massive sulphide (VMS) deposit were analysed and exposed to a set of weathering experiments.

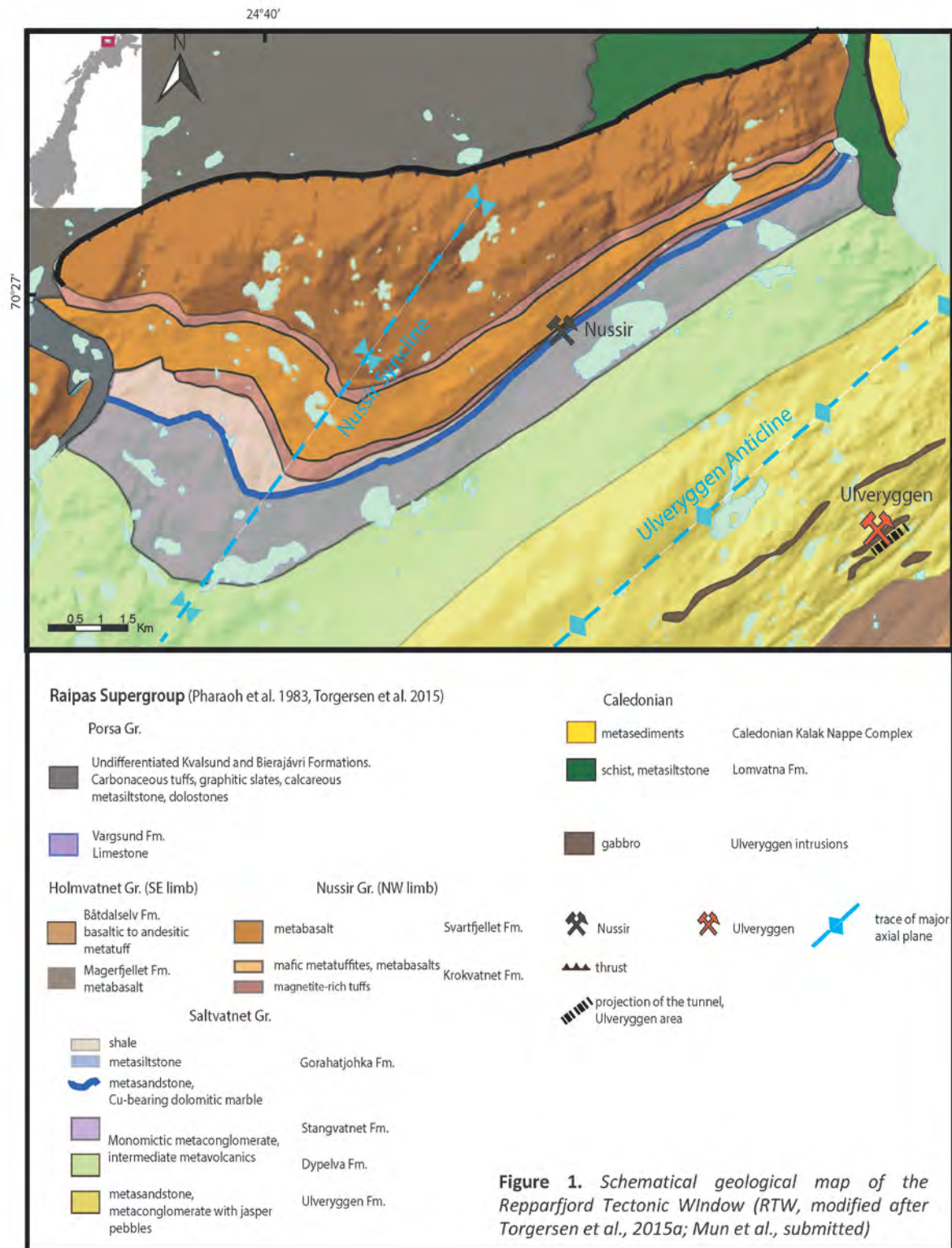
Scientific background

Ore potential of the Repparfjord Tectonic Window

A high ore potential of the Paleoproterozoic Greenstone Belts on the Fennoscandian Shield was confirmed during geological, geophysical, structural investigations and resulted in extensive mining activities in Fennoscandia (e.g., Viola et al., 2008; Olesen & Sandstad, 1993; Eilu et al., 2015; Henderson et al., 2015; Melezhik et al., 2015; Nasuti et al., 2015 and references therein; Torgersen et al., 2015a). The mineral deposits (Eilu, 2012; Eilu et al., 2015) have been found in the Kiruna District (Parák, 1975), Aitik (Wanhainen et al., 2003), Karasjok (Often, 1985), and Central Lapland (Ward et al., 1988; Yang et al., 2013). The Repparfjord Tectonic Window (RTW) is a basement culmination of Paleoproterozoic (circa 2.1 Ga) Greenstone Belt within the Kalak Nappe Complex of the Norwegian Caledonides in Northern Norway. It is widely correlative with neighbouring Alta-Kvanangen Tectonic Window (Melezhik et al., 2015; Nasuti et al., 2015). Generally, the Greenstone Belts are composed of a classic succession of mafic metavolcanics and carbonate-siliciclastic rocks (Torske & Bergh, 2004).

The RTW is composed of mafic metavolcanics and carbonate-siliciclastic sequences of the Raipas Supergroup that were compressed in SE-NW direction during the Svecofennian Orogeny at ca. 1840 Ma (Fig. 1; Pharaoh et al., 1982; Torgersen et al., 2015a). The rocks are metamorphosed to greenschist - lower amphibolite facies.

A number of different scale Cu mineralization such as Porsa, Bratthammer, Vesterdalen, Skreivatnet sites are known in the RTW (Viola et al., 2008, Torgersen et al., 2015b). However, the biggest prospects for Cu are sediment-hosted Nussir and Ulveryggen deposits (Viola et al. 2018). Mining is planned to be launched in 2020 by Nussir ASA.



Sedimentary-hosted Cu-deposits are found worldwide and make up about 23% of the global Cu production (Singer, 1995). The biggest are the Siberian Kodaro-Udokan basin, the African Katangan basin and the European Kupferschiefer basin (Hitzman et al., 2010). The Zambian, Zairian, and Kalahari Copperbelts in Africa, the Redstone Copperbelt in Canada, and the Donchuan and Zongtiaoshan regions in China are smaller in scale (Brown, 1971; Ripley et al., 1980; Chartrand and Brown, 1985; Selley et al., 2005; Dewaele et al., 2006; Brems et al., 2009; El Desouky et al., 2009; Sillitoe et al., 2010; Jiang et al., 2014). Stratiform-Cu deposits are mostly formed as results of circulating basinal brines with a high oxidation potential that are able to leach base metals from volcanic or intrusive rocks and transport them to the site of deposition. They are often characterized by the presence of evaporate sequence, red beds (i.e. hematite-rich sedimentary rocks such as sandstone, siltstone or conglomerate) and organic-rich sediments or pyrite-bearing shales where base metals are deposited in a form of sulphides.

Torgersen et al. (2015b) determined the age of the mineralization in the Porsa and Brattahammer mineralized veins and suggested that the first emplacement of veins occurred at 2.69 Ga (Torgersen et al. 2015a). Perelló et al. (2015) determined the age of host mafic metavolcanics to be circa 2.1 Ga and the Nussir mineralization age to be 1765 Ma. In spite of a prolonged research history of the Repparfjord Tectonic Window (e.g. Reitan, 1963; Stribrny, 1985; Fabricius, 1979) the source of metals, the mechanisms that triggered their transportation and deposition remained unknown. In Paper 1, we have constrained the nature of mineralizing fluids, the possible source of base metals and PT conditions characteristic for the Repparfjord Tectonic Window during the time of the Cu mineralizing event.

VMS type of deposits. Røros mining area in Central Norway.

Volcanogenic massive sulphides (VMS) type of deposits significantly contribute to the world's production of Cu, Zn, Pb, Au, and Ag. Tin, Mo, Co, Ba, Be, Se, Bi, Te, Mn, Cr, In, PGE, Ni, Cd, Ge, and Ga are common co- or by-products (Hutchinson, 1973; Galley et al., 2007; Koski & Mosier, 2010). The VMS type of deposits are formed from Early Archean (3.55 Ga) to the present time in modern oceanic settings (Koski & Mosier, 2010). They are typically formed in extensional tectonic regime, in submarine depressions where seawater reacts with heated upper crustal rocks leaching the metals from country rocks (Ohmoto, 1996). In Norway numerous VMS deposits are found along the Upper Allochthon of the Scandinavian Caledonides (Grenne et al., 1999).

The Røros mining area located in the Trøndelag County, southeastern Norway (Fig. 2), represents one of ten VMS districts in Norway. The area was mined from 1644 until 1977 (Sandstad et al., 2012) in numerous mines. Among the biggest are Storwartz and Olav mines in the eastern part and the Kongens mine in the north-western part (Fig. 2). The average Cu and Zn content is about 2.7% and 4.2-5%, respectively (Bjerkgård et al., 1999). The major ore minerals are chalcopyrite, sphalerite, pyrite, pyrrhotite and galena. The mineralization is hosted by metagraywacke interbedded with tuffite, metabasalts and gabbroic sills and dykes (Rui and Bakke, 1975; Bjerkgård et al., 1999; Sandstad et al., 2012).

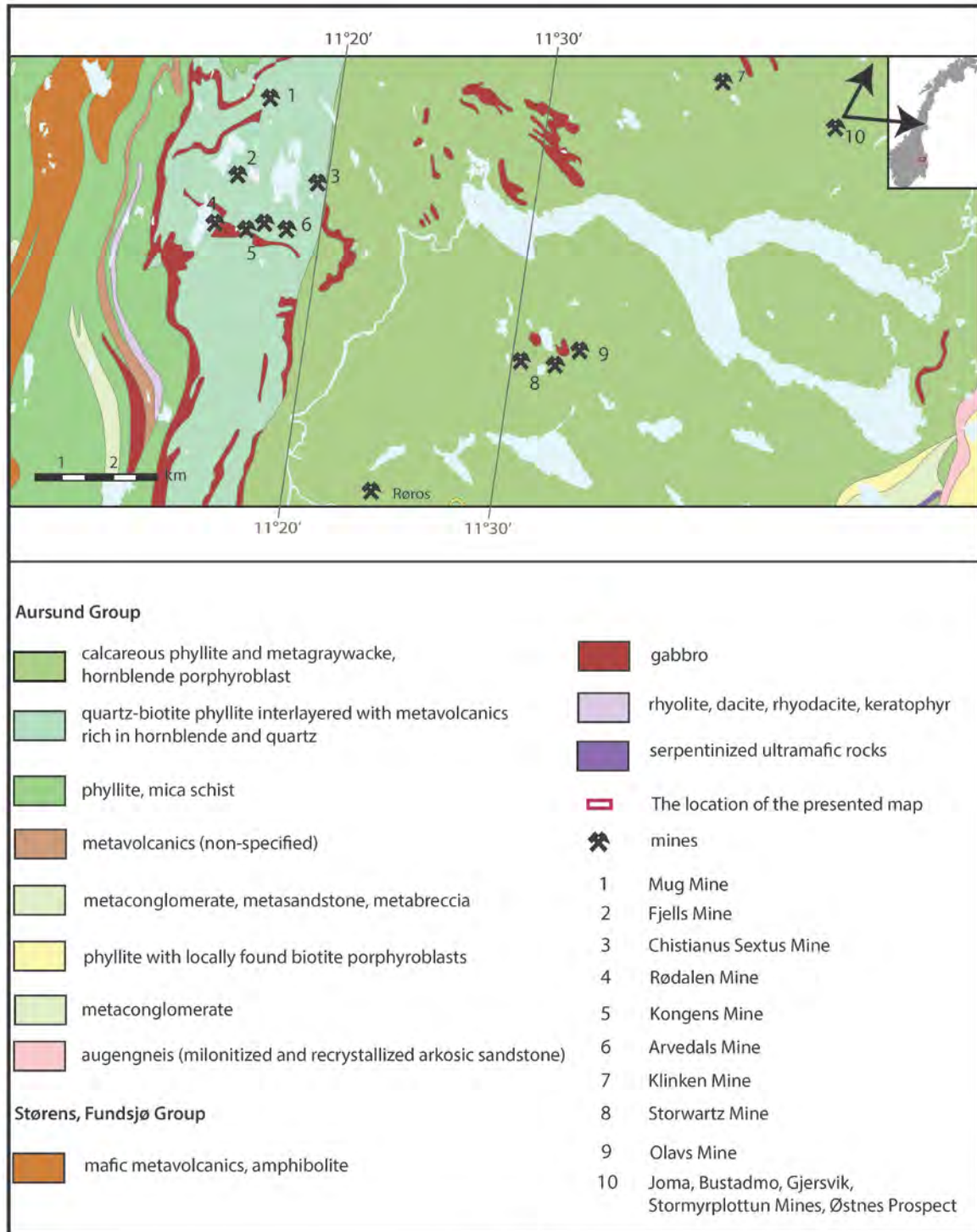
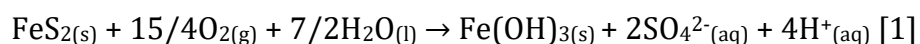


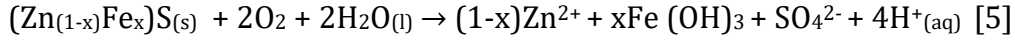
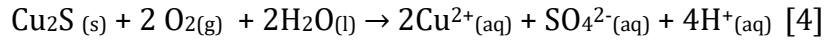
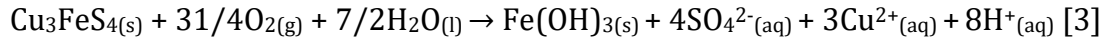
Figure 2. Geological map of the Røros mining area (modified after http://geo.ngu.no/kart/berggrunn_mobil/).

Mine tailings and AMD: synthesis

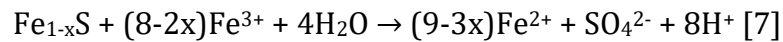
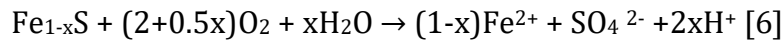
Mining production creates large amounts of mine waste that can be in solid, liquid and gaseous phase. Mine waste is a common term that includes mining waste, processing wastes and metallurgical wastes. Mine waste is a heterogeneous geological material that can contain fragments of sedimentary, metamorphic and igneous rocks as well as ore minerals, industrial minerals, metals, coal or mineral fuels in a sub-economic concentration, as well as process chemicals (Lottermoser, 2010). Mine tailings is only one type of mine waste, which is in focus of this thesis. Herein, we consider only sulphide-rich mine tailings – a slurry mixture of crushed rock with mud and metals in sub-economic concentration remained after the extraction. The biggest issue that is raised during poorly planned mine waste disposal site of mine tailings containing sulphides is the formation of acid mine drainage (AMD). AMD refers to highly acidic drainage waters containing a vast amount of dissolved sulphate, metals and metalloids that are formed during the reaction of sulphide rich mine wastes in an oxygenated environment (e.g. España et al., 2005; Bussièrre, 2009; Simate & Ndlovu, 2014; Kefeni et al., 2017). Several factors influence the generation and neutralization of acidic drainage waters. Among others, sulphur content, grain size of sulphides and buffering minerals (e.g. carbonates, silicates), ore mineral assemblages that can trigger a galvanic effect (e.g. Jambor et al., 2002; Kwong et al., 2003; Li et al., 2006).

Pyrite is the most reactive mineral in this process (Eq. 1). The major sulphides at the Ulveryggen and Nussir are bornite (Eq.2), chalcopyrite (Eq.3), chalcocite (Eq.4), covellite, pyrite and sphalerite (5) (Stirbrny, 1985; Sandstad, 2010; Perelló et al., 2015). Simplified chemical reactions occurring in AMD can be described as followed (Steger & Desjardins, 1980; Lottermoser, 2010; Lindsay et al., 2015):





Mine tailings can be stored under on-land or submarine conditions. Under on-land conditions, heavy metals release can affect the whole ecosystem in a long-term perspective (e.g. Tinto River, Spain; Ok Tedi River, Papua New Guinea; Hettler et al., 1997, Leblanc et al., 2000; Braungardt et al., 2003). In Norway, a negative experience of AMD can be observed in Røros mining area where predominant sulphides are pyrite and pyrrhotite (e.g. Ettner, 2007). Pyrrhotite dissolution occurs under the reaction with oxygen or ferric iron (Eqs. 6, 7; Janzen et al., 2000)



For several decades, after the cessation of mining activity in the Røros area, sulphide-rich mine tailings are still present in impoundments around the mining area and are subjected to weathering (Fig. 3). A number of rivers and streams including seasonal streams are continuously polluted by heavy metals liberated due to weathering of waste rocks dumps, smelting slag, tailings impoundments (Gundersen & Steinnes, 2001; Ettner, 2007; Iversen, 2012). The amount of dissolved metals (Cu, Zn, Cd, and Al) is negatively correlated with seasonal fluctuations of river discharge and more related to an increase of sediments, presumably sulphide rich, during high water flow episodes (Gundersen & Steinnes, 2001).

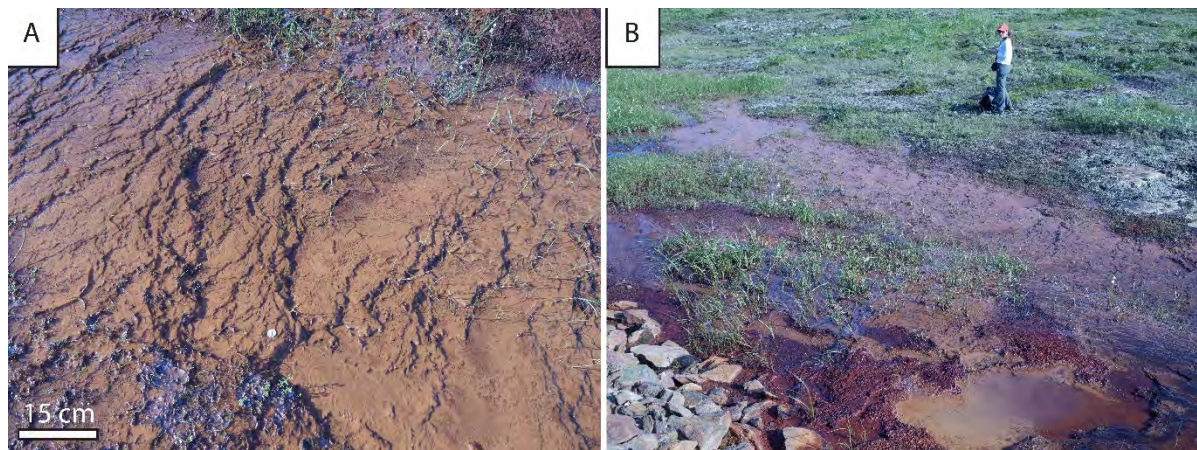


Figure 3. *A) travertine-like steps made by amorphous Fe hydroxides in small stream close to Krestenbekken; B) pond of reddish-brown water with strong odour formed along the stream close to Lergruvbakken Mine.*

The river sediments located in the vicinity of piles of mine waste have brown to reddish colour due to presence of amorphous iron hydroxides, (Fig. 3), the sediments have strong mouldy odour and the vegetation is poor. All around the area, ponds with small amount of water with bright brownish-red colour can be observed (Fig. 3). In the northern part of the mining area, leaching of heavy metals to the Orva river resulted in severe pollution and fish devastation (Ettner, 2007; Iversen 2012).

Submarine mine tailings disposal (STD) is, however, a controversial topic too, which has been under the discussion during the last decade. Norway is among few countries, along with Papua New Guinea, Philippines, Chile, Indonesia and Turkey, where submarine disposal is allowed. Submarine mine tailings disposal was also practiced in Canada (Island Copper Mine, Jordan River Mine) and Greenland (Black Angel Mine; Dold, 2014), however due to environmental considerations this practice was banned. Marine disposals are differentiated according to the depth of deposition and subdivided into three categories: coastal shallow-water disposal (CTD), submarine tailing disposal (STD) and deep-sea tailing placement (DSTP) (Ramirez-Llodra et al., 2015). This research was

focused on STD disposal in Repparfjord, Finnmark, Northern Norway (Fig. 4). As it was documented by Pedersen et al. (2018) 80-390 t of Cu still remains in the sediments of the Repparfjord. Andersson et al. (2018) describes a hardpan – Fe-Mn-hydroxide horizon that can be formed either at the border between oxidized and reduced layers or where pore water reacts with carbonates resulting in hydroxides precipitation. (Lottermoser, 2010). Hardpan is often associated with AMD-related processes (Lottermoser, 2010).

In both, off-shore and on-land conditions, dissolved heavy metals can be bioavailable and lead to significant changes in the ecosystem (Chapman et al., 1998, Lottermoser, 2010, Ramirez-Llodra et al., 2015, Pedersen et al. 2017, Sternal et al., 2017). As an example, Pb and Zn uptake by mussels, as well as by seaweeds was registered in Agfardlikavsa and Quarmarijuk fjords in western Greenland where STD was practiced between 1973 and 1990 (Loring & Asmund, 1989; Larsen et al., 2001; Dold, 2006). Bioavailable heavy metals and metalloids can be bioaccumulated and biomagnified up the feeding chain leading to intoxication of biota (Chapman et al., 1998; Bowles et al., 2001; Macdonald et al., 2002).

In 1970-s Folldall Verk AS was mining the sediment-hosted Ulveryggen Cu deposit and discharged about 1Mt of mine tailings into Repparfjorden. The slurry was transported into the inner part of the fjord through a pipeline about 600 m long with opening intervals at 100 m (Kvassnes & Iversen, 2013; Pedersen et al., 2016; Sternal et al., 2017). A number of national projects (EWMA – Environmental Waste Management, Pedersen et al., 2017; Sternal et al., 2017; AkplanNiva; FIMITA, Andersson et al., 2018; Reinardy et al. 2019) were funded in order to investigate the present state of tailings, monitor heavy metals distribution around the fjord, the reaction of biota to elevated concentrations of heavy metals etc. in the Repparfjord. The investigations revealed the

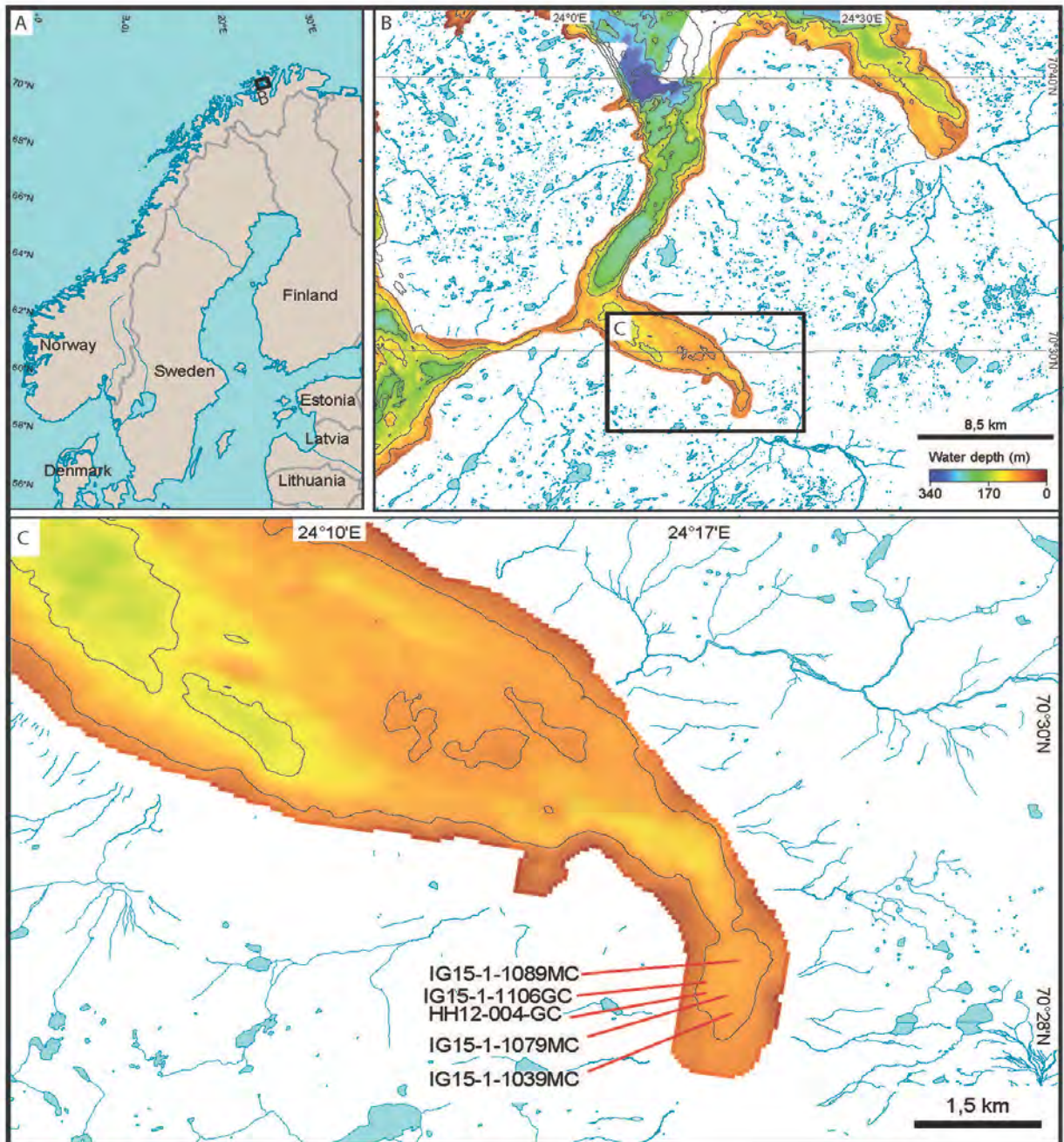


Figure 4. A) overview map; B) Map of the study area; C) map of the Repparfjord showing the location of cores studied in Mun et al. (in preparation): MC - multi cores, GC – gravity core. The maps are modified after Sternal et al. (2017).

Cu contamination and dispersion of Cu within the fjord (Sternal et al., 2017), the bioavailability of Cu and its potential negative impact on biota (Pedersen et al. 2017; Reinardy et al. 2019). In Paper 2 we are presenting the results of geochemical studies of the Cu mineralization from the Nussir and Ulveryggen deposits as well as sedimentological, mineral and geochemical data obtained from tailings and natural sediments in Repparfjorden.

Tools to predict AMD.

Kinetic and static tests

Kinetic tests represent a powerful and relatively cheap instrument to predict generation of AMD. They are designed to simulate sulphide-weathering processes in different physicochemical conditions. Kinetic leaching tests can be industrial or performed in the laboratory. Industrial tests are run in leaching columns, heaps, tanks, vasts, dumps, large bins or drums (Lottermoser, 2010). They are placed in the field and subjected to meteoric waters, oxygen from the atmosphere, changing temperature depending on the season. These tests can be conducted for several months to several years and but only infrequently sampled for concentrations of dissolved metals and metalloids, sulphate and changing pH and Eh parameters (e.g. Lima, 2004). The tests can be accelerated by adding additional water (Lottermoser, 2010).

However, more often the leaching tests are performed in miniature versions and run in laboratory size equipment – batch reactors, leaching columns, humidity cells (e.g. Gottschalk & Buehler, 1912; Cheng & Lawson, 1991; Falk et al., 2006; Rzepka et al., 2014; Embile Jr. et al., 2018; Embile Jr. & Walder, 2018). The results are later extrapolated or mathematically modelled for larger volumes (Lima, 2004). The tests are well-controlled and parameters such as water pH and Eh, metals and metalloids concentrations are continuously measured. The tests are often accelerated by increased temperature or

addition of hydrogen peroxide (e.g. Silva et al., 2011). The laboratory leaching tests also allow determination of an acid neutralizing capacity of gangue minerals and acid producing potential of sulphides as well as to test remediation mechanisms, (e.g. Gottschalk & Buehler, 1912, Jambor et al., 2002; Ruan et al., 2010; Plante et al., 2012). However, many authors (e.g. Banwart et al., 1998) argue that laboratory tests cannot be simply extrapolated to the field conditions. For example, a faster oxidation of pyrite and chalcopyrite from the Aitik site in Northern Sweden has been observed in the laboratory compared to the field conditions (Banwart et al., 1998).

During this PhD project, we applied a series of leaching experiments and test typical ore assemblages from three Cu sulphide deposits: sediment-hosted Nussir and Ulveryggen deposits and the Røros VMS deposit. The main focus was given to simulation of physicochemical conditions relevant for submarine and on-land tailing sites. The results of the experiments are presented in Manuscript 3.

Thermodynamical modelling of sulphides weathering

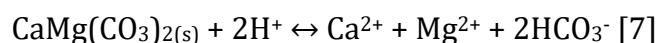
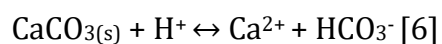
Thermodynamic modelling allows prediction of stability of Cu-sulphide minerals as well as of acid mine drainage generation. Various variables, such as temperature, pressure, redox potential, pH value, conductivity, concentrations of various anions (e.g., Cl^- , SO_4^{2-} , HCO_3^- , etc.), the presence of solid phases (e.g., carbonates, quartz, pyrite) can be added to the calculations of predominant dissolved species (e.g. Ayora et al., 1998). Visual Minteq 3.1. (Visual Minteq, 2019) was applied in Manuscript 2 for calculation of chalcopyrite solubility and speciation of Cu.

Remediation of AMD

Mine tailings are products that can have irreversible negative impact on the environment. Therefore, the main objective of all methods applied to detailed study of AMD is to find the best solution how to minimize the impact on the environment. Johnson & Hallberg

(2005), Lottermoser (2010), and Kefeni et al. (2017) give a review on AMD remediation. An alternative usage of mine waste and tailings is more often discussed (e.g. Bonden, 2011; Lottermoser, 2011) also because many authors agree that long-term stability predictions are difficult to make based on short-term laboratory tests. The remediation and treatment are often difficult and no universal solution exists (Chapman et al., 1998; Johnson and Hallberg 2005; Hudson-Edwards et al., 2011; Kefeni et al. 2017). Lottermoser (2011), Bonden (2011), and Kefeni et al. (2017) suggest the recycling of on-land deposited mine tailings with further remediation by introducing of metal opportunistic plants providing enough soils and nutrients to secure their growth (Bakker, 1981; Bradshaw, 1997; Lottermoser et al., 2011). Among other ways to prevent AMD and bioavailability of dissolved metals, Chapman et al. (1998) proposes capping, dredging, solidification/stabilization. However dredging can destroy anoxic conditions therefore provoking oxidation of tailings (Chapman et al. 1998). Capping is a process of covering the storage place with a thin layer of inert material, which is placed in order to create anoxic conditions. One variety of capping is introduction of silty material to grinded mine tailings material in order to increase adsorption capacity and therefore immobilization of metals (Chapman et al., 1998; Kefeni et al., 2017). Layers of desulphurized tailings can also be used as capping material (Benzaazoua et al., 2000, 2008; Benzaazoua and Kongolo, 2003; Demers et al., 2008).

Oxidation of pyrite, which is one of the most common minerals associated with metallic mineral deposits, leads to the decrease in pH (Eq. 1) and consequently mobilization of heavy metals, including Cu (e.g., Lindsay et al., 2015) which is in the focus of this research. In processes of remediation, pH can be maintained by the addition of carbonates or by dilution with hydroxides. Carbonates commonly keep the aquifer pH in the range from 6.5 to 7.5 (Lindsay et al. 2015):



An addition of lime ($\text{Ca}(\text{OH})_2$) have been proposed by several researchers (Blowes et al. 1994; Ziemkiewicz et al., 1994; Yanful & Orlanda, 1999; Cravotta III, 2003). Bernier et al., (2002), however, emphasise that following factors and investigation should be made before the choice of passive lime treatment: annual sulphide load, flow rates, armouring effects, internal porosity, water chemistry, and seasonable variations in hydraulic conductivity. In anoxic conditions the usage of lime can take place during limited time until the equilibrium and calcite saturation are achieved (Cravotta III, 2003; Kefeni et al., 2017). Oxic conditions would lead to dissolution of calcite (Lottermoser, 2010).

In addition, adsorption processes can significantly affect mobility of metals and metalloids in various environments, including tailing disposal sites (e.g., Kadirvelu et al, 2001; Kumpiene et al., 2008; Motsi et al., 2009; Gitari et al., 2011).

The Røres area nowadays represents a UNESCO historical site heritage, which complicates mitigation efforts, including prevention of AMD. However, several attempts were done in Røros area to diminish and control AMD and ARD (acid rock drainage; Ettner, 2007). Among them there are: capping of mine waste and removal of waste rocks dumps, designation of anaerobic passive treatment (bioreactors). The *Induced bacterial-sulphate reduction (BSR)* method was also tested in the Røros mining area (Ettner, 2007). This type of remediation is also well known and successful tests of BSR application are reported (e.g. Nancucheo et al., 2017, Ayangbenro, 2018, Liu et al., 2018). The recent observations, however, demonstrated that the metals are still being released into the riverine system (Iversen, 2012).

Overall, prevention of AMD generation is often cheaper and wiser the rehabilitation and remediation of it (e.g. Bradshaw, 1997; Johnson & Hallberg, 2005). As demonstrated by

Younger et al. (2005) the combination of scientific and governmental forces in order to prevent AMD distribution often leads to great results.

Materials

Materials from the Nussir and Ulveryggen sediment hosted Cu deposits were collected during several field campaigns from 2013 to 2015 in the Repparfjord Tectonic Window as well as at the National Drill Core and Sample Centre (NBPS) in Løkken (Papers 1, 3). Sediments from Repparfjorden were sampled during the research cruise on Research Vessel Helmer Hansen in 2015 (Paper 2). Two gravity cores studied and applied for Papers 2 and 3 were retreated in 2012 from RV Helmer Hansen and kindly provided by Matthias Forwick for further investigation. River sediments from the Repparfjordelva were kindly provided by the Norwegian Geological Survey (Paper 2). The Røros mining area was sampled in 2014. In addition, the massive sulphide mineralization from the Joma Mine (Nord Trøndelag) and Røros Mine was subsampled from the mineral collection at UiT The Arctic University of Norway.

In total approximately 90 thin polished sections were prepared at the geological laboratory of the Department of Geosciences at the UiT. The thin polished sections were further used for petrographical and mineralogical studies as well as for SEM investigations of ore mineral assemblages. Twenty-seven thin polished sections were used in weathering tests described in Paper 3.

The reconstruction of PT conditions of hydrothermal fluids required preparation of double-sided polished wafers from vein quartz (Nussir) and host rock quartz (Ulveryggen). Stable isotope analysis ($\delta^{13}\text{C}$ and $\delta^{18}\text{O}$) were made on 14 samples containing carbonates both in host dolomites and vein carbonate (Nussir) and marble from the Vargsund Formation in the Repparfjord Tectonic Window for the comparison (Paper 1). Supplementary Tables 1 & 2 give a full overview on samples and methods applied.

The material for Paper 2 was obtained from two gravity cores: HH12-004-GC and IG15-1-1106GC and three multi cores: IG15-1-1089MC, IG-15-1-1079MC, and IG15-1-1039. The multi cores were sliced at 1 cm interval on board and immediately frozen. The gravity cores were immediately frozen on-board and further sliced at the UiT at 0.5 cm interval. Marine sediments were sampled for determination of total organic carbon, grain size analysis. Heavy concentrates were extracted from marine sediments in the 0-2, 3-4, 43, 100, 155, 167, 181, and 216 cm intervals of HH12-004-GC. The same samples were used for sequential extraction and XRD bulk and clay analyses. Heavy concentrates were also isolated from IG-15-1-1039/1089/1079 multi corers at 3-4 cm, 7-8, 8-9, 11-12, 14-14.5 cm intervals.

HH12-004-GC was subsampled and TOC was determined from 0-30 cm with 0.5 cm steps, and deeper from 43, 100, 155, 167, 188 and 216 cm depths. TOC was also determined in HH12-002-GC prior to the use of marine sediments in weathering tests described in paper 3. HH12-002-GC was subsampled 1 cm step, the uppermost part was not used for the tests in order to avoid the effect of marine sediments effected by mine tailings from the Ulveryggen. Supplementary table 2 gives an overview of samples location, depth, coordinates of cores and methods applied.

Thirteen river sediments from the streams affected by mining were sampled in the Røros mining area. Air-dried samples were consequently sampled for XRD bulk, XRD of clay mineralogy, as well as amorphous Fe hydroxides were hand-picked and mounted to the epoxy for further investigation using SEM technique (supplementary Table 3).

Methods and techniques

Petrography and mineralogy of host rocks and ore mineralization

Petrography and ore mineral analyses were performed at the Department of Geosciences at UiT using transmitted and reflected polarized light techniques. The Leica DM LM microscope was equipped with 2.5x, 5x, 10x, and 63x objectives.

Chemical analyses of individual ore minerals were performed using a Cameca SX 100 electron microprobe at the Department of Geosciences at the University of Oslo; a Jeol YXA 8800R Superprobe at the Institute of Geology and Geophysics of the Republic of Uzbekistan; a Zeiss Merlin compact VP field emission scanning electron microscope (SEM-FE) equipped with Energy-dispersive X-ray spectrometer (EDS) and wavelength-dispersive spectrometer (WDS) at UiT The Arctic University of Norway; and a NovaNanoSEM 450 at the University of California, Riverside. The analyses performed with the Cameca SX 100 were carried out at 15 kV accelerating voltage, 15 nA beam current, focused beam, and 10 s counting time on a peak. Standardization was made on synthetic minerals (As: gallium arsenide), metal (Fe, Co, Cu, Ni, Ag, and Au) and on natural minerals (Zn: sphalerite, Pb: galena). The optical system and electron backscattered images were used for recognition. The analyses obtained with Jeol Superprobe were carried out at 20 kV accelerating voltage, under the regime of high and low vacuum. The NovaNanoSEM 450 was set in a high vacuum regime at 20 kV accelerating voltage, 10 s counting time, and with the aperture of 60 μm . The Zeiss Merlin SEM field emission microscope was run in a high vacuum regime at 20 kV accelerating voltage, 20 s counting time, and with an aperture of 60 μm .

The heavy fraction was extracted from marine sediments using sodium polytungstate (max density 3.1 g/cm³; Fig. 5). The fraction was subsequently mounted into crystal bond

and thereafter polished. Polished samples were investigated using Zeiss Merlin Compact VP field emission scanning electron microscope (SEM) equipped with Energy-dispersive X-ray spectrometer (EDS) and wavelength-dispersive spectrometer (WDS) at UiT. The analyses were carried out in a high vacuum regime at 20 kV accelerating voltage, 20 s counting time, and with an aperture of 60 μm .

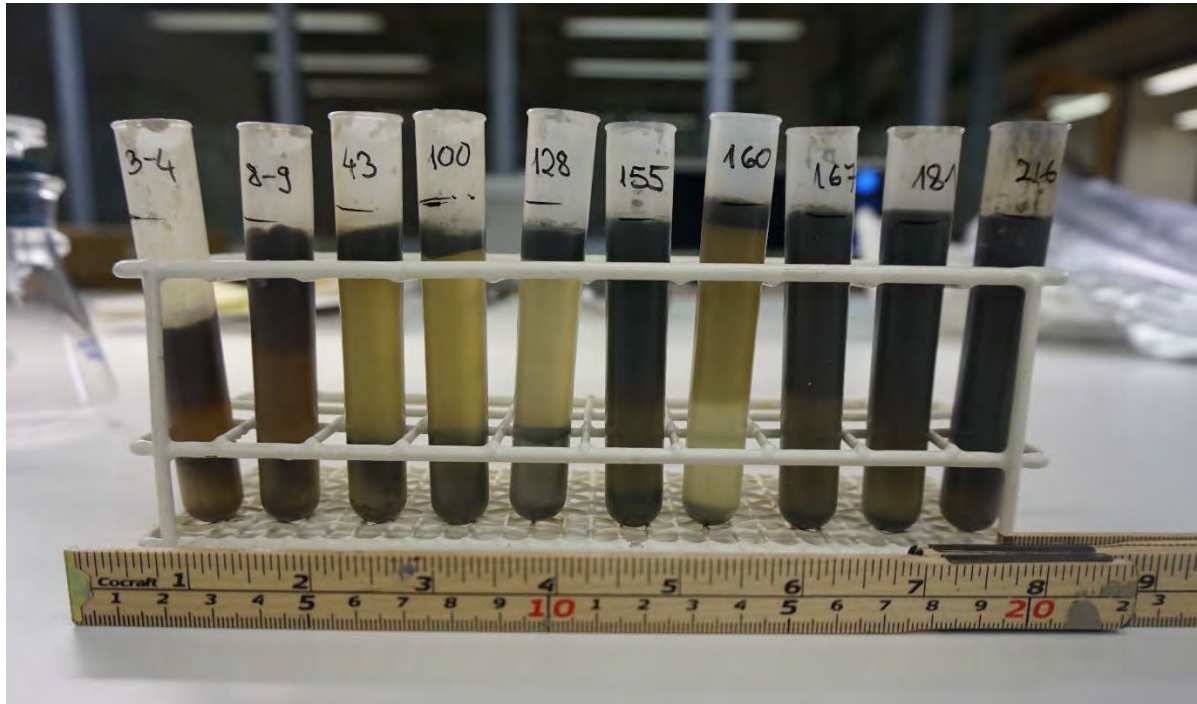


Figure 5. *Separation of heavy concentrates from marine sediments*

Twenty-seven polished thin sections, prepared for weathering tests, were firstly examined under reflected light using Leica DM LM microscope and SEM. The fresh samples were investigated under high vacuum regime at SEM; the samples after 90-days tests were investigated under low vacuum regime and using secondary electrons (SE).

Litho geochemistry

Whole-rock geochemical analyses were performed at Activation Laboratories (Actlabs, Canada). About 10 g of crushed material was fused together with the lithium metaborate/tetraborate to ensure total acid dissolution of minerals such as zircon,

monazite, and xenotime prior to analyses. The analyses were performed using ICP and ICP-MS (inductively coupled plasma mass-spectrometry) to determine major and trace element contents. Actlabs uses replicate analyses of samples and certified reference materials to assure the precision and accuracy of data.

Individual sulphide grains of Cu sulphides were hand-picked under a binocular microscope, washed in an ultrasonic bath and pulverized in an agate mortar. The amount of 0.5 g was analysed for bulk trace element composition at Acmelabs (Vancouver, Canada), using the ICP MS method with the LF202 analysis code.

Stable isotopes

Stable isotope composition of host mineralized dolomitic marbles of the Gorahatjohka Formation of the Nussir deposit as well as marbles from the Vargsund Formation in Repparfjord were analysed. Carbon and oxygen isotope analyses of carbonates were performed at UiT The Arctic University of Norway and at the SIFIR laboratory of the Department of Geological Sciences, University of Manitoba, Canada. At UiT, 50 - 150 μg of microdrilled carbonate powder was loaded into sealed reaction vessels, then flushed with helium gas and reacted at 50°C with phosphoric acid, during >2hours. The evolved carbon dioxide was sampled using a Thermo Fisher Gasbench II and isotope ratios were measured in a continuous flow mode using a Thermo Fisher MAT253 isotope-ratio mass-spectrometer. The stable isotope ratios of carbon and oxygen are reported in the delta (δ) notation as per mil (‰) deviation relative to the Vienna Pee Dee Belemnite (V-PDB). The analytical reproducibility was better than $\pm 0.1\text{‰}$ for $\delta^{13}\text{C}$ and $\delta^{18}\text{O}$.

At the SIFIR laboratory, carbonates were microdrilled with 1 mm in diameter diamond drill bits from the least altered (i.e., lacking veins, discoloration, weathering rinds, and silicification) and finest-grained portions of polished thick sections; slabs were subsequently stained to determine carbonate mineralogy. Carbonate powders were

reacted at 70 °C with anhydrous phosphoric acid using a GasBench II carbonate device and delivered in a stream of high-purity He to a Thermo Fisher Delta V Plus isotope ratio mass spectrometer via an open-split interface (ConFlo IV, Thermo Fisher). All C and O isotope ratios are reported in delta notation relative to international standards on the Vienna Pee Dee Belemnite (V-PDB) scale. All C isotope ratios are reported in delta notation

$$\delta^{13}\text{C} = \left(\frac{{}^{13}\text{R}_{\text{sample}}}{{}^{13}\text{R}_{\text{V-PDB}}} - 1 \right) \times 1000$$

Calibration was performed by analyzing two international calcite standards (NBS-18 and NBS-19) at the beginning, middle, and end of each run. A calibration line was calculated by least squares linear regression using the known and measured isotope values of the calibration standards. To check the quality of analysis performance, one calibrated internal calcite standard (CHI, $\delta^{13}\text{C} = -8.01\text{‰}$ V-PDB and $\delta^{18}\text{O} = -11.67\text{‰}$ V-PDB) and one calibrated internal dolomite standard (Tytyri, $\delta^{13}\text{C} = +0.78\text{‰}$ V-PDB and $\delta^{18}\text{O} = -7.07\text{‰}$ V-PDB) were analyzed together with unknown samples. Replicate analyses of internal standards yielded the results of $\delta^{13}\text{C} = -7.98 \pm 0.08\text{‰}$ and $\delta^{18}\text{O} = -11.63 \pm 0.14\text{‰}$ (n=23) for CHI, and $\delta^{13}\text{C} = +0.74 \pm 0.09\text{‰}$ and $\delta^{18}\text{O} = -6.02 \pm 0.15\text{‰}$ (n=17) for Tytyri. Correction using the known oxygen isotope value for the Tytyri dolomite standard was performed for $\delta^{18}\text{O}$ values of dolomite samples.

Fluid inclusions study

Petrographic and microthermometric studies of fluid inclusions were performed at UiT The Arctic University of Norway. Double-polished, 0.1 to 0.3 mm-thick, quartz wafers were prepared. Measurements were carried out on Linkam THMS 600 stage mounted on an Olympus BX 2 microscope using 10× and 50× Olympus long-working distance objectives. Two synthetic fluid inclusion standards (SYN FLINC; pure H₂O and mixed H₂O-

CO₂) were used to calibrate the equipment. The precision of the system was $\pm 2.0^{\circ}\text{C}$ for homogenization temperatures, and $\pm 0.2^{\circ}\text{C}$ in the temperature range between -60° and $+10^{\circ}\text{C}$. Apparent salinity of two-phase inclusions was calculated from final ice melting temperatures. The salinity of three-phase (L+V+S) inclusions was calculated from halite melting temperatures. In both cases the equation of Bodnar (1993) was applied. The computer package FLUIDS (Bakker 2003; Bakker and Brown, 2003) was used to calculate fluid properties, including the bulk density. The fluid inclusions bulk density and isochores were calculated according to the equation of state published by Zhang and Frantz (1987).

The measured microthermometric parameters included: eutectic temperature, last melting temperature of ice and/or hydrohalite, and total homogenization temperature. The studied fluid inclusions were further decrepitated by quick heating of the samples (100°C per min) up to 600°C and keeping the samples at this temperature for 30 minutes, following the procedure described by Kontak (2004). The samples were subsequently inspected under reflected light for the presence of evaporite mounds and then placed on carbon tape for analysis on SEM using EDS detector at UiT The Arctic University of Norway.

X-ray Powder Diffraction (XRD)

The HH12-004-MF-0312 gravity core was sampled up to 12 cm depth with 2 cm interval for the XRD analysis of bulk marine sediments. Clay minerals were separated from the 3-4, 8-9, 43, 100, 128, 155, 160, 167, 181, 216 cm and analysed by the XRD technique. In order to sample clays, marine sediments were mixed with distilled water and centrifuged for about 3 minutes. The suspension was further sampled, and dropped with pipette onto the thin section glass that was primarily roughed with diamond paper. The XRD analyses were conducted at the Department of Geology, University of Zagreb, Croatia, using a

Philips PW 3040/60 X'Pert PRO powder diffractometer (45 kV, 40 μ A), with CuK α -monochromatized radiation ($\lambda = 1.54056 \text{ \AA}$) and θ - θ geometry. The area between 4° and $63^\circ 2\theta$, with 0.02° steps, was measured with a 0.5° primary beam divergence. Compound identifications from the bulk samples were based on a computer program X'Pert high score 1.0B and literature data. Highly oriented samples of the $<2 \mu\text{m}$ fraction were prepared for clay mineral identification on air-dried, ethylene-glycol saturated, and heated (at 400 and 550°C , respectively) samples according to the procedure described by Starkey et al. (1984). Instrumental conditions were 40 kV , 40 mA and constant time 5 s , with step scanning ($0.02^\circ 2\theta$).

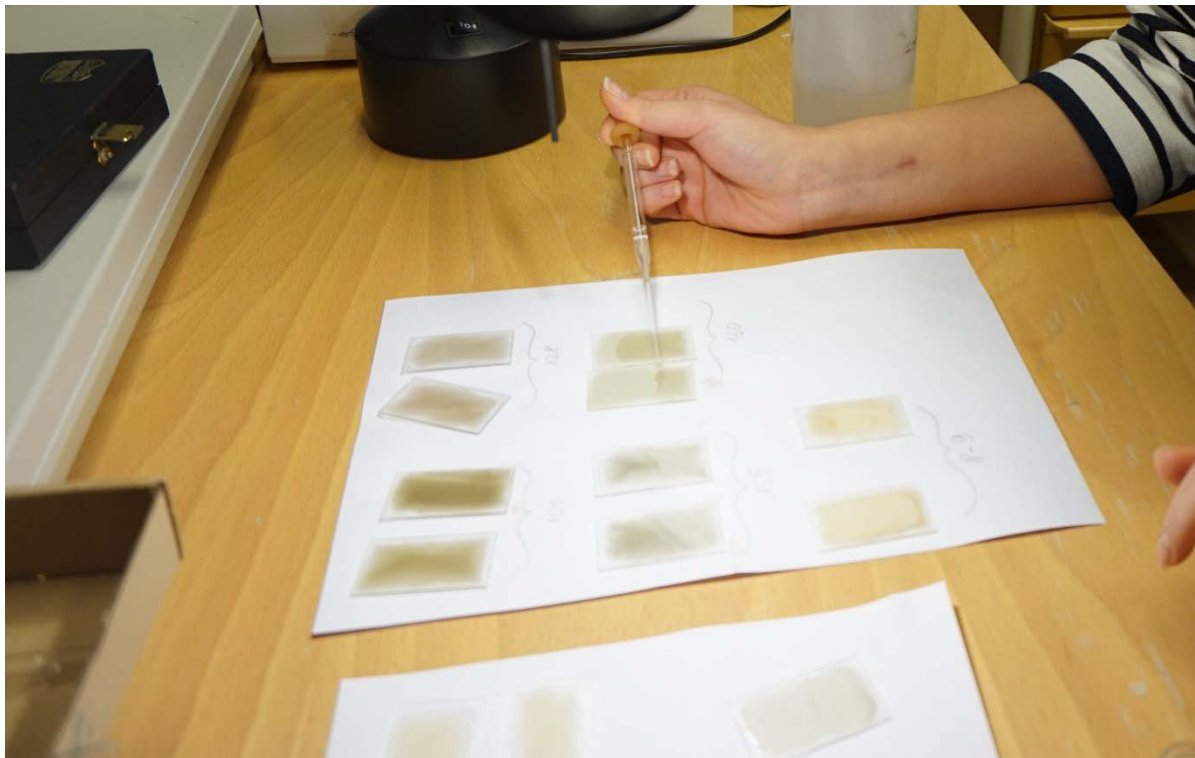


Figure 6. *Separation of clay minerals for XRD analysis*

Grain-size analysis

Grain-size analysis was performed on HH12-004-MF-0312 GC core sub-sampled at every 0.5 cm interval using Diffraction Particle Size Analyzer at UiT (Beckman Coulter LS 13 320). All samples were prepared and analysed following the procedures described by

Dijkstra et al. (2017) and processed as described in Sternal et al. (2017) using the GRADISTAT program and applying the geometric methods of moments (Blott & Pye, 2001).

TOC

Total organic carbon (TOC) was measured in sediment samples of the HH12-004-MF-0312-GC core using the LECO CS-200 instrument at UiT. The samples were prepared following the procedure described in Sternal et al. (2017). For the purpose of this study the following intervals were sampled (all samples are of 1-cm thickness) and analysed: 0-30 cm, followed by 43, 100, 155, 167, 181, and 216 cm depth.

Thermodynamical modelling

Visual Minteq version 3.1 (Visual Minteq, 2019), a freeware for simulation of chemical equilibrium models and calculation of metal speciations, mineral solubility and sorption capacities in natural waters (Gustafsson, 2012) and the geochemical modeling software PHREEQC (Parkhurst & Appelo, 2013) were used to calculate Cu speciation and Cu-mineral solubility using the concentrations of major dissolved components defined for on-land and submarine conditions.

Sequential extraction

The rocks, sediments or mine tailings can contain elevated concentrations of trace metals, including hazardous ones. However, as long as they are bound to hardly soluble fraction, e.g. in the lattice of silicates they remain stable and non-effective for the environment. Sequential extraction is a method that allows determination of metals and metalloids speciation (e.g. Tessier et al., 1979; Arroyo & Siebe, 2007). For this study, 5 steps consequent dissolution was applied to marine sediments following the procedure described in Ure et al., 1993, Pedersen et al., 2017 and improved by Simonsen et al. (*in*

press, Paper 2). Sequential extraction was performed for partitioning of Cu, Ni, Pb, Zn, Fe, Al, Fe, K, Mg, Mn and Ba among 5 fractions: residual, oxidisable, reducible, acid-soluble and exchangeable. The analyses were made on seven samples from HH12-004-GC-MF-0312 GC taken from following intervals: 3-4, 43, 100, 155, 167, 181, and 216 cm.

	Chemical form	Sequential extraction method	Fractionation pattern	
Total	Weakly adsorbed	Sediment (0.5g) extracted with nitrate acid (0.5M, 20mL) for 16h	Exchangeable	Bioavailable
	Associated with carbonates	Sediment is extracted with acetic acid (0.11M, 20mL, pH3) for 16h	Acid soluble	
	Associated with Fe and Mn oxides	Sediment is extracted with hydroxylammonium chloride (0.1M, 20mL, pH2) for 16h	Reducible	
	Associated with organic matter and sulphides	Sediment was extracted with hydrogen peroxide (8.8M, 5mL) for 1h followed by extraction at 85°C for 1h, evaporation of liquid at 85 °C, and extraction of cooled solid with ammonium acetate (1M, 25mL, pH2) for 16h	Oxidisable	Potential bioavailable
	Bound in mineral lattice	Sediment and nitric acid (9M, 20mL) were autoclaved (200kPa, 120 °C , 30min). Solid particles removed and liquid is diluted	Residual	Not-bioavailable

Figure 6. Five-steps sequential extraction applied in this research (Simonsen et al., in press).

Raman spectrometry

Raman spectroscopy was conducted at the Department of Earth Science, The Faculty of Mathematics and Natural Sciences, University of Bergen (UiB). A JobinYvon LabRAM HR800 confocal Raman spectrometer equipped with a frequency doubled Nd-YAG laser (100 mW, 532 nm) and LMPlan FI 50× objective (Olympus) were used to identify mineral phases in the studied ore samples, as well as the degree of weathering after simulation of weathering conditions in on-land and submarine conditions. The identifications were based on Raman spectra published in the literature.

Synopsis of research

Paper 1 – Evolution of metal-bearing fluids at the Nussir and Ulveryggen sediment-hosted Cu deposits, Repparfjord Tectonic Window, Northern Norway

The main goal of this paper was to better understand the evolution of Early Proterozoic Repparfjord basin from the mineralization point of view. Regardless prolonged exploration history, the nature of mineralizing fluids and the source of base metals remain unclear. The combination of lithogeochemistry of host rocks, fluid inclusion study (FI) and stable isotope analyses allowed reconstruction of the evolution of the mineralizing fluids. The FI study revealed an involvement of highly saline brines. The combination of microthermometry and SEM/EDS analyses of evaporated mounts formed after the decrepitation of FIs suggest that these saline brines were metal-bearing. Oxidizing fluids penetrated through the volcanogenic-sedimentary sequence dissolved evaporates and leached base metals from mafic volcanics abundantly present in the area. The metals were further transported by chloride complexes to the reductive boundary. The major part of the mineralization at the Nussir deposit was concentrated in dolomites in quartz-carbonate veins as well as in disseminated form, partly the mineralization was precipitated in rare quartz-carbonate veins within metavolcanogenic sequence. The Cu content of sphalerite that occurs in the chemical equilibrium with chalcopyrite allowed the calculation of the formation temperature in an interval between 330 and 340°C. Diverse assemblages of FIs and homogenization temperatures varying from 135 to 350°C at the Nussir deposit and 102-520°C at the Ulveryggen deposit evidence a prolonged evolution history of the basin. The combination of independent sphalerite geothermometer with homogenization temperatures obtained from FIs revealed the pressure during mineralization formation to be 1.1-2.7 kbars which is in agreement with regionally observed greenschist facies metamorphism. Overlapping $\delta^{13}\text{C}$ (-0.9 to +2.9‰

V-PDB) and $\delta^{18}\text{O}$ (-18.3 to -15.9‰ V-PDB) values in host dolomites and ore bearing carbonate veins in metavolcanites suggest that the system was closed and rock-buffered without significant contribution of magmatic or hydrothermal CO_2 .

Paper 2 – Stability of Cu-sulphides in submarine tailing disposals: A case study from Repparfjorden, northern Norway

During the mining activities at the Ulveryggen sediment-hosted Cu deposit from 1972 to 1978/79 approximately 1 Mt of mine tailings were deposited in the inner part of Repparfjorden (Sandstad et al., 2007; Kvassness & Iversen, 2013). The main objective of Paper 2 is to observe the stability of sulphides in submarine tailings and estimate their geochemical impact on marine sediments. Litho-geochemistry of marine sediments up to 12 cm depth and river sediment from the Repparfjordelva demonstrated that both types of sediments contain elevated concentrations of Ni and Cr. Both elements are sourced from mafic country rocks. In contrast, elevated concentrations of Cu and Ba in marine sediments are considered as a result of mining activities in the area.

Bulk chemical analyses of chalcopyrite and bornite from Nussir and Ulveryggen deposits respectively, demonstrated that ore minerals contain minor amounts of potentially hazardous elements like As, Cd, and Hg. SEM investigations of heavy concentrates separated from marine sediments revealed well preservation of bornite and pyrite in the submarine tailings. Chalcopyrite from the shallow depth (0-4 cm) was found in well preserved grains, but some of the grains have oxidized rims. Bulk XRD analyses revealed that marine sediments contain mostly quartz, plagioclase, muscovite, chlorite, zinnwaldite. Clay minerals determination using XRD analysis demonstrated the presence of montmorillonite – an expandable clay – in the marine sediments together with non-expandable illite, kaolinite and chlorite. Thermodynamic modelling of Cu speciation for pore waters within anoxic marine sediments and under oxic conditions common for on

land disposal sites confirmed that pH and redox potential are major factors affecting Cu sulphides dissolution. The buffering of marine sediments with carbonates can lead to remobilization of Cu in a form of $\text{CuCO}_3(\text{aq})$ complex. This fact should be accounted when planning mine tailings disposal from the Nussir deposit since the latter is hosted by dolomitic marbles (Torgersen et al., 2015; Perelló et al., 2015; Mun et al., *submitted*).

Paper 3 – The role of ore-forming processes and tailing disposal site conditions on a contrasting environmental impact of Cu-sulphide deposits in Norway.

Twenty-seven thin-polished sections containing sulphides from three Cu deposits in Norway: 1) the Nussir sediment-hosted Cu deposit; 2) the Ulveryggen sediment-hosted Cu deposit; 3) the Røros VMS type of deposit were weathered under laboratory conditions. Prior to the tests the samples were investigated under reflected light and using SEM. The samples from the Nussir deposit contained chalcopyrite, bornite, galena, sphalerite, and minor amount of pyrite. The Ulveryggen samples contained bornite and chalcocite. The Røros samples contain abundant pyrite, sphalerite and chalcopyrite. The bulk lithogeochemistry of hand-picked chalcopyrite from the Røros mining area demonstrated high concentration of As, Cd, Hg.

The glass beakers (400 ml) were filled with marine sediments from Repparfjorden and prefabricated sand simulating reductive and oxidative conditions. Sediments were buffered or non-buffered with carbonates and/or organic matter combined with either seawater or meteoric water. After 90-days test the samples were investigated using reflected light microscopy, SEM and Raman spectrometry. Reflected light microscopy demonstrated various degree of oxidation and the additive of organic matter to be the best to prevent weathering. Raman spectrometry revealed the presence of secondary minerals containing OH and CO_3 in their composition.

Conclusion

Paleoproterozoic terrains are complex and yet fascinating place for studying. Methods traditionally applied to mineral deposits investigation should be in many cases modified in order to smoothen the impact of changing geodynamic settings leading to regional metamorphism, multiple fluid remobilizing events, disappearance of particular lithologies etc. In many cases, the suggestions are made based on indirect features and guesswork. In spite of the more than 2.0 Ga years of evolution history the Repparfjord Tectonic Window remained a well-preserved, well-outcropped site for making scientific research and be a nice “text-book style” study place. High ore potential makes the RTW especially attractive in the moment of “Green Shift”. In this research, we present new data on the evolution of the mineralization of the RTW. Based on the information obtained from petrographical, mineralogical, geochemical observations, fluid inclusions study, stable isotopes combined with the data from previous researchers, we give evidence of the metals source, PT conditions and mechanisms triggered the deposition of ore in the Nussir and Ulveryggen deposit.

This thesis was intended to show a bridge between fundamental study of the deposit with detailed petrographical, mineralogical, geochemical characterization and post mining reactions occurring in the residuals (mine tailings) when stored in submarine conditions on the example of Repparfjorden where some indications of acid mine drainage (AMD) are found. The AMD from the sulphide ores and sulphide-rich mine tailings is the main emphasis of this research. In order to show the contrast, on-land mine waste placement was studied in the Røros mining area. Field observations demonstrated the formation of acidic drainage waters in the Røros mining area where different types of mine waste is subjected to weathering under atmospheric conditions rich in dissolved oxygen and Fe

(III) species. The tailings disposed in Repparfjorden are less oxidized, i.e. the majority of ore minerals are well-preserved with an exception of chalcopyrite from upper most horizons which in some samples was found partly weathered. In addition, the presence of Fe-Mn hydroxide hardpan is one of the AMD presence signs. Laboratory tests combined with thermodynamic modelling of Cu speciation demonstrated the leading role of pH and redox potential in the sulphide oxidation rate and the predominance of particular species in the environment with various pH values. Thus, at pH below 8, Cu^{2+} are predominant dissolved Cu species, while at pH ranging from 8 to 11 $\text{Cu}_3(\text{OH})_4^{+2}$ and CuOH^+ prevail. In more alkaline environment, $\text{Cu}(\text{OH})_3^-$ are the most abundant species. In the marine environment buffered with carbonates Cu^{2+} and CuHCO_3^+ prevail at pH below 7, while in alkaline conditions Cu-hydroxides complexes are most abundant. In near-neutral conditions $\text{CuCO}_3(aq)$ complexes are dominant. Marine sediments are near-neutral to slightly alkaline therefore the mobilization of Cu in $\text{CuCO}_3(aq)$ complexes should be especially considered. The weathering tests demonstrated that addition of carbonate lead to higher oxidation degree of Cu-sulphides.

While pH controls the speciation of Cu, the redox potential controls the rate of sulphide oxidation, in marine sediments due to low content of dissolved oxygen the solubility of sulphides is relatively low in comparison to the atmospheric conditions. Therefore, the choice of remediation approach should be directed to the decrease of dissolved oxygen and creation of anoxic conditions. The weathering tests demonstrated that oxidizing atmospheric conditions can be buffered by the additive of organic matter thus preventing the oxidation of sulphides regardless the complexity of mineral assemblages. This research was a minor attempt to combine the knowledge from primary to processed ore.

References

- Andersson, M.; Finne, T.E.; Jensen, L.K.; Eggen, O.A. (2018) Geochemistry of a copper mine tailings deposit in Repparfjorden, northern Norway. *Science of Total Environment* 644: 1219-1231.
- Arroyo, Y.R. & Siebe, C. (2007) Weathering of sulphide minerals and trace element speciation in tailings of various ages in the Guanajuato mining district, Mexico. *Catena* 71, 497-506
- Ayangbenro, A.S.; Olanrewaju, O.S.; Babalola, O.O. (2018) Sulfate-reducing bacteria as an effective tool for sustainable acid mine bioremediation. *Frontiers in Microbiology* 9, 1-10.
- Ayora, C.; Chinchón, S; Aguado, A.; Guirado, F. (1998) Weathering of iron sulfides and concrete alteration: thermodynamic model and observation in dams from Central Pyrenees, Spain. *Cement and Concrete Research* 28 (9), 1223-1235.
- Bakker, R.J. (2003) Fluids, package of computer programs for fluid inclusion studies. *Chemical Geology* 194, 3-23.
- Bakker, R.J.; Brown, P.E. (2003) Computer modelling in fluid inclusion research. In: Samson, I.; Anderson, A.; Marshall, D. (eds.) *Fluid Inclusions: Analysis and Interpretation. Short Course 32, Mineralogical Association of Canada*, 175-212.
- Banwart, S.A.; Destouni, G.; Malmström, M. (1998) Assessing mine water pollution: from laboratory to field scale. *Groundwater Quality: Remediation and Protection. Processing of the CQ'98 Conference, Tübingen, Germany, IAHS Publ 250*, 307-311.
- Benzaazoua, M.; Bussière, B.; Kongolo, M.; McLaughlin, J.; Marion, P. (2000) Environmental desulphurization of four Canadian mine tailings using froth flotation. *International Journal of Mineral Processing* 60, 57-74.
- Benzaazoua, M.; Kongolo, M. (2003) Physico-chemical properties of tailing slurries during environmental desulphurization by froth flotation. *International Journal of Mineral Processing* 69, 221-234.
- Benzaazoua, M.; Bussière, B.; Demers, I.; Aubertin, M.; Fried, É.; Blier, A. (2008) Integrated mine tailings management by combining environmental desulphurization and cemented paste backfill: Application to mine Doyon, Quebec, Canada. *Minerals Engineering* 21, 330-340.
- Bernier, L.R.; Aubertin, M.; Poirier, C.; Bussière, B. (2002) On the use of limestone drains in the passive treatment of acid mine drainage (AMD). Symposium Les Mines ET l'ENVIRONNEMENT, Rouyn-Noranda.
- Bjerkgård, T.; Sandstad, J.S.; Sturt, B.A. (1999) Massive sulphide deposits in the south-eastern Trondheim region Caledonides, Norway: a review. In: Stanley et al. (eds.) *Mineral Deposits: Processes to Processing*, London: 935-938.
- Blott, S.J.; Pye, K. (2001) Gradistat: a grain size distribution and statistics package for the analysis of unconsolidated sediments. *Earth Surface Processes and Landforms* 26, 1237-1248.
- Blowes, D.W.; Johnson, R.H.; Robertson, W.D.; Molson, J.W. (1994) Acid-neutralization reactions in inactive mine tailings impoundments and their effect on the transport of dissolved metals. *Proceedings of the international land reclamation and mine drainage conference and third international conference on the abatement of acidic drainage. Volume 1: Mine drainage*, 429-438.
- Bodnar, R.J. (1993) Revised equation and table for determining the freezing point depression of H₂O-NaCl solutions. *Geochemica et Cosmochimica* 57, 683-684.

- Bonden, A. (2011) Alternativ disponering av avgangsmasse fra Nussir og Ulveryggen. Report. Bergfald miljørådgivere: 22 pp.
- Bowles, K.C.; Apte, S.C.; Maher, W.A.; Kawei, M.; Smith, R. (2001) Bioaccumulation and biomagnification of mercury in Lake Murray, Papua New Guinea. *Canadian Journal of Fisheries and Aquatic Science* 58, 888-897.
- Bradshaw, A. (1997) Restoration of mined lands – using natural processes. *Journal of Ecological Engineering* 8, 255-269.
- Braungardt, C.B., Achterberg, E.P., Elbaz-Poulichet, F., Morley, N.H. (2003) Metal geochemistry in a mine-polluted estuarine system in Spain. *Applied Geochemistry* 18, 1757-1771.
- Brems, D., Muchez, Ph., Sikazwe, O., Mukumba, W. (2009) Metallogenesis of the Nkana copper-cobalt South Orebody, Zambia. *Journal of African Earth Sciences* 55, 185-196.
- Brown, A.C. (1971) Zoning in the White Pine copper deposit, Ontogon County, Michigan. *Economic Geology* 66, 543-573.
- Bussi re, B. (2009) Acid mine drainage from abandoned mine sites: problematic and reclamation approaches. *Proceedings of the International Symposium on Geoenvironmental Engineering*. ISGE2009. September 8-10, Hangzhou, China.
- Chapman, P.M.; Wang, F.; Janssen, C.; Persoone, G.; Allen, H.E. (1998) Ecotoxicology of metals in aquatic sediments: binding and release, bioavailability, risk assessment, and remediation. *Canadian Journal of Fisheries and Aquatic Sciences* 55, 2221-2243.
- Chartrand, F.M. & Brown, A.C. (1985): The diagenetic origin of stratiform copper mineralization, Coates Lake, Redstone Copper Belt, N.W.T., Canada. *Economic Geology* 80, 325-343.
- Cheng, C.Y. & Lawson, F. (1991) The kinetics of leaching covellite in acidic oxygenated sulphate-chloride solutions. *Hydrometallurgy* 27, 269-284.
- Cravotta III, C.A. (2003) Size and performance of anoxic limestone drains to neutralize acidic mine drainage. *Journal of Environmental Quality* 32, 1277-1289.
- Demers, I.; Bussi re, B.; Benzaazoua, M.; Mbonimpa, M.; Blier, A. (2008) Column test investigation on the performance of monolayer covers made of desulphurized tailings to prevent acid mine drainage. *Minerals Engineering* 21, 317-329.
- Dewaele, S., Muchez, Ph., Vets, J., Fenandez-Alonzo, M., Tack, L. (2006): Multiphase origin of the Cu-Co ore deposits in the western part of the Lufilian fold-and-thrust belt, Katanga (Democratic Republic of Congo). *Journal of African Earth Sciences* 46, 455-469.
- Dijkstra, N.; Junttila, J.; Skirbekk, K.; Carroll, J.; Husum, K.; Hald, M. (2017) Benthic foraminifera as bio-indicators of chemical and physical stressors in Hammerfest harbour (Northern Norway). *Marine Pollution Bulletin* 114, 384-396.
- Dold, B. (2006) Element flows associated with marine shore mine tailings deposits. *Environmental Science and Technology* 40, 752-758.
- Dold, B. (2014) Submarine tailings disposal (STD) – a review. *Minerals* 4, 642-666.
- Eilu, P. (ed., 2012) Mineral deposits and metallogeny of Fennoscandia. *Geological Survey of Finland, Special Paper* 53, 401 pp.
- Eilu, P.; Hallberg, A.; Bergman, T.; Bjerkg rd, T.; Feoktistov, V.; Korsakova, M.; Krasotkin, S.; Lampio, E.; Lauri, L.; Litvinenko, V.; Philippov, N.; Sandstad, J.S.; Shchiptsov, V. (2015) Fennoscandian Ore Deposit Database. Annual update. Available at: <http://en.gtk.fi/information-services/databases/fodd/index.html>
- El Desouky, H.A.; Muchez, Ph.; Cailteux, J. (2009) Two Cu-Co sulfide phases and contrasting fluid systems in the Katanga Copperbelt, Democratic Republic of Congo. *Ore Geology Reviews* 36, 315-332.

- Embile Jr., R.F.; Walder, I. (2018) Galena non-oxidative dissolution kinetics in seawater. *Aquatic Geochemistry* 24, 107-119.
- Embile Jr., R.F.; Walder, I.F.; Schuh C.; Donatelli J.L. (2018) Cu, Pb and Fe release from sulphide-containing tailings in seawater: Results from laboratory simulation of submarine tailings disposal. *Marine Pollution Bulletin* 137, 582-592.
- España, J.S.; López Pamo, E.; Santofimia, E.; Aduvire, O.; Reyes, J.; Baretino, D. (2005) Acid mine drainage in the Iberian Pyrite Belt (Odiel river watershed, Huelva, SW Spain): Geochemistry, mineralogy and environmental implications. *Applied Geochemistry* 20, 1320-1356.
- Ettner, D.C. (2007) Passive mine water treatment in Norway. In: Cidu, R.; Frau, F. (eds.) *Water in Mining Environments*. IMWA Symposium 2007. Italy.
- Fabricius, J. (1979) Kobberforekomsten på Ulveryggen, Finnmark, Norge. *Dansk Geologisk Forening. Årsskrift for 1979*, 107-110.
- Falk, H.; Lavergren, U.; Bergbäck (2006) Metal mobility in alum shale from Öland, Sweden. *Journal of Geochemical Exploration* 90, 157-165.
- Galley, A. G., Hannington, M. D., & Jonasson, I. R. (2007). Volcanogenic massive sulphide deposits. Mineral deposits of Canada: A synthesis of major deposit-types, district metallogeny, the evolution of geological provinces, and exploration methods: *Geological Association of Canada, Mineral Deposits Division, Special Publication* 5, 141-161.
- Gitari, W.M.; Kaseke, C.; Nukuzani, B.B. (2011) Passive remediation of acid mine drainage using bentonite clay: a laboratory batch experimental study. In: Råde, Freund and Wolkersdorfer (eds.) *IMWA 21011: Mine water – managing the challenges*. 325-329.
- Gottschalk, V.H.; Buehler, H.A. (1912) Oxidation of sulphides. *Economic Geology* 7, 15-34.
- Grenne, T.; Ihlen, P.M.; Vokes, F.M. (1999) Scandinavian Caledonide metallogeny in a plate tectonic perspective. *Mineralium Deposita* 34, 422-471.
- Gundersen, P.; Olsvik, P.A.; Steinnes, E. (2001) Variations in heavy metal concentrations and speciation in two mining-polluted streams in Central Norway. *Environmental Toxicology and Chemistry* 20 (5), 978-984.
- Gundersen, P.; Steinnes, E. (2001) Influence of temporal variations in river discharge, pH, alkalinity and Ca on the speciation and concentration of heavy metals in some mining polluted rivers. *Aquatic Geochemistry* 7, 173-193.
- Gustafsson, J.P., Mwamila, L.B., Kergoat, K. (2012) The pH dependence of phosphate sorption and desorption in Swedish agricultural soils. *Geoderma* 189-190, 304-311.
- Henderson, I.H.C.; Viola, G.; Nasuti, A. (2015) A new tectonic model for the Palaeoproterozoic Kautokeino Greenstone Belt, northern Norway, based on high-resolution airborne magnetic data and field structural analysis and implications for mineral potential. *Norwegian Journal of Geology* 95 (3-4), 339-363.
- Hettler, J.; Irion, G.; Lehmann, B. (1997) Environmental impact of mining waste disposal on a tropical lowland river system: a case study on the Ok Tedi Mine, Papua New Guinea. *Mineralium Deposita* 32, 280-291.
- Hitzman, M.W.; Selley, D.; Bull, S. (2010) Formation of sedimentary rock-hosted stratiform copper deposits through Earth history. *Economic Geology* 105, 627-639.
- Hudson-Edwards, K.A.; Jamleson, H.E.; Lottermoser, B.G. (2011) Mine Waste: past, present, future. *Elements* 7, 375-380.
- Hutchinson, R.W. (1973) Volcanogenic sulphide deposits and their metallogenic significance. *Economic Geology* 68: 1223-1246.
- Iversen, E.R. (2012) Avrenning fra Nordgruvefeltet, Røros kommune Undersøkelser i 2011-2012. *Niva Rapport L. Nr. 6420-2012*, 24 pp.

- Jambor, J.L.; Dutrizac, J.E.; Groat, L.A.; Raudsepp, M. (2002) Static tests of neutralization potentials of silicate and aluminosilicate minerals. *Environmental Geology* 43, 1-17.
- Janzen, M.P.; Nicholson, R.V.; Scharer, J.M. (2000) Pyrrhotite reaction kinetics: Reaction rates for oxidation by oxygen, ferric iron, and for nonoxidative dissolution. *Geochimica et Cosmochimica Acta* 64 (9), 1511-1522.
- Jiang, Yu.; Niu, H.; Bao, Zh.; Shan, Q.; Yang, W.; Yan, Sh. (2014) Fluid evolution of the Paleoproterozoic Hujiayu copper deposit in the Zhongtiaoshan region: evidence from fluid inclusions and carbon-oxygen isotopes. *Precambrian Research* 255, 734-747.
- Johnson, D.B.; Hallberg, K.B. (2005) Acid mine drainage remediation options: a review. *Science of Total Environment* 338, 3-14.
- Kardirvelu, K.; Thamaraiselvi, K.; Namasivayam, C. (2001) Removal of heavy metals from industrial wastewaters by adsorption onto activated carbon prepared from an agricultural solid waste. *Bioresource Technology* 76, 63-65.
- Kefeni, K.K.; Msagari, T.A.M.; Mamba, B.B. (2017) Acid mine drainage: prevention, treatment options, and resource recovery: A review. *Journal of Cleaner Production* 151, 475-493.
- Kontak, D.J. (2004) Analysis of evaporate mounds as a complement to fluid-inclusion thermometric data: case studies from granitic environments in Nova Scotia and Peru. *Canadian Mineralogist* 42, 1315-1329.
- Koski, R.; Mosier, D.L. (2010) Deposit type and associated commodities In: Shanks III, W.C.P & Thurston, R. (eds.) Volcanogenic massive sulphide occurrence model. *U.S.G.S. Scientific Investigations Report* 2010-5070-C, 15-21.
- Kumpiene, J.; Lagerkvist, A.; Maurice, C. (2008) Stabilization of As, Cr, Cu, Pb and Zn in soil using amendments – A review. *Waste Management* 28, 215-225.
- Kvassnes, A.J.S.; Iversen, E. (2013) Waste sites from mines in Norwegian fjords. *Mineralproduksjon* 3, A27-A-38.
- Kwong, Y.T.; Swerhone, G.W.; Lawrence, J.R. (2003) Galvanic sulphide oxidation as a metal-leaching mechanism and its environmental implications. *Journal of Geochemical Exploration* 3, 337-343.
- Larsen, T.S.; Kristensen, J.A.; Asmund, G.; Bjerregaard, P. (2001) Lead and zinc in sediments and biota from Maarmorilik, West Greenland: an assessment of the environmental impact of mining wastes on an Arctic fjord system. *Environmental Pollution* 114, 275-283.
- Leblanc, M.; Morales, J.A.; Borrego, J.; Elbaz-Poulichet, F. (2000) 4500-year-old mining pollution in southwestern Spain: long-term implications for modern mining pollution. *Economic Geology* 95, 655-662.
- Levings CD, Barry KL, Grout JA, Piercey GE, Marsden AD, Coombs AP, and Mossop B (2004) Effects of acid mine drainage on the estuarine food web, Britannia Beach, Howe Sound, British Columbia, Canada. *Hydrobiologia* 525: 185-202.
- Li, Zh.; Heping, LI.; Lining, X. (2006) Galvanic interaction between galena and pyrite in an open system. *Chinese Journal of Geochemistry* 25, 230-237.
- Lindsay, M.B.J.; Moncur, M.C.; Bain, J.G.; Jambor, J.L.; Ptacek, C.J. (2015) Geochemical and mineralogical aspects of sulphide mine tailings. *Applied Geochemistry* 57, 157-177.
- Liu, Z.; Lihua, L.; Li, Z.; Tian, X. (2018) Removal of sulfate and heavy metals by sulfate-reducing bacteria in an expanded granular sludge bed reactor. *Environmental Technology* 39, 1814-1822.
- Loring, D.H.; Asmund, G. (1989) Heavy metal contamination of a Greenland fjord system by mine wastes. *Environmental Geology and Water Sciences* 14, 61-71.

- Lottermoser, B.G. (2010) Mine Wastes. Characterization, treatment and environmental impacts. 3rd ed. Springer – Verlag Berlin Heidelberg. 400 pp.
- Lottermoser, B.G. (2011) Recycling, reuse and rehabilitation of mine wastes. *Elements* 7, 405-410.
- Macdonald, R.; Mackay, D.; Hickie, B. (2002) A new approach suggests that phenomena, such as bioconcentration, biomagnification, and bioaccumulation, result from two fundamental processes. *Environmental Science & Technology*: 457A-462A.
- Melezhik, V.A.; Bingen, B.; Sandstad, J.S.; Pokrovsky, B.G.; Solli, A.; Fallick, A.E. (2015) Sedimentary-volcanic successions of the Alta–Kvænangen Tectonic Window in the northern Norwegian Caledonides: Multiple constraints on deposition and correlation with complexes on the Fennoscandian Shield. *Norwegian Journal of Geology* 95, 245-284.
- Motsi, T.; Rowson, N.A.; Simmons, M.J.H. (2009) Adsorption of heavy metals from acid mine drainage by natural zeolite. *International Journal of Mineral Processing* 92 (1-2), 42-48.
- Mun, Y.; Strmić Palinkaš, S.; Kullerud, K.; Nilsen, K.S.; Neufeld, K.; Bekker, A. Evolution of metal-bearing fluids at the Nussir and Ulveryggen sediment-hosted Cu deposits, Repparfjord Tectonic Window, Northern Norway (*submitted to Norwegian Journal of Geology*).
- Mun, Y.; Strmić Palinkaš, S.; Forwick, M.; Junttila, J.; Pedersen, K.B.; Sternal, B.; Neufeld, K.; Tibljaš, D.; Kullerud, K. The stability of Cu-sulphides in submarine tailing disposals: A case study from the Repparfjord disposal site, Norway (*to be submitted to Minerals*).
- Nancuqueo, I.; Bitencourt, J.A.P.; Sahoo, P.K.; Alves, J.O.; Siqueira, J.O.; Oliveira, G. (2017) Recent developments for remediating acidic mine waters using sulfidogenic bacteria. *BioMed Research International*, 1-17.
- Nasuti, A.; Roberts, D.; Dumais, M.-A.; Ofstad, F.; Hyvönen, E.; Stampolidis, A.; Rodionov, A. (2015) New high-resolution aeromagnetic and radiometric surveys in Finnmark and North Troms: linking anomaly patterns to bedrock geology and structure. *Norwegian Journal of Geology* 95, 217-243.
- Often, M. (1985) The Early Proterozoic Karasjok Greenstone Belt, Norway; a preliminary description of lithology, stratigraphy and mineralization. *Norges Geologiske Undersøkelse Bulletin* 403, 75-88.
- Ohmoto, H. (1996) Formation of volcanogenic massive sulphide deposits: the Kuroko perspective. *Ore Geology Reviews* 10, 135-177.
- Olesen, O. & Sandstad, J.S. (1993) Interpretation of the Proterozoic Kautokeino Greenstone Belt, Finnmark, Norway from combined geophysical and geological data. *Norges Geologiske Undersøkelse Bulletin* 425, 41-62.
- Parák, T. (1975) Kiruna iron ores are not “intrusive-magmatic ores of the Kiruna type”. *Economic Geology* 70, 1242-1258.
- Parkhurst, D.L.; Appelo, C.A.J. (2013) Description of Input and Examples for PHREEQC Version 3—A Computer Program for Speciation, Batch-Reaction, One-Dimensional Transport, and Inverse Geochemical Calculations. *U.S.G.S. Chapter 43, Section A Groundwater. Book 6, Modeling Techniques*.
- Pedersen, K.B.; Jensen, P.E.; Sternal, B.; Ottosen, L.M.; Vesterskov Henning, M.; Kudahl, M.M.; Junttila, J.; Skirbekk, K.; Frantzen, M. (2017) Long-term dispersion and availability of metals from submarine mine tailing disposal in a fjord in Arctic Norway. *Environmental Science and Pollution Research* 25(33), 32901-32912.

- Pedersen, K.B.; Reinardy, H.C.; Jensen, P.E.; Ottosen, L.M.; Junttila, J.; Frantzen, M. (2018): The influence of Magnafloc10 on the acidic, alkaline, and electro-dialytic desorption of metals from mine tailings. *Journal of Environmental Management* 224: 130-139.
- Perelló, J.; Clifford, J.A.; Creaser, R.A.; Valencia, V.A. (2015) An example of synorogenic sediment-hosted copper Mineralization: geologic and geochronologic evidence from the Paleoproterozoic Nussir deposit, Finnmark, Arctic Norway. *Economic Geology* 110, 677–689.
- Plante, B; Bussi re, B.; Benzaazoua, M. (2012) Static tests response on 5 Canadian hard rock mine tailings with low net acid-generating potentials. *Journal of Geochemical Exploration* 114: 57-69.
- Ramirez-Llodra, E.; Trannum, H.C.; Evenset, A.; Levin, L.A.; Andersson, M.; Finne, T.E.; Hilario, A.; Flem, B.; Christensen, G.; Schaanning, M.; Varreusel, A. (2015) Submarine and deep-sea mine tailing placement: A review of current practices, environmental issues, natural analogs and knowledge gaps in Norway and internationally. *Marine Pollution Bulletin* 97, 13-35.
- Reinardy, H.C.; Pedersen, K.B.; Nahrgang, J.; Frantzen, M. (2019) Effects of mine tailings exposure on early life stages of Atlantic cod. *Environmental Toxicology and Chemistry* 00, 1-9.
- Reitan, P.H. (1963) The geology of the Komagfjord tectonic window of the Raipas suite, Finnmark, Norway. *Norges Geologiske Unders kelse* 221, 1-71.
- Ripley, E.M.; Lambert, M.W.; Berendsen, P. (1980) Mineralogy and paragenesis of Red-Bed copper mineralization in the Lower Permian of South Central Kansas. *Economic Geology* 75, 722-729.
- Ruan, R.; Zhou, E.; Xingyu, L.; Biao, W.; Guiying, Z.; Jiankang, W. (2010) Comparison on the leaching kinetics of chalcocite and pyrite with or without barteria. *Rare Metals* 29, 552-556.
- Rui, I.J.; Bakke, I. (1975) Stratabound sulphide mineralization in the Kj li area, R ros District, Norwegian Caledonides. *Norsk Geologisk Tidsskrift* 55, 51-75.
- Rzepka, P.; Walder, I.F.; Aagaard, P.; Bo ecki, P.; Rzepa, G. (2014) Sub-sea tailings deposition leach modeling. *Geology, Geophysics and Environment* 40, 123-124.
- Sandstad, J.S.; Viola, G.; Nilsson, L.P. (2007) Reconnaissance structural geological mapping and field XRF-analyses of the Ulveryggen copper deposit, Finnmark, Norway. *Norges Geologiske Unders kelse* Report no.: 2007.064., 16 pp.
- Sandstad, J.S.; Bjerkg rd, T.; Boyd, R.; Ihlen, P.; Korneliussen, A.; Nilsson, L.P.; Often, M.; Eilu, P.; Hallberg, A. (2012) Metallogenic areas in Norway. In: Eilu, P. (ed.) Mineral deposits and metallogeny of Fennoscandia. *Geological Survey of Finland, Special Paper* 53, 35-138.
- Selley, D.; Broughton, D.; Scott, R.; Hitzman, M.; Bull, S.; Large, R.; McGoldrick, P.; Croaker, M.; Pollington, N.; Barra, F. (2005) A new look at the Geology of the Zambian Copperbelt. *Economic Geology 100th Anniversary Volume*, 965-1000.
- Sillitoe, R.H.; Perell , J.; Carc a, A. (2010): Sulfide-bearing veinlets throughout the stratiform mineralization of the Central African Copperbelt: temporal and genetic implications. *Economic Geology* 105, 1361-1368.
- Silva, L.F.O.; Querol, X.; da Boit, K.M.; Fdez-Ortiz de Vallejuelo, S.; Madariaga, J.M. (2011) Brazilian coal mining residues and sulphide oxidation by Fenton's reaction: An accelerated weathering procedure to evaluate possible environmental impact. *Journal of Hazardous Materials* 186, 516-525.
- Simate, G.S.; Ndlovu, S. (2014) Acid mine drainage: challenges and opportunities. *Journal of Environmental Chemical Engineering* 2, 1785-1803.

- Simonsen, A.M.T.; Pedersen, K.B.; Jensen, P.E.; Elberling, B.; Bach, L. Lability of toxic elements in Submarine Tailings Disposal: The relationship between metal fractionation and metal uptake by sandworms (*Alitta virens*). *The Journal of Total Environment* (in press).
- Singer, D.A. (1995) World-class base and precious metal deposits – a quantitative analysis. *Economic Geology* 90, 88-104.
- Starkey, H.C.; Blackmon, P.D.; Hauff, P.L. (1984) The routine mineralogical analysis of clay-bearing samples. *U.S.G.S. Bulletin* 1563, 1–32.
- Steger, H.F. & Desjardins, L.E. (1980): Oxidation of sulfide minerals. V. Galena, sphalerite and chalcocite. *Canadian Mineralogist* 18, 365-372.
- Sternal, B.; Junttila, J.; Skirbekk, K.; Forwick, M.; Carroll, J.; Pedersen, K.B. (2017) The impact of submarine copper mine tailing disposal from the 1970s on Repparfjorden, northern Norway. *Marine Pollution Bulletin* 120, 136-153.
- Stribrny, B. (1985) The conglomerate-hosted Repparfjord copper ore deposit, Finnmark, Norway: Monograph Series on Mineral Deposits 24. Gebrüder Borntraeger, Berlin, Stuttgart, 75 pp.
- Tessier, A.; Campbell, P.G.C.; Bisson, M. (1979) Sequential extraction procedure for the speciation of particulate trace metals. *Analytical Chemistry* 51, 844-851.
- Torgersen, E.; Viola, G.; Sandstad, J.S. (2015a) Revised structure and stratigraphy of the northwestern Repparfjord Tectonic Window, Northern Norway. *Norwegian Journal of Geology* 95, 397-421.
- Torgersen, E.; Viola, G.; Sandstad, J.S.; Stein, H.; Zwingmann, H.; Hannah, J. (2015b): Effects of frictional – viscous oscillations and fluid flow events on the structural and Re-Os pyrite – chalcopyrite systematics of Cu-rich carbonate veins in northern Norway. *Tectonophysics* 659, 70-90.
- Torske, T.; Bergh, S.G. (2004) The Caravari Formation of the Kautokeino Greenstone Belt, Finnmark, North Norway Palaeoproterozoic foreland basin succession. *Norges Geologiske Undersøkelse Bulletin* 442, 5-22.
- Ure, A.M.; Quevauviller, P.; Muntau, H.; Griepink, B. (1993) Speciation of heavy metals in soils and sediments. An account of the improvement and harmonization of extraction techniques undertaken under the auspices of the BCR of the Commission of the European Communities. *International Journal of Environmental Analytical Chemistry* 51, 135-151.
- Viola, G.; Sandstad, J.S.; Nilsson, L.P.; Heincke, B. (2008) Structural and ore geological studies in the northwestern part of the Repparfjord Window, Kvalsund, Finnmark, Norway. *Norges Geologiske Undersøkelse Report no. 2008.029.*, 93 pp.
- Visual Minteq 3.1 <https://vminteq.lwr.kth.se/>
- Wanhainen, C.; Broman, C.; Martinsson, O. (2003) The Aitik Cu-Au-Ag deposit in northern Sweden: a product of high salinity fluids. *Mineralium Deposita* 38, 715-726.
- Ward, P.; Härkönen, I.; Nurmi, P.A.; Pankka, H.S. (1998) Structural studies in the Lapland Greenstone Belt, Northern Finland and their application to gold mineralization. *Geological Survey of Finland, Special Paper* 10, 71-79.
- Yang, S.-H.; Maier, W.D.; Hanski, E.J.; Lappalainen, M.; Santaguids, F.; Määttä, S. (2013) Origin of ultra-nickeliferous olivine in the Kevitsa Ni-Cu-PGE-mineralized intrusion, northern Finland. *Contributions to Mineralogy and Petrology* 166, 81-95.
- Younger, P.L.; Coulton, R.H.; Froggatt, E.C. (2005) The contribution of science to risk-based decision-making: lessons from the development of full-scale treatment measures for acidic mine waters at Wheal Jane, UK. *Science of Total Environment* 338, 137-154.

- Zhang, Y.-G. & Frantz, J.D. (1987) Determination of the homogenization temperatures and densities of supercritical fluids in the system NaCl-KCl-CaCl₂-H₂O using synthetic fluid inclusions. *Chemical Geology* 64, 335-350.
- Ziemkiewicz, P.; Skousen, J.; Lovett R. (1994) Open limestone channels for treating acid mine drainage: A new look at an old idea. *Green Lands* 24(4): 36-41.

Paper 1

Evolution of metal-bearing fluids at the Nussir and Ulveryggen sediment-hosted Cu deposits, Repparfjord Tectonic Window, Northern Norway,

Mun Y., Strmić Palinkaš S., Kullerud K., Nilsen K.S., Neufeld K., Bekker A.

submitted to Norwegian Journal of Geology.

**Evolution of metal-bearing fluids at the Nussir and Ulveryggen sediment-hosted Cu deposits,
Repparfjord Tectonic Window, Northern Norway**

Yulia Mun¹, Sabina Strmić Palinkaš¹, Kåre Kullerud², Kjell S. Nilsen³, Kai Neufeld¹, Andrey Bekker⁴

¹*Department of Geosciences, The Arctic University of Norway, Tromsø, 9037, Norway*

²*Norsk Bergverksmuseum, 3602 Kongsberg, Norway*

³*Kjell Nilsen Geoconsulting, Landingsveien 80, 0767 Oslo, Norway*

⁴*Department of Earth and Planetary Sciences, University of California, Riverside, CA 92521, USA*

E-mail corresponding author (Yulia Mun): Yulia.mun@uit.no

Abstract

The Paleoproterozoic Greenstone Belts of Fennoscandia, such as Kautokeino, Karasjok, and Central Lapland, are metamorphosed and deformed volcano-sedimentary basins with a high base-metal ore potential. The Repparfjord Tectonic Window (RTW) in Northern Norway, an exposed fragment of the Paleoproterozoic greenstone belt, contains several sediment-hosted Cu deposits including Nussir and Ulveryggen. The RTW is composed of mafic metavolcanics (metabasalts, volcanoclastic metabreccia, and metatuffite) intercalated with carbonate-siliciclastic sediments (dolomitic marble, metasandstone, metasilstone, and metapelite). The whole sequence is highly deformed and metamorphosed up to greenschist to lower amphibolite facies.

The Cu-mineralization at the Nussir deposit is hosted by a dolomitic marble. It occurs mostly in the form of quartz-carbonate veins with chalcopyrite, bornite, chalcocite, and covellite as the main ore minerals. Minor amounts of pyrite, galena, sphalerite, as well as Ag and Bi minerals, accompany the Cu mineralization. In contrast, the Ulveryggen mineralization is predominantly disseminated within a metasiliciclastic succession. Chalcopyrite, bornite, chalcocite, covellite, and neodigenite dominate the ore-mineral assemblage. Pyrite, cuprite, tenorite, a wide spectrum of Fe-oxides/oxyhydroxides

(hematite, magnetite, maghemite, and goethite), Ti minerals (ilmenite, anatase, and titanite), as well as wittichenite, renierite, and idaite, are also found in minor amounts.

Mineralogical, geochemical, stable isotope, and fluid inclusion studies carried out at the Nussir and Ulveryggen deposits gave an insight to the evolution of Cu-bearing fluids within the RTW. A wide range in homogenization temperatures (135-350°C at the Nussir deposit and 102-520°C at the Ulveryggen deposit) and fluid inclusion salinities (from 0.35 up to 36 wt.% NaCl equivalents) suggest an evolving system with brines developed by subsurface evaporite dissolution. Alternatively, late orogenic retrograde metamorphic reactions involving rehydration of pre-existing metamorphic assemblages could have developed the salinity approaching that of circulating basinal brines. The fluid inclusion and Cu-sphalerite geothermometry data reveal that the Cu mineralization in the Nussir area was formed within the temperature range between 330 and 340°C at the pressure between 1.1 and 2.7 kbars and that the basin experienced gradual cooling under the constant pressure. High salinity at a relatively high temperature of the ore-bearing fluids implies that Cu was transported predominantly by Cu-chloride complexes. Interaction with carbonate-rich host lithologies is proposed as the main mechanism for Cu mineralization at the Nussir deposit, whereas at the Ulveryggen mineralization was mostly controlled by dilution and cooling when ore-bearing fluids mixed with groundwaters. Locally, reaction of Cu-bearing fluids with sediment-hosted pyrite might also have triggered copper precipitation. Similar ranges of $\delta^{13}\text{C}$ (-0.9 to +2.9‰ V-PDB) and $\delta^{18}\text{O}$ (-18.3 to -15.9‰ V-PDB) values in carbonates from ore-bearing veins and underlying host dolomitic marbles reflect a carbonate rock-buffered system without significant contribution of magmatic or hydrothermal CO_2 .

Keywords Copper mineralization, sediment-hosted mineralization, basin evolution, fluid inclusions, stable isotopes, lithogeochemistry

Introduction

Stratiform Cu deposits contribute with about 23% to the global Cu production (Singer, 1995). The supergiant deposits include Siberian Kodaro-Udokan basin, African Katangan basin and northern Europe Kupferschiefer basin (Hitzman et al., 2010). However smaller scale deposits are also found worldwide, like in Zambian, Zairian, and Kalahari Copperbelts in Africa, Redstone Copperbelt in Canada, and Donchuan and Zongtiaoshan regions in China (Brown, 1971; Ripley et al., 1980; Chartrand and Brown, 1985; Selley et al., 2005; Dewaele et al., 2006; Brems et al., 2009; El Desouky et al., 2009; Sillitoe et al., 2010; Jiang et al., 2014). It is widely accepted that the stratiform Cu deposits are formed during the large-scale circulation of basinal fluids, derived from high mountains formed during rifting or continental collision, capable to transport base metals to the precipitation site due to their moderate to high salinities and high oxidation potential, and presence of mafic volcanic or intrusive rocks that provide base-metals while leached with these fluids (e.g., Hitzman et al., 2005, 2010). The stratiform Cu deposits are usually associated with sediments indicating extreme aridity and continentality such as red beds and evaporites that are laterally and stratigraphically bordered by organic-rich and pyrite-bearing shales (e.g., Gablina & Malinovskii, 2008). The oldest stratiform Cu deposits formed at the very early stage of the Great Oxidation Event (GOE; Bekker, 2013), in the early Paleoproterozoic, on several cratons (Kirkham, 1989). While sedimentary successions of the early Paleoproterozoic age, bracketing the rise of atmospheric oxygen, are extensively developed on the Fennoscandian Shield and contain redbeds as well as sulfate and halite evaporites (e.g., Melezhik et al., 2013), Cu stratiform deposits were not well characterized from these successions.

The Nussir and Ulveryggen sediment-hosted Cu deposits are located within the Repparfjord Tectonic Window (RTW), one of several exposures of the Paleoproterozoic Greenstone Belts within the Norwegian Caledonides in Northern Norway (Fig. 1; Viola et al., 2008; Torgersen et al., 2015b). In general, the Paleoproterozoic Greenstone Belts in Northern Norway are composed of a classic succession with mafic metavolcanics (metamorphosed pillow lavas, volcanoclastic breccia, and tuffite)

at the base succeeded by carbonate-siliciclastic deposits (dolomitic marble, metasandstone, metasilstone, and metapelite) (Torske & Bergh, 2004). These greenstone belt successions record episodic deposition over several hundred million years that corresponds to different stages in basin evolution (Nordgulen & Andresen, 2008). Later, in the Svecofennian time (1.92-1.75 Ga; Pharaoh et al., 1990), the whole Fennoscandian Shield was subjected to compression during the assembly of the Nuna or Columbia supercontinent, resulting in the regional greenschist facies and locally amphibolite and granulite facies of metamorphism, e.g., near the Lapland-Kola and Svecofennian orogens (Bogdanova et al., 2015, 2016).

Mining activities at the Ulveryggen deposit lasted between 1972 and 1978/1979, while the Nussir deposit was discovered in late 1970's and has not been in the exploitation yet. Indicated resources of Cu at the Ulveryggen deposit are 3.7 million tons at 0.8 wt.% Cu, and the Nussir area contains 5.8 million tons at 1.15 wt.% Cu with Au and Ag as by-products (Nussir ASA, 2019).

Despite the protracted exploration history at the RTW, the nature of ore-bearing fluids, the source of metals, and the evolution of the basin remain poorly constrained. Fabricius (1979) discussed three possible models for the genesis of the Ulveryggen mineralization: 1) hydrothermal with gabbroic rocks being a possible source for metals; 2) diagenetic with detrital Cu-bearing sulfide minerals in associated siliciclastic units releasing metals; and 3) diagenetic associated with ilmenite to rutile transformation with chalcopyrite formed as a side product ($\text{FeTiO}_3 + \text{Cu}^{2+} + 2\text{H}_2\text{S} = \text{TiO}_2 + \text{CuFeS}_2 + \text{H}_2\text{O} + 2\text{H}^+$). Stribrny (1985) suggested that the Repparfjord Copper Deposit (former name of the Ulveryggen deposit) is a marine placer deposit with a diagenetic overprint. Subsequently, Sandstad et al. (2007) inferred structural control on the Ulveryggen mineralization, but also reported ore minerals with features consistent with both diagenetic and epigenetic modes of development. Viola et al. (2008) further reported strong structural control on Cu mineralization hosted in mesothermal veins in the RTW along the NE-SW dextral ductile shear corridor. Perelló et al. (2015) obtained Re-Os date for molybdenite syngenetic with Cu-bearing mineralization at ca. 1765 Ma, which they interpreted to indicate

syntectonic origin for the mineralization. In contrast, Torgersen et al. (2015a) argued for progressive development of ore mineralization under rapidly evolving extensional and compressional regimes in the basin and related the ca. 1765 Ma Re-Os molybdenite date obtained by Perelló et al. (2015) to regional metamorphism and remobilization event. Torgersen et al. (2015a) also inferred a multi-stage evolution of the mineralization system and favoured the early diagenetic origin with the first emplacement of mineralized veins at ca. 2069 ± 14 Ma (Re-Os date on sulphides from the Porsa and Bratthammer mesothermal Cu veins associated with tholeiitic metabasalts of the Nussir Group; Torgersen et al., 2015b) and subsequent syntectonic ore remobilization.

The main focus of this study is to constrain the origin and the nature of Cu-bearing fluids that circulated in the RTW during the early Proterozoic. The study presents new petrographic and lithogeochemical data for mineralized and barren host rocks, mineral chemistry of ore minerals, petrography and microthermometry of fluid inclusions entrapped by quartz in ore-bearing veins as well as carbon and oxygen isotope compositions of carbonates from mineralized veins and host metadolostones.

Geological setting

The RTW is a part of the ca. 2.1 Ga greenstone belt (Torgersen et al., 2015a) that represents a basement culmination of the Paleoproterozoic metasedimentary rocks of the Raipas Supergroup within the Kalak Nappe Complex of the Caledonian Middle Allochthon (Fig. 1; Corfu et al., 2007; Kirkland et al., 2006; Pharaoh et al., 1983; Reitan, 1963; Viola et al., 2008). The sequence is broadly correlative with those in the Kautokeino and Karasjok greenstone belts (Pharaoh et al., 1983; Siedliecka et al., 1985). The Paleoproterozoic Raipas Supergroup of the RTW was subjected to compression in SE-NW direction during the Svecofennian Orogeny at ca. 1840 Ma (Pharaoh et al., 1982), which resulted in the regional metamorphism of greenschist to lower amphibolite facies. During the Silurian stage of the Caledonian orogeny (425–400 Ma ago), the Norwegian Caledonides were thrust over the western margin of the Fennoscandian Shield in southeastern to eastern direction (Corfu et al., 2007; Gee et al., 2008). U-Pb

zircon dating of mafic tuffites from the Krokvatnet Formation of the Nussir Group yielded 2.1-2.06 Ga ages (Perelló et al., 2015).

The stratigraphy of the Raipas Supergroup of the RTW has been described by numerous authors (e.g. Reitan, 1963; Pharaoh et al., 1982; Pharaoh & Pearce, 1984; Pharaoh et al., 1983; Viola et al., 2008; Mun, 2013) and recently revised by Torgersen et al. (2015a) (Fig. 1). Four lithological sequences, from the oldest to the youngest are: (1) the Saltvannet Group, a volcano-sedimentary sequence outcropping in the hinge of the Ulveryggen anticline (Fig. 1); the subaerial metavolcanic rocks of (2) the Holmvatnet and (3) the Nussir groups, represented by tholeiitic, metabasaltic lavas and metatuffs outcropping on the southeastern and northwestern limbs of the Ulveryggen anticline, respectively; (4) the Porsa Group including the Vargsund, Kvalsund, and Bierajávri formations (Fig. 1) composed of carbonate-rich rocks, with locally developed stromatolites, quartz metasandstones, metatuffs, schists, and slates, thrust in SE direction along the Kvenklubben Fault upon the Nussir Group sediments at the northwestern edge of the RTW (Torgersen & Viola, 2014; Torgersen et al., 2014). In some places, the basal polymictic metaconglomerate indicates erosion of the Nussir Group prior to deposition of the Porsa Group sediments (Pharaoh et al., 1983; Torgersen et al., 2015a). The Saltvannet Group has been of the major economic interest in the RTW where it hosts Cu-deposits of Ulveryggen and Nussir (Fig. 1). The group can be further subdivided to four formations (listed from the oldest to the youngest): the Ulveryggen, Djupelv, Stangvatnet, and Gorahatjohka formations (Fig. 1; Torgersen, 2015a).

The Ulveryggen deposit is predominantly hosted by coarse-grained, braided fluvial arkosic metasandstones of the Ulveryggen Formation. The Ulveryggen Formation is overlain by metaconglomerates of the Dypelva and Stangvatnet formations. The metaconglomerate changes stratigraphically upward from green-coloured, containing pebbles of metabasalt and metatuffite with rare pebbles of jasper, quartzite, and dolostone, towards a purple polymictic metaconglomerate with dacite clasts (Pharaoh et al., 1983; Torgersen et al., 2015a). The Gorahatjohka Formation that was

previously described as a part of the Stangvatnet Formation (Pharaoh et al., 1983; Viola et al., 2008) hosts the Nussir Cu deposit and it is composed of volcanoclastic metasilstones and dolomitic marble (Torgersen et al., 2015a).

In the central to southern part of the RTW, the supracrustal rocks are intruded by numerous ultramafic to mafic intrusions of the Svecofennian age. The Rødfjellet (Raudfjellet) Suite of gabbro-peridotite-pyroxenite-norite composition forms sheets or podiform intrusions (Reitan, 1963; Pharaoh et al., 1983; Pharaoh, 1985; Jensen, 1996; Viola et al., 2008), and the Kvitfjell Suite consists of tonalites and trondhjemites in the SW part of the RTW. All intrusive rocks were subjected to low-grade metamorphism similar to that of their host rocks. The lithologies are crosscut by a number of tectonic dislocations such as the Kvenklubben Fault in the NW, the Skifergangen shear zone, the Porsavannet Fault, and the Markopp Fault as well as thrusts with top-to-the-SE transport direction that are common in the region (Torgersen et al., 2015a). They are located beyond Figure 1.

Sediment-hosted Cu mineralization

Nussir deposit

The Cu mineralization at the Nussir deposit is mostly hosted by a dolomitic marble horizon that is intercalated with metapelites in the lowermost part of the Gorahatjohka Formation (Figs. 1, 2 & 3). The dolomitic marble of the Gorahatjohka Formation is subdivided by Torgersen et al. (2015a) into three members of which the lower and middle are mineralized. Their thickness does not exceed 5 m and they can be followed for several kms from NE to W (Fig. 1). The dolomitic marble of the Gorahatjohka Formation is underlain by metaconglomerates of the Stangvatnet Formation. Within the dolomitic interval, greenish to light-grey dolomitic marble layers intercalate with 2 to 5 cm thick beds of metapelites, metadolobrecias, metasandstones, and metaconglomerates. The green colour of the host rocks is related to the ubiquitously developed chlorite, muscovite, and sericite. The Cu mineralization predominantly occurs at the depth of about 210 m. The mineralized horizon is approximately 3 m thick in the NS-DD-08-006 drill core. Cu-mineralization in dolomitic marble,

metasandstone, and metasiltstone forms irregular masses and fine-grained aggregates within thin carbonate and quartz veinlets as well as it occurs in disseminated form (Fig. 4, Sandstad, 2010; Perelló et al., 2015; Torgersen et al., 2015a).

Locally the mineralization extends to the overlying metavolcanic rocks of the Holmvatnet and Nussir groups (Figs. 1, 2 & 3; Torgersen et al., 2015a). The Cu-mineralization within metavolcanic rocks is associated with extensive carbonatization and chloritization (Figs. 2 & 3). The mineralization is hosted by quartz-carbonate veinlets and forms interstitial grains between the fragments of the rocks. Small, nest-shaped accumulations and rare disseminations have been found in the overlying metatuffs and intercalated metasandstones (Fig. 3).

The ore mineralization (Fig. 2) consists of chalcopyrite, bornite, chalcocite, and covellite intergrown with pyrite, galena, sphalerite, and Ag and Bi minerals (e.g., Sandstad, 2010; Mun, 2013, Perelló et al., 2015). In metatuffites, chalcopyrite and pyrite dominate, while carbonates contain mostly bornite, chalcocite, and, to lesser extent, chalcopyrite. Cinnabar (Hg), native Au, electrum (Au, Ag), amalgam (Ag), Au-Ag-tellurides, sperrylite (PtAs_2), bohdanowiczite (AgBiSe_2), naumannite (Ag_2Se), native Bi, and wittichinite (Cu_3BiS_3) are found in association with the Cu mineralization (Sandstad, 2010). Figure 2 schematically shows modal distribution of ore minerals at the Nussir ore field.

Ulveryggen deposit

Cu mineralization at the Ulveryggen deposit is hosted by the metasedimentary complex comprised of fine-grained, polymictic reddish arkosic to quartz metasandstone, conglomeratic metasandstone, metasiltstone containing grains of quartz, feldspar, chlorite, muscovite, biotite, and epidote (Stribrny, 1985). The mineralization is disseminated and, to a lesser extent, occurs in veins and veinlets controlled by tectonic structures (Sandstad et al., 2007; Perelló et al., 2015). The disseminated mineralization is also controlled by the sediment grain size and sorting within the host sedimentary lithology. The underlying, coarse conglomeratic layers are characterized by higher Cu grade, although the grade distribution is rather heterogeneous within the host rocks (Stribrny, 1985). Fine-grained, irregularly

shaped aggregates are smaller in size than in the Nussir deposit and mostly range from 0.5 to 2 cm in size (Fig. 4).

The Cu mineralogy is similar to that observed in the Nussir area. It consists of chalcopyrite, bornite, chalcocite, and neodigenite in an association with pyrite and covellite. Cuprite and tenorite have been observed as well (Stribrny, 1985). A wide spectrum of Fe (hematite, magnetite, maghemite, goethite, and turgite) and Ti minerals (ilmenite, anatase, and titanite) as well as wittichenite, renierite, and idaite have been found in minor quantities (Stribrny, 1985).

Samples and methods

Samples were collected from 9 drill cores from the Nussir deposit (Fig. 1, Supplementary Table 1) and 5 drill cores from the Ulveryggen deposit. The sampled drill cores from the Ulveryggen deposit are located close to the tunnel shown on Fig. 1. Samples were collected from 1) barren host rocks (i.e., volcanic and sedimentary rocks), and 2) Cu-mineralized rocks including hydrothermal veins. The drill core NS-DD-08-006 from the Nussir deposit was sampled in detail in order to get a deeper insight into the stratigraphic section.

Whole-rock geochemical (lithochemical) analyses were performed at Activation Laboratories (Actlabs, Canada). Lithium metaborate/tetraborate fusion was used as a dissolution method to ensure total acid dissolution of minerals such as zircon, monazite, and xenotime prior to analyses using ICP and ICP-MS to determine major and trace element contents. Replicate analyses of samples and certified reference materials were used to assure the precision and accuracy of data. Repeated analysis of standards reproduced certified values within 1% accuracy for major elements and 20 ppm for trace elements. The mean precision of analyses is within 1% for major elements and within 30 ppm for trace elements.

Chemical analyses of individual ore minerals were performed using a Cameca SX 100 electron microprobe at the Department of Geosciences at the University of Oslo; a Jeol YXA 8800R Superprobe

at the Institute of Geology and Geophysics of the Republic of Uzbekistan; a Zeiss Merlincompact VP field emission scanning electron microscope (SEM) equipped with Energy-dispersive X-ray spectrometer (EDS) and wavelength-dispersive spectrometer (WDS) at UiT The Arctic University of Norway; and a NovaNanoSEM 450 at the University of California, Riverside. The analyses performed with the Cameca SX 100 were carried out at 15 kV accelerating voltage, 15 nA beam current, focused beam, and 10 s counting time on a peak. Standardization was made on synthetic minerals (As: gallium arsenide), metals (Fe, Co, Cu, Ni, Ag, and Au), and on natural minerals (Zn: sphalerite, Pb: galena). Mostly the optical system was used, and backscattered images were obtained for recognition. The analyses obtained with the Jeol Superprobe were carried out at 20 kV accelerating voltage, under both high and low vacuum regimes. The NovaNanoSEM 450 was set in a high vacuum regime at 20 kV accelerating voltage, 10 s counting time, and with an aperture of 60 μm . The Zeiss Merlin SEM field emission microscope was run in a high vacuum regime at 20 kV accelerating voltage, 20 s counting time, and with an aperture of 60 μm .

Carbon and oxygen isotope analyses of carbonates were performed at UiT The Arctic University of Norway and at the SIFIR laboratory of the Department of Geological Sciences, University of Manitoba, Canada. At UiT, 50 - 150 μg of microdrilled carbonate powder was loaded into sealed reaction vessels, then flushed with helium gas and reacted at 50°C with phosphoric acid, during >2h. The evolved carbon dioxide was sampled using a Thermo Fisher Gasbench II and isotope ratios were measured in a continuous flow mode using a Thermo Fisher MAT253 isotope-ratio mass-spectrometer. The stable isotope ratios of carbon and oxygen are reported in the delta (δ) notation as per mil (‰) deviation relative to the Vienna Pee Dee Belemnite (V-PDB). The analytical reproducibility was better than $\pm 0.1\%$ for $\delta^{13}\text{C}$ and $\delta^{18}\text{O}$. The UiT mass-spec laboratory used three in-house calibration standards calibrated with international NBS18, NBS19, and LSVEC standards. Quality control was performed by the replicate runs of the reference samples.

At the SIFIR laboratory, carbonates were microdrilled with diamond drill bits 1 mm in diameter, from the least altered (i.e., lacking veins, discolouration, weathering rinds, and silicification) and finest-grained portions of polished thick sections; slabs were subsequently stained to determine carbonate mineralogy. Carbonate powders were reacted at 70°C with anhydrous phosphoric acid using a GasBench II carbonate device and delivered in a stream of high-purity He to a Thermo Fisher Delta V Plus isotope ratio mass spectrometer via an open-split interface (ConFlo IV, Thermo Fisher). All C and O isotope ratios are reported in delta notation relative to international standards on the Vienna Pee Dee Belemnite (V-PDB) scale. Calibration was performed by analysing two international calcite standards (NBS-18 and NBS-19) at the beginning, middle, and end of each run. A calibration line was calculated by least squares linear regression using the known and measured isotope values of the calibration standards. To check the quality of analysis performance, one calibrated internal calcite standard (CHI, $\delta^{13}\text{C} = -8.01\text{‰}$ V-PDB and $\delta^{18}\text{O} = -11.67\text{‰}$ V-PDB) and one calibrated internal dolomite standard (Tytyri, $\delta^{13}\text{C} = +0.78\text{‰}$ V-PDB and $\delta^{18}\text{O} = -7.07\text{‰}$ V-PDB) were analysed together with unknown samples. Replicate analyses of internal standards yielded the results of $\delta^{13}\text{C} = -7.98 \pm 0.08\text{‰}$ and $\delta^{18}\text{O} = -11.63 \pm 0.14\text{‰}$ (n=23) for CHI, and $\delta^{13}\text{C} = +0.74 \pm 0.09\text{‰}$ and $\delta^{18}\text{O} = -6.02 \pm 0.15\text{‰}$ (n=17) for Tytyri. Correction using the known oxygen isotope value for the Tytyri dolomite standard was performed for $\delta^{18}\text{O}$ values of dolomite samples.

Petrographic and microthermometric studies of fluid inclusions were performed at UiT. Double-polished, 0.1 to 0.3 mm-thick, quartz wafers were prepared. Measurements were carried out on Linkam THMS 600 stage mounted on an Olympus BX 2 microscope using 10× and 50× Olympus long-working distance objectives. Two synthetic fluid inclusion standards (SYN FLINC; pure H₂O and mixed H₂O-CO₂) were used to calibrate the equipment. The precision of the system was $\pm 2.0^\circ\text{C}$ for homogenization temperatures, and $\pm 0.2^\circ\text{C}$ in the temperature range between -60° and $+10^\circ\text{C}$. Apparent salinity of two-phase inclusions was calculated from final ice melting temperatures. The salinity of three-phase (L+V+S) inclusions was calculated from halite melting temperatures. In both cases the equation of Bodnar (1993) was applied. The computer package FLUIDS (Bakker, 2003; Bakker

& Brown, 2003) was used to calculate fluid properties, including the bulk density. The fluid inclusion bulk density and isochores were calculated according to the equation of state published by Zhang & Frantz (1987).

After measuring microthermometric parameters of about eighty fluid inclusions from Nussir samples NS-51 (a-k), NS-52 (a-c), and NS-53 (eutectic temperature, last melting temperature of ice and/or hydrohalite, and total homogenization temperature), the fluid inclusions were decrepitated by quick heating of the samples (100°C per min) up to 600°C and by keeping the samples at this temperature for 30 minutes, following the procedure described by Kontak (2004). The samples were subsequently inspected under reflected light for the presence of evaporate mounds and then placed on carbon tape for analysis on SEM using EDS detector at UiT The Arctic University of Norway.

Results

Petrography of the host rock

Nussir deposit

The petrographic description given here for the Nussir deposit sedimentary-volcanogenic sequence is based on samples from the depth interval 65.64-234.69 m of the drill core NS-DD-08-006 (Fig. 1), which is shown in Fig. 3. The lower part of the sequence is composed of carbonate-siliciclastic strata, whereas the uppermost part represents thick strata of altered mafic metavolcanics. The carbonate-siliclastic package consists of interlayered metasandstone, marble, dolomitic marble, and metasiltstone with few layers of metaconglomerate. The sequence is cut by a shear zone (Fig. 3).

The fragments are composed of quartz and sericitized feldspar. Quartz fragments vary in size from 0.1 to 0.6 mm, are often rounded, but there are also anhedral varieties. Feldspar fragments are euhedral, up to 1.2 mm in size. The fragments are cemented by chlorite and muscovite. Beds of pelitic schist, quartz semischist, metasiltstone, and metabreccia alternate from 225 to 214 m depth. This sequence

is overlain by dolomitic marble interlayered with metapelite, which represents the typical Nussir deposit ore-bearing dolomitic marble (Fig. 3).

Mafic metavolcanics, predominantly metatuffites, dominate the upper, almost 150 m thick, part of the section starting from a depth of approximately 210 m. In the lower part, the rocks are intensely carbonatized and chloritized and the chlorite content decreases towards the top. The metatuffite is composed of quartz, plagioclase, and biotite grains in a fine-grained matrix. Quartz is represented mostly by anhedral grains, smaller than 0.05 mm in size. Biotite has a tabular shape, often replaced by chlorite, and varies from 0.1 to 1 mm in size. Feldspar has also a tabular shape, and is often sericitized (Figs. 5B, C). At a depth of about 81 m, metatuffite is strongly carbonatized and mineralized (uppermost horizon marked as highly carbonatized volcanic rocks (HCVR on Fig. 3). The mafic metavolcanics are also crosscut by quartz-carbonate veins, but they are less abundant than in the underlying carbonate-siliciclastic section.

Between 229.64 and 231.90 m depth, a shear zone characterised by intensely crushed, chloritized, and schistose rocks developed. The whole sequence is crosscut by quartz-carbonate veins and veinlets (Figs. 5C-F). The width of veins varies from mms to cms across. Carbonate in veins is mainly dolomite with either deformed and stretched grains (Fig. 5D), up to 5 mm in size, or euhedral to subhedral crystals ranging in size from 0.1 to 0.3 mm. Fig. 5D shows the early generation of carbonate veins. Fig. 5E, F shows the late generation of carbonate veins. Carbonate grains in the late generation veins are not deformed and considerably smaller in size. Several samples have folded veins (Fig. 5E).

The rocks from the uppermost (28.45-28.92 m) part of the drill core NUS-DD-06-007 were also petrographically examined. Deformation structures such as crenulation cleavage in mica-rich layers, sigmoidally shaped aggregates of quartz and carbonate as well as elongated and recrystallized quartz grains in the veinlets suggest that the rock experienced compression after its formation (Fig. 5E). Veins having deformed and undeformed carbonate grains indicate at least two generations of carbonate

veins and that the last generation of carbonate in veins formed after compressional deformation subsequent to extension (Figs. 5D, F).

The DD-14-001, DD-13-012, DD-13-020, DD-90-002, NUS-DD-11-004, and NUS-06-005 drill cores were also sampled (Fig. 1). Samples for analyses were selected from intervals with high Cu-sulphide content. The samples have similar lithologies to those observed in the drill core NS-DD-08-006 and most likely correspond to the typical Nussir deposit mineralized layer containing intercalations of thin layers of metasandstones, dolomitic marble, metasiltsstones, and metapelites.

Abundant chlorite and actinolite, as well as sericitization of K-feldspar and plagioclase indicate that the rocks have undergone greenschist facies metamorphism and hydrothermal alteration (Fig. 5B, C).

Ulveryggen deposit

In contrast to the Nussir deposit, which is stratigraphically higher than Ulveryggen deposit, the host rocks at the Ulveryggen deposit are represented by massive arkosic metasandstone interlayered with metaconglomerate (Fig. 5G, H). The main components are quartz, feldspars, and muscovite, which formed along grain boundaries. The size of the quartz grains ranges from < 0.03 mm up to ~ 0.2 mm in diameter. The mineralization is predominantly disseminated, filling space between plagioclase and quartz grains. Rare quartz veinlets, up to 1 cm in length, with aggregates of recrystallized quartz and carbonate grains were also observed. Quartz crystals within the veinlets do not exceed 20 µm in diameter (Fig. 5H).

Lithogeochemistry

The whole-rock geochemical (lithogeochemical) composition of the studied rocks is shown in Tables 1-3. Samples chosen for the whole-rock geochemical analyses were collected from Cu-mineralized zones; parts of the drill cores with visible quartz-carbonate veins were avoided. Volcanic rocks were subdivided into mineralized and non-mineralized taking about 75 ppm of Cu as an average content for mafic rocks (Engel et al., 1965; Doe, 1994). Major elements in non-mineralized and mineralized volcanics show slight difference in abundance. The CaO content is slightly higher in Cu-mineralized

metavolcanics with the mean value of 6.49 wt.% compared to 4.95 wt.% for non-mineralized samples (Table 1). The Na₂O content is also higher in mineralized volcanic rocks (4.23 ± 1.36 wt.%) than in non-mineralized volcanics (2.61 ± 1.47 wt.%). In contrast, the K₂O content shows lower values in mineralized volcanic rocks (0.78 ± 0.44 wt.%) than in non-mineralized volcanic rocks (1.67 ± 0.23 wt.%). The SiO₂ contents in non-mineralized and mineralized volcanic rocks are similar (50.31 ± 6.82 and 49.08 ± 4.76 wt.%, respectively).

In contrast, trace element contents in mineralized and non-mineralized volcanic rocks (Table 1) show significant variations. The Cu content ranges from background level reported for mafic volcanics (Engel et al., 1965; Doe, 1994) in non-mineralized rocks up to about 8600 ppm in mineralized volcanics. Zinc and Ni show slightly elevated concentrations relative to the average mafic volcanic rock (Gale et al., 2013), but without significant difference between non-mineralized and mineralized rocks. Zinc varies from less than 30 ppm up to 200 ppm in non-mineralized rocks; mineralized rocks contain 30 to 210 ppm of Zn. The Ni content is higher, up to 700 ppm, in rocks with lower Cu content, while in Cu-rich volcanic rocks the maximum content of Ni is 280 ppm.

Major element contents in carbonate-siliciclastic rocks from the Nussir deposit, represented predominantly by intercalation of dolomitic marbles with metapelites, metasilstones, and metasandstones, show a wide range (Table 2). The CaO content varies from 0.75 to 35.48 wt.%, while Na₂O content from 0.01 to 3.26 wt.%. Significant variation is also present in K₂O and MgO contents; from 0.02 up to 6.70 wt.% and from 0.38 to 12.89 wt.%, respectively.

The whole-rock chemical analyses of the mineralized rocks, predominantly arkosic metasandstones, from the Ulveryggen deposit are listed in Table 3. They contain 77.96 ± 2.74 wt.% SiO₂, 1.45 ± 0.57 wt.% MgO, 2.51 ± 0.73 wt.% Na₂O, and 0.13 ± 0.07 wt.% CaO. The average content of Cu, Zn, and Co is 7045 ± 2643.4 ppm, 25 ± 20 ppm, and 11.63 ± 3.53 ppm, respectively.

Ore mineralogy and mineral chemistry

Nussir deposit

A range of ore minerals has been observed in the studied samples from the Nussir deposit. Copper minerals include chalcopyrite, bornite, digenite, chalcocite, and covellite. In addition, pyrite, sphalerite, galena, clausthalite, molybdenite, gersdorffite, argentite, stromeyerite, chlorargyrite, amalgam, cobaltite, hessite, and native Bi were found (Fig. 6A-I).

The studied drill core (NS-DD-08-006; Fig. 3) shows a gradual change with depth in distribution of copper and associated ore minerals. In the upper part of the drill hole, chalcopyrite is the dominant ore mineral together with pyrite, iron oxides, and galena, whereas bornite and chalcocite are more abundant in the lower part.

Chalcopyrite occurs throughout the mineralized sequence and appears predominantly in quartz-carbonate veinlets. It is noted, however, that in the upper part of the drill core, chalcopyrite is present as a pure mineral nearly without inclusions. In the lower part, bornite dominates and chalcopyrite occurs in minor amounts, usually as a secondary mineral. From 230 to 730 m depth, chalcopyrite is also intergrown with bornite (Fig. 6 a) as well as with pyrite (Fig. 6H). Sphalerite inclusions in chalcopyrite (Fig. 6I) appear at relatively shallow (33 m) depth. Chalcopyrite also occurs together with galena (Fig. 6A) and cobaltite (Fig. 6E). Spot EDS chemical analyses of chalcopyrite are given in Table 4. Chalcopyrite contains trace amounts of Zn (0.05 - 0.12 wt.%), As (0.01 - 0.04 wt.%), Ag (0.03 - 0.05 wt.%), and Au (0.09 wt.%).

Bornite contains trace amounts of Ni, Zn, As, Se, Mo, Ag, Au, Te, and Hg (Table 4). Locally, bornite contains silver with concentrations reaching up to 3.70 wt.% (for example in sample NS-4).

In the studied section (drill core NS-DD-0608-006; Fig. 4), bornite appears below 198.0 m depth. It is nearly always altered and partly replaced by chalcopyrite, chalcocite (Figs. 6B, D, F), digenite, and/or covellite. Inclusions of galena and clausthalite as well as of native Bi (Figs. 6A-D, F) have been observed within bornite.

Digenite, chalcocite, and covellite are usually observed as secondary minerals. Chalcocite is often intergrown with bornite (Figs. 6B-D, F). Both chalcocite and covellite have a minor As content (Table 4). Chalcocite also contains trace amounts of Co, Se, Mo, and Hg. Trace amounts of Ag have been found in chalcocite, digenite, and covellite (Table 4). Chalcocite was identified in the lower part of the drill core NUS-DD-08-006 at depths below 203 m. Covellite occurs as a secondary copper mineral replacing chalcopyrite, bornite, and chalcocite.

Pyrite (Fig. 6H) has been observed throughout the studied samples. The mineral is distributed both in the matrix as single grains, but it is also intergrown with chalcopyrite when the last forms around the rim of pyrite. Pyrite contains trace amounts of Ag and Au (Table 4). Sphalerite (Figs. 6B, I) is paragenetically linked with chalcocite and chalcopyrite. Sphalerite ranges in grain size from 25 to 50 μm and contains 0.6 to 0.77 wt.% Cu and 0.71 to 1.18 wt.% Cd (Table 4).

Galena forms inclusions within bornite, chalcocite (Figs. 6A, B), and chalcopyrite and shows trace concentrations of Ag, Au, Te, Co, and Ni (Table 4). The grain size is often too small (2-6 μm in diameter) to avoid interference of adjacent copper minerals during analysis, which explains high trace contents of Fe and Cu for galena crystals. Clausthalite was found in microinclusions within chalcocite and bornite (Figs. 6B, C, G). Clausthalite grains do not exceed 1 μm in diameter, and it was not possible to avoid interference of adjacent minerals during analysis.

Cobaltite grains, up to 10 μm in diameter, occur together with chalcopyrite (Fig. 6E). Cobaltite contains trace amounts of Ni, Se, Mo, Ag, Hg, and Bi (Table 4).

Silver compounds with Cl (chlorargyrite), Cu (stromeyerite), Bi (possibly matildite), and argentite, together with clausthalite and native bismuth (Bi), were predominantly found at shallow depths (29 to 150 m) (Figs. 6B-D, F, H), while hessite was found below 360 m depth (Fig. 6G). Silver has been observed in its native form (amalgam) with up to 13 wt.% Hg, as argentite, chlorargyrite, stromeyerite, and hessite (Table 4). Silver minerals occur as small inclusions, 2 to 20 μm in diameter, in grains of bornite,

chalcocite, and chalcopyrite. Chemical analyses of silver minerals are given in Table 4. Other minerals that have rarely been observed include gersdorffite and molybdenite (Table 4).

Ulveryggen deposit

Samples from the Ulveryggen deposit show ore mineralogy similar to that of the samples from the Nussir deposit (Figs. 6J-L). Ore minerals from the Ulveryggen deposit include bornite, chalcopyrite, chalcocite, covellite, hessite, amalgam, iron oxide, and an unidentified CuBiS phase. The distribution of ore minerals does not show any zonation and minerals fill the space between quartz and feldspar grains.

Bornite and chalcocite are more abundant than chalcopyrite. Bornite replaces chalcopyrite (Fig. 6J) and chalcocite forms vermicular intergrowths with bornite (Figs. 6K, L). Bornite also contains inclusions of hessite (Fig. 6L). Chalcocite contains inclusions of native Bi (Fig. 6K). Chalcopyrite, bornite, chalcocite, pyrite, and galena contains trace amounts of Au and Ag. Chemical analyses of selected ore minerals from the Ulveryggen deposit are given in Table 4.

Fluid inclusion study

In total, about 80 fluid inclusions (FIs) hosted by vein (Fig. 7A-D; 8) and host-rock quartz from the Nussir and Ulveryggen deposits, respectively, were analyzed. The Ulveryggen deposit host-rock quartz contains fluid inclusions that are hard to recognize and work with. Consequently, the most of fluid inclusion data were collected from the mineralized intervals within metatuffite (Fig. 7A) and metasiltstone (Fig. 7B) at the Nussir deposit. Multiple generations of fluid inclusions have been recognized in quartz veins hosted by both lithologies. The studied inclusions have been described as primary or secondary in their origin, applying the diagnostic criteria proposed by Roedder (1984). Primary inclusions show very diverse phase relations at room temperature. According to a number of phases present at room temperature, fluid inclusions have been classified into the following types: Type 1: liquid-rich two-phase (L+V) inclusions; Type 2: polyphase (L+V+S) inclusions; Type 3: two-phase

(L+S) inclusions; Type 4: liquid-only (L) inclusions; and Type 5: vapour-only (V) inclusions (Figs. 7E-H), where L, V and S stand for liquid, vapour and solid phase, respectively.

The great majority of fluid inclusions have sizes less than 10 μm across and show irregular to subrounded shapes. At room temperature, the vapour bubble occupies about 25% of the volume in fluid inclusions of types 1 and 2. The solid phase (daughter crystal) is transparent, isotropic, and usually occupies about 20 to 25% of the volume in the type 2 fluid inclusions. In the type 3 fluid inclusions, the daughter crystal occupies up to 30% of the volume.

The type 1 inclusions are present in quartz from both the Nussir and Ulveryggen deposits. At the Nussir deposit, they are characterized by a wide range of homogenization temperatures (168-430°C) and a low salinity (0.4-3.2 wt.% NaCl equiv.). The Ulveryggen deposit type 1 FIs have even wider range of homogenization temperatures (102-550°C) and a higher salinity (13.9 wt.% NaCl equiv.). The type 2 FIs prevail over all other types of inclusions. They are further subdivided into three groups according to their homogenization mode: FIs of the group 2a homogenize with vapour disappearing as the last phase; FIs of the group 2b homogenize with salt disappearing as the last phase; and the FIs of the group 2c have both vapour and salt disappear at the same temperature. FIs from the 2a group are homogenized at 247-350°C; their salinity varies from 30 to 36 wt.% NaCl equiv. The 2b group FIs are homogenized at the temperature between 200 and 270°C and have the salinity ranging from 31 to 36 wt.% NaCl equiv.

The type 3 FIs are found in the Nussir deposit quartz. The ultimate halite melting temperature ranges from 220 to 260°C indicating the salinity between 32 and 35 wt.% NaCl equiv. The type 4 and 5 FIs occur as isolated FI sets and they do not show evidence for boiling during entrapment. Both of these types of FIs do not show evidence for phase transition during the microthermometry experiments.

Secondary inclusions are of types 1 and 2a (Fig. 7E). They are found along the cracks in the vein quartz. Secondary FIs have rounded and subrounded shapes and are about 1-3 μm in size. Vapour bubble occupies about 25% of the type 1 fluid inclusions at room temperature. For the type 2, the vapour

bubble occupies around 10% of the inclusion and the solid phase occupies around 10-15% of the inclusion. The homogenization temperature of type 1 secondary FIs varies from 150 to 220°C. The type 2a secondary FIs homogenize at 200-220°C. The salinity for these FIs is hard to measure due to their small size. For the fluid inclusions in quartz from the Ulveryggen deposit, only a limited amount of data was collected due to the absence of sufficiently large transparent crystals associated with the mineralization.

Decrepitated fluid inclusion analysis showed that the evaporate mounds formed from primary fluid inclusions have a complex chemical composition including Na, Ba, Mg, Mn, Ca, K, and Cl (, Figs. 7I, J, 9 & 10, Table 5). In addition, minor amounts of Ni, Fe, S, and Cu were detected, suggesting that these fluids were metal-bearing. Evaporate mounds formed after decrepitation of secondary inclusions contain Ca, Ba, Mn, Ti, Fe, S, and Cl (Fig. 10).

Stable isotopes

Carbon and oxygen isotope values were measured for 12 samples of the dolomitic marble hosting the mineralization as well as from the ore-bearing veins of the Nussir deposit (Figure 11, Table 6). $\delta^{13}\text{C}$ values for host dolomitic marble range from +1.8 to +2.9‰ V-PDB, and $\delta^{18}\text{O}$ values range from -18.2 to -15.9‰ V-PDB. Ore-bearing vein dolomite from the Nussir deposit has $\delta^{13}\text{C}$ values ranging from -1.0 to +2.3‰ and $\delta^{18}\text{O}$ values varying from -17.0 to -16.0‰. Two samples from limestone in the Vargsund Formation were analyzed and the results are provided here for comparison. Calcite has slightly higher $\delta^{13}\text{C}$ and $\delta^{18}\text{O}$ values, ranging from +3.1 to +3.2‰ and from -9.6 to -9.5‰, respectively.

Discussion

Sulphide mineralization at the Nussir and Ulveryggen deposits

Despite the numerous geological studies in the Nussir and Ulveryggen areas, remarkably little is known about the ore-forming processes that resulted in formation of the Cu mineralization (e.g., Sandstad et al., 2007; Sandstad, 2010; Perelló et al., 2015; Torgersen et al., 2015a). Although the Nussir and

Ulveryggen deposits are considered to be the products of the same mineralizing event, they show significant differences in the style of the mineralization, predominantly controlled by the difference in the host rock lithology of these two deposits. The less permeable volcano-sedimentary sequence at the Nussir area focussed the fluid flow and deposited the mineralization mostly in the form of quartz-carbonate veins (Figs. 5C & 7A). In contrast, the porous arkosic metasandstones at the Ulveryggen deposit did not have a capability to focus fluid flow. The circulating fluids were penetrating through the whole sequence resulting in disseminated mineralization in form of cement along grain boundaries and in the formation of only few veins (Fabricius, 1979; Sandstad et al., 2007).

Studied drill cores from the Nussir volcanic-sedimentary sequence suggest vertical zonation in distribution of Cu-bearing sulphides. In the upper part of the sequence, chalcopyrite dominates. At the top of the NS-DD-08-006 drill core, galena and silver minerals were also found. Deeper in the sequence, pyrite was gradually replaced by chalcopyrite (Fig. 6H), bornite, digenite, chalcocite, and covellite. The Ulveryggen deposit is different to some extent. In this study, no sulfide zonation was observed. However, vein-type mineralization hosted by a series of shear zones was described by Sandstad et al. (2007) from the Ulveryggen deposit. In these shear zones, Cu-sulfide mineralization is associated with quartz veins and has zonal distribution across stratigraphy and laterally. Therefore, shear zones might have acted as fluid pathways and controlled zonal sulfide distribution (Perelló et al., 2015). In addition, while Stribrny (1985) documented chalcopyrite as the dominant copper sulfide, this study found that bornite was also abundant. Therefore, lateral zonation of copper sulfides might be also developed at the Ulveryggen deposit, but further detailed investigation is needed

Origin and composition of metal-bearing fluids. Source for base metals: metamorphosed redbeds or hosting volcanics?

Both deposits have undergone greenschist to lower amphibolite facies metamorphism and significant deformation (Torgersen et al., 2015a). Petrographic study of the host rocks from the Nussir deposit reveals the abundant presence of chlorite and sericite. Chlorite mostly replaced biotite reflecting its

formation during the retrograde metamorphic stage. Deformation structures including crenulation cleavage in mica-rich beds, sigmoidally shaped aggregates of quartz and carbonate as well as elongated grains of quartz in veins, and recrystallized quartz suggest that the succession was affected by compression after its deposition (Fig. 5E, D). At least two generations of mineralized quartz-carbonate veins indicate at least two corresponding hydrothermal events (Fig. 5D-F, Sandstad, 2010).

At the Ulveryggen deposit, which is stratigraphically lower than the Nussir deposit, the host lithology is laterally changing across the deposit from the coarser-grained metasediments described by Stribny (1985) to finer-grained metasediments observed in this study. Greenschist facies metamorphism resulted in the formation of mica-rich layers, sericitization of feldspar fragments (Fig. 5G, H), and chloritization. Both brittle and ductile deformation styles and mineralized major shear zones were observed by Sandstad et al. (2007). In contrast to the Nussir deposit, carbonatization of the ore-bearing sequence is not typical for the Ulveryggen deposit.

Red-bed sandstones (hematite-coated quartz- and feldspar-rich sediments) are often considered as a critical component for the formation of sediment-hosted Cu deposits as a source of base metals including copper (e.g., Kirkham, 1989; Hitzman et al., 2005, 2010) and for maintaining oxidizing conditions in the basin necessary for the metal transport. In addition, alkaline mafic intrusions have been recognized as a potential source of chalcophile metals at several deposits (Brown, 1984, 1992; Carmichael & Ghiorso, 1986; Keith et al., 1997; Hitzman et al., 2005, 2010). The major difference between the Nussir and Ulveryggen deposits and similar sediment-hosted Cu deposits, including Kurferschiefer (Germany, Poland), Zambian Copper Belt (Zambia), Zairian Copperbelt (DRC), Redstone Copperbelt (Canada), Udokan Belt (Siberia, Russia), Kalahari Copperbelt (Namibia and Botswana), White Pine (Michigan, USA), Donchuan (China), and a number of smaller deposits (Brown, 1971; Ripley et al., 1980; Chartrand & Brown, 1985; Selley et al., 2005; Dewaele et al., 2006; Brems et al., 2009; El Desouky et al., 2009; Sillitoe et al., 2010) is an absence of red-bed sandstones in the former deposits. However, Jensen (1996) and Pharaoh (1990) described mafic intrusions in the RTW with alkaline

composition. At the Kipushi Zn-Cu deposit in DRC (Heijlen et al., 2008), which share many similarities with the Nussir and Ulveryggen deposits, mafic volcanics were inferred as one of the possible sources for metals that were leached out by highly saline brines during their deep convection and subsequent drainage along the Kipushi Fault. In the case of the Klein Aub Cu-Ag deposit of Namibia (Borg & Maiden, 1986), the underlying basaltic lavas were documented as a potential source of Cu and other base metals.

Even though the red beds were not previously described in the Repparfjord area, indirect features show that Ulveryggen metaconglomerates and metasandstones might be metamorphosed red-beds. Gablina (1990) and Eriksson & Cheney (1992) indicate that Precambrian sedimentary sequences loses their original reddish coloration due to hematite metamorphism to magnetite. Iron for the diagenetically formed hematite is derived from alteration or dissolution of unstable ferromagnesium minerals or infiltration of oxidized meteoric waters (Bancole et al., 2016). SEM analysis of Ulveryggen metasandstone performed for this study showed the presence of a big amount of magnetite, however, the grains are more detrital rather than authigenic in origin. Stribny (1985) in his monograph describes red to violet rim around metaconglomerate grains. Hematite and magnetite are the most abundant minerals after chalcopyrite among opaque minerals. In addition, magnetite also forms rims around chromite. Pyrite is also present in the abundant amount at the Ulveryggen deposit. However, the predominance of iron oxides upon pyrite is an evidence that ferric iron prevails upon ferrous form. In addition, a relatively high Fe_2O_3 content in arkosic metasandstone (Table 3) which is up to 5.65 wt.% is also in favour that these might be metamorphosed red beds. For this study, the whole rock geochemistry was done on samples with no visible mineralization and no visible pyrite. We, however, can not at the moment calculate the coefficient of distribution of ferric versus ferrous iron to support this idea. Therefore further investigation with additional emphasis on the abundance of Fe(II) vs. Fe (III) shall be done. Mathews (1976) calculated the PT conditions of minimum 365°C and 1.5 kbars necessary for the full conversion of hematite into magnetite. Assuming that reconstructed PT conditions are fair also for the Ulveryggen for the basin are 330-340°C and 1.1-2.7 kbars (see the

discussion below). Therefore, not sufficiently high temperature explains contemporaneous presence of hematite and magnetite in Ulveryggen metaconglomerate.

As mentioned above mafic metavolcanics are recognized as a source rocks for base metals at some sedimentary-hosted Cu deposits worldwide. To constrain another potential source of metals in the Nussir and Ulveryggen areas, whole-rock geochemical data (Tables 1-3) were used to construct the isocon diagrams according to the method developed by Grant (1986, 2005). The constructed isocon diagrams compare concentrations for a suite of mobile and immobile elements in non-mineralized vs. mineralized samples and illustrate their geochemical behaviour in response to the mineralization processes at the Nussir and Ulveryggen deposits. Volcanic and carbonate-siliciclastic rocks were plotted on different graphs (Figs. 12A, B). NS-13 and NS-15 samples were chosen as non-mineralized samples for mafic volcanic and carbonate-siliciclastic rocks, respectively, since they contain the lowest amounts of Cu. The isocon diagrams reveal that Cu, Mo, Pb, Sn, Bi, and Ag were added to the rocks with hydrothermal fluids during the formation of the Nussir deposit, while Co, Ni, Ba, and V were leached out. Zn was leached out from volcanic rocks and introduced into carbonate-siliciclastic rocks. The same pattern is also observed for the Ulveryggen deposit where Zn, Cu, Mo, Pb, Ni, Ba, and Co were introduced to the system (Fig. 12C). Phosphorus was leached out from the Nussir carbonate-siliciclastic rocks and the Ulveryggen siliciclastic rocks, while its concentration in the volcanic sequence of the Nussir deposit was not affected. The isocon diagrams also confirmed that the Cu mineralization at the Nussir deposit is associated with an extensive carbonization, whereas at the Ulveryggen deposit Ca was leached out with hydrothermal fluids. This is in agreement with Sandstad (2010) who suggested that Cu content increased in carbonate rich rocks. In addition, petrographic study revealed that carbonate rich volcanic rocks that are observed at shallow depth in the NS-08/06 drill core (Fig. 2) are also enriched in Cu.

The fluid inclusion (FI) study was conducted with the main aim to get a better insight into the nature of transport media for Cu and associated metals. Fig. 16 shows the temperature versus pressure

isochrons, calculated from Th and salinity of the FIs. For simplification, only end-member isochores for each type of FIs are plotted on Figure 14. The multiple generations of FIs and very diverse FI assemblages reflect a complex and potentially multi-stage evolution of hydrothermal fluids that circulated through the Nussir and Ulveryggen areas. Here, we present FI data for the Nussir deposit and refer to the data of Fabricius (1979) for FIs from the Ulveryggen deposit. The two-phase (L+V, Type 1) inclusions from the Nussir deposit show a very broad range of homogenization temperatures, but a relatively narrow range of salinities (Fig. 13). The low salinity of the entrapped fluids (< 3.2 wt.% NaCl equiv.) limited their capacity to transport metals such as Cu and Zn, whereas these elements are easily transported in the form of Cl-complexes (Seward et al., 2013). In contrast, fluid inclusions that belong to the Types 2 and 3 correspond to highly saline hydrothermal fluids, with a greater capacity to transport base metals. The SEM/EDS analyses of the selected Type 2 fluid inclusions confirmed that they contain detectable amounts of Cu, Fe, and Ni (Fig. 9). An independent geothermometer was used to constrain formation temperatures. In this study, we have applied sphalerite geothermometer described by Hutchison and Scott (1981), who have constrained the relationship between the Cu content in sphalerite in equilibrium with chalcopyrite and the formation temperature at 1 b and 5 kb with the following equations:

$$(1b) \text{ Log mole \%CuS in ZnS} = 4.202 - 3735 T^{-1} (\text{°K}) [1]$$

$$(5kb) \text{ Log mole \%CuS in ZnS} = 4.084 - 3791 T^{-1} (\text{°K}) [2]$$

The Cu content in the studied sphalerite that was in chemical equilibrium with chalcopyrite ranges between 0.47 and 0.96 wt.%, resulting in the calculated mineralization temperatures in the range of 320 to 350°C at 1 bar and 335 to 370°C at 5 kbars. Hutchison and Scott (1981) observed that the solubility of CuS in sphalerite is almost not affected by pressure, the equations are linear regression equations that can be described by least squares. Considerable changes will be observed at temperatures exceeding 550°C at 1b and 600°C at 5kb. The range of temperatures obtained during this study is lower, therefore we can assume linear relations between 1b and 5kb. Combining isochores

with the calculated mineralization temperatures, the formation temperatures were estimated to be 330-340°C and pressures to be in the range of 1.1 to 2.7 kbars (Fig. 14), defined by the intersection of the line passing through the calculated mineralization temperatures and the field for the type 2 and 3 Fls. Assuming lithostatic pressure, mineralization occurred at the depth varying from approximately 3.4 to 9 km. The basin and the mineralization either had a long and continuous history or experienced multiple, episodic remobilization events upon progressive burial of the basin.

In our study, the main focus was on the fluid inclusions from the Nussir deposit. Fabricius (1979) studied petrography and microthermometry of fluid inclusions in quartz veins and quartz from the matrix from the Ulveryggen deposit. The L+V and L+V+S types of fluid inclusions were described. The wide range of reported homogenization temperatures and salinities, ranging from 145 to 550°C and from 20 to 42 wt.% NaCl equiv., respectively, closely overlaps with the data obtained in this study (Fig. 8 & 13).

High salinity fluids have been reported from other sediment-hosted Cu deposits (e.g. Hitzman et al., 2005; Cailteux et al., 2005; Heijlen et al., 2008). The source of the salinity still remains uncertain for many of these deposits and different interpretations have been proposed including the evolved seawater, connate waters, gypsum dehydration, or low-grade metamorphic dehydration as well as inflow of meteoric waters (e.g., Hitzman et al., 2005). The high salinities indicated by fluid inclusions from both the Nussir and Ulveryggen deposits could reflect fluids derived from evaporite dissolution, contribution of magmatic fluids, or, alternatively, an effect of retrograde metamorphism involving rehydration of amphiboles and high metamorphic grade minerals such as biotite (e.g. Bennett & Barker, 1992) as well as mixing with meteoric water or gradual cooling under constant pressure (Fig. 13).

Figure 11 and Table 6 show $\delta^{13}\text{C}$ and $\delta^{18}\text{O}$ values for the host dolomitic marble and carbonates in the mineralized veins from the Nussir deposit. Based on carbon and oxygen isotope compositions, all carbonate samples analysed in this and previous studies from the RTW and AKTW plot in the field of

marine carbonates. Marbles from the Paleoproterozoic Vargsund Formation show ^{13}C -enrichment, likely reflecting secular variations in seawater C isotope composition. While O isotope values of both the host dolomitic marble and ore-bearing carbonates are more negative than those of other Paleoproterozoic unmineralized carbonates in the Repparfjord Tectonic Window (RTW), their C isotope values, with the exception of two outliers, are similar to each other and to those of the other Paleoproterozoic carbonates in the RTW and Alta-Kvanangen Tectonic Window (Melezhik & Fallick, 1996; Torgersen et al., 2014; Melezhik et al., 2015).

Considering that carbonate-water exchange affects first oxygen isotope values and only at a higher water-rock ratio C isotope values in carbonates (cf. Banner & Hanson, 1990), the data indicate a rock-buffered system with most of carbon in veins derived from the host dolostones with little to no CO_2 contributed by magmatic, hydrothermal, or organic sources.

Salinity derived due to retrograde metamorphism of highly metamorphosed rocks is also not supported by field and petrographic observations. The highest degree of metamorphism reported for the area is amphibolitic. Therefore, we suggest that dissolution of evaporates caused the formation of highly saline brines. Although evaporites have not been found in the Nussir and Ulveryggen deposits, sulphate-bearing evaporites were described in the nearby and broadly correlative Alta-Kvanangen Tectonic Window (Melezhik et al., 2015; Nasuti et al., 2015), as well as from the broadly correlative sedimentary successions in Fennoscandia and worldwide (e.g., Bekker et al., 2006; Schröder et al., 2008; Melezhik et al., 2015) deposited during the ca. 2.2-2.06 Ga Lomagundi carbon isotope excursion in seawater composition (e.g., Bekker et al., 2006; Schröder et al., 2008; Melezhik et al., 2015). Furthermore, a significant increase in seawater sulphate reservoir during the Lomagundi carbon isotope excursion has been inferred (Bekker & Holland, 2012; Planavsky et al., 2012), which ended at about the same time as deposition of the Raipas Supergroup started. Based on these correlations and evidence for evaporite deposition on the Fennoscandian Shield and worldwide at roughly the same time, we suggest that the evaporites were also present in the RTW and were entirely consumed

subsequent to their deposition. The presence of no longer preserved evaporates is also supported by the SEM-EDS study of the decrepitated FIs that revealed the presence of S and Cl in addition to Fe, Cu, Ca and Ba. We suggest that warm basinal fluids have been circulating through carbonate rocks, reaching equilibrium with carbonates via dissolution-precipitation. Evaporites, originally present in the volcano-sedimentary sequence, were dissolved enriching basinal fluids in sulphate and chlorine. Hot (330-340°C) saline brines circulating through the volcano-sedimentary sequence and leached Cu and other metals from mafic volcanic rocks and alkaline mafic intrusions. Reaching to the shallow levels in the basin, metal-charged saline fluids were cooled, sulphate was reduced, and metals were bounded with hydrogen sulphide and precipitated, following the reactions:



Copper sulphides could be also deposited after deposition when Cu-rich fluids enter initially iron sulphide-rich beds as was described at White Pine in Michigan. This process often results in a Cu-sulphide rim around the pyrite, when the latter is served as a sink for Cu (Fig. 6H; Eq. 2; Brown, 1971, 1992).

Na, Mg, K, Mn, and Ca were the major cations in the fluids (Table 5, Figs. 11-14). Presence of Cu, Fe, Ni, and Co suggests that these fluids were metal-bearing; in addition, S was found in the precipitated salts. The studied fluid inclusions represent at least one generation of metal-bearing fluids (primary FI). In case of secondary fluid inclusions, Cu was not detected. However, fluid composition did not change among different generations of fluid inclusions bearing Na, Mg, K, Mn, Ca, Cl, SO₄, Fe, S, and Ba. This suggests that the evolved fluids were also metal-bearing even though their Cu-bearing potential diminished. Oxidizing fluids transported sulphur in sulphate form. Although at the Nussir deposit the Cu mineralization occurs in different lithologies, including dolomitic marbles, metasandstones, metasiltsstones, and, to some extent, volcanic rocks, the highest-grade mineralization is hosted by dolomitic marbles and carbonatized intervals. Consequently, dolostones must have

formed an efficient reducing front due to the presence of organic matter to promote reduction of sulphate to sulphide, resulting in precipitation of the Cu-sulphide mineralization. Similar processes have been described for numerous carbonate-hosted base-metal deposits (e.g. Anderson & Garven, 1987; Machel, 1989; Shelton et al., 2009).

Metallogenetic model

The coexistence of oversaturated (L+S) and undersaturated (L+V) fluid inclusions together with the dominant fluid inclusions of L+V+S type, combined with variable homogenization temperatures, indicate remobilization of the fluids, inflow of and dilution with meteoric waters. Taking into consideration all data discussed above, we propose a scenario for the basin evolution (Fig. 15). Evidence for the presence of several fluid inclusion types and generations as well as a wide range of homogenization temperatures indicate a long history of fluid circulation in the basin. The fluid inclusions reflect the progressive evolution of the fluids (Figs. 14 & 13). The Type 1 FIs have a very wide range of homogenization temperatures, overlapping with those for the Type 2 and 3 FIs. The latter indicate the presence of brines with salinities as high as 36 wt.% NaCl equiv., which is only possible to achieve via evaporite dissolution, assuming that there was no input of magmatic fluids. Therefore, connate waters must have circulated through and dissolved evaporite sequence, progressively increasing their metal mobilization potential. Evaporites are commonly developed on carbonate platforms (e.g. Warren, 1999). Presence of evaporites is an important factor for the formation of the copper stratiform deposits (Pirajno, 2009), since dissolved salts and sulphate are necessary to transport metals, including Cu, with brines as metal-carrying complexes with chlorine, sulfate, and sulfide to the redox front or shallow level in the basin, where cooling and reduction result in metal precipitation. These brines are also efficient in leaching Cu and forming mobile CuCl_2 complexes (Rose, 1976), whereas dissolved sulphate in these brines helps to trap metals as sulphides at the reduction front via sulphate reduction. In order to create a sulphide deposit, large amounts of dissolved sulphate should be transported with the brine to the precipitation site within the basin. Therefore, dissolution of gypsum or anhydrite in the subsurface was necessary in the Repparfjord Tectonic Window to form

the Nussir and Ulveryggen deposits. It is likely that sediment burial, and, as a consequence, increase in subsurface temperatures in a compressional regime heated connate waters and induced their circulation through the host mafic volcanics, siliciclastic rocks, sulphate evaporites, alkaline mafic intrusions, and carbonates. Dissolution of dolostones at this stage contributed Ca and Mg to basinal waters, resulting in calcite precipitation in veins, which are frequently observed in the sequence. Notably, mineralization of the Nussir deposit is predominantly developed in quartz-calcite veins.

The basinal fluids form as a result of the evolution of the sedimentary basin (Hanor, 1979; Garven & Raffensperger, 1997; Pirajno, 2009). The key controls on the formation of the fluids are diagenesis and compaction in the basin. During the compaction, pore waters trapped in the sediments are released and subjected to overpressuring because of the overlying sediments and dehydration reactions, and their chemistry modified via pressure solution (dissolution of minerals at grain-to-grain contacts). In addition, regional compressional tectonic regime (Torgersen et al., 2015a) increased pressure and triggered dehydration reactions, and the evolved fluids were forced to circulate convectively and along the shear zones.

Alternative scenario for the formation of Nussir-Ulveryggen mineralized system is that continental braded river deposits of Ulveryggen were former red-beds creating the oxidizing conditions necessary for the mobilization of metals. The fluids circulating in the basin were penetrating and as a result dissolving no longer preserved evaporates and through red-beds consisting of metaconglomerates and metasandstones and dropped the metals in disseminated form in the Ulveryggen metasedimentary rocks and in the Nussir dolomites as the latter played the reduction front. Metavolcanics were additional source for base metals. However, this model is rather speculative and requires further investigation.

Conclusions

The early Paleoproterozoic Nussir and Ulveryggen sediment-hosted Cu deposits were formed by the basinal, moderately to highly saline fluids that transported Cu and Fe with metal-carrying complexes in the aftermath of the GOE.

Both deposits were hydrothermally altered with the addition of Cu, Mo, Pb, Sn, Bi, Ag, and Be to both the Ulveryggen and Nussir deposits. In contrast, Co, Ni, Ba, and V were leached out. Zn was leached out from volcanic rocks and added to the carbonate-siliciclastic deposits of the Nussir deposit and to the sandstone to conglomerate succession at the Ulveryggen deposit. Volcanic rocks of the volcano-sedimentary sequence hosting the Nussir deposit could be a potential metal source.

Alteration and low-grade metamorphism took place when quartz-carbonate veins formed and subsequently deformed. Presence of both deformed and undeformed quartz-carbonate veins indicates at least two fluid migration events.

Presence of both primary and secondary inclusions and similar composition of decrepitated evaporate mounts suggest multiple remobilization events involving metalliferous fluids. Combined with the previously published Re-Os dates, our data suggest a multi-stage mineralization process that started shortly after deposition of the sediments and continues until the very late stage of the Svecofennian Orogeny.

High salinity of basinal fluids suggests the involvement of evaporites that are no longer present. The circulating brines had high ionic strength with Na, Mg, Mn, Ba, and Ca enrichments. The temperature of metal-bearing fluids was 330 - 340°C and the pressure was 1.1 to 2.7 kbars, which constrains the maximum burial depth to approximately 3.4 - 9 km, consistent with greenschist facies metamorphism.

Overlapping $\delta^{13}\text{C}$ and $\delta^{18}\text{O}$ values for host carbonates and carbonates in the quartz-carbonate veins suggest closed, rock-buffered system with little to no carbon added from magmatic, hydrothermal, and organic sources. Metal-bearing fluids must have reached equilibrium with the host carbonates.

Acknowledgements

The authors would like to thank Troms Fylkeskommune and SINTEF for financing this research through a Ph.D. project of the first author. Participation of AB was made possible with the funding from the NSERC Discovery and Accelerator grants. We would like to express our gratitude to the former and current staff of Nussir AS and Øystein Rushfeld for supporting us on field trips and providing us with access to the samples. Special thanks to Margarita Kim (The Institute of Geology and Geophysics of the Republic of Uzbekistan) and laboratory staff of the UiT and, especially, Trine Merete Dahl for timely help with sample preparation and analysis.

Reference list

Bakker, R.J. 2003: Fluids, package of computer programs for fluid inclusion studies. *Chemical Geology* 194, 3-23.

Bakker, R.J., Brown, P.E. 2003: Computer modelling in fluid inclusion research. *In*: Samson, I., Anderson, A., Marshall, D. (eds.): *Fluid Inclusions: Analysis and Interpretation*. Mineralogical Association of Canada 32, 175-212.

Bancole, O.M., El Albani, A., Meunier, A., Rouxel, O.J., Gauthier-Lafaye, F. & Bekker, A. 2016: Origin of red beds in the Paleoproterozoic Franceville Basin, Gabon, and implications for sandstone-hosted uranium mineralization. *American Journal of Science* 316, 839-872.

Banner, J.L. & Hanson, G.N. 1990: Calculation of simultaneous isotopic and trace element variations during water-rock interaction with applications to carbonate diagenesis. *Geochimica et Cosmochimica Acta* 54, 3123-3137.

Bekker, A., Karhu, J.A., Kaufman, A.J. 2006: Carbon isotope record for the onset of the Lomagundi carbon isotope excursion in the Great Lakes area, North America. *Precambrian Research* 148, 145-180.

Bennett, D.G. & Barker, A.J. 1992: High salinity fluids: the result of retrograde metamorphism in thrust zones. *Geochimica et Cosmochimica Acta* 56, 81-95.

Bodnar, R.J. 1993: Revised equation and table for determining the freezing point depression of H₂O-NaCl solutions. *Geochimica et Cosmochimica Acta* 57, 683-684.

Bogdanova, S., Gorbatshev, R., Skridlaite, G., Soesoo, A., Taran, L., Kurlovich, D. 2015: Trans-Baltic Palaeoproterozoic correlations towards the reconstruction of supercontinent Columbia/Nuna. *Precambrian Research* 259, 5-33.

Bogdanova, S.V., Gorbatshev, R., Garetsky, R.G. 2016: Europe|East European Craton. Reference Module in Earth Systems and Environmental Sciences. Elsevier. doi: 10.1016/B978-0-12-409548-9.10020-X

Borg, G., Maiden, K.J. 1986: A preliminary appraisal of the tectonic and sedimentological environment of the Sinclair sequence in the Klein Aub area. *Communications of the Geological Survey of South Western Africa/Namibia* 2, 65-73.

Brems, D., Muchez, Ph., Sikazwe, O., Mukumba, W. 2009: Metallogensis of the Nkana copper-cobalt South Orebody, Zambia. *Journal of African Earth Sciences* 55, 185-196.

Brown, A.C. 1971: Zoning in the White Pine copper deposit, Ontogon County, Michigan. *Economic Geology* 66, 543-573.

Brown, A.C. 1984: Alternative sources of metals for stratiform copper deposits. *Precambrian Research* 25, 61-74.

Brown, A.C. 1992: Sediment-hosted stratiform copper deposits. *Geoscience Canada* 19, 125-141.

Cailteux, J.L.H., Kampunzu, A.B., Lerouge, C., Kaputo, A.K., Milesi, J.P. 2005: Genesis of sediment-hosted stratiform copper-cobalt deposits, Central African Copperbelt. *Journal of African Earth Sciences* 42, 134-158.

- Carmichael, I.S.E. & Ghiorso, M.S. 1986: Oxidation-reduction relations in basic magma: a case for homogeneous equilibria. *Earth and Planetary Science Letters* 78, 200-210.
- Chartrand, F.M. & Brown, A.C. 1985: The diagenetic origin of stratiform copper mineralization, Coates Lake, Redstone Copper Belt, N.W.T., Canada. *Economic Geology* 80, 325-343.
- Corfu, F., Roberts, R.J., Torsvik, T.H., Ashwal, L.D., Ramsay, D.M. 2007: Peri-Gondwanan elements in the Caledonian Nappes of Finnmark, Northern Norway: Implications for the paleogeographic framework of the Scandinavian Caledonides. *American Journal of Science* 307, 434-458.
- Dewaele, S., Muchez, Ph., Vets, J., Fernandez-Alonzo, M., Tack, L. 2006: Multiphase origin of the Cu-Co ore deposits in the western part of the Lufilian fold-and-thrust belt, Katanga (Democratic Republic of Congo). *Journal of African Earth Sciences* 46, 455-469.
- Doe, B.R. 1994: Zinc, copper, and lead in mid-ocean ridge basalts and the source rock control on Zn/Pb in ocean-ridge hydrothermal deposits. *Geochimica et Cosmochimica Acta* 58, 2215-2223.
- El Desouky, H.A., Muchez, Ph., Cailteux, J. 2009: Two Cu-Co sulfide phases and contrasting fluid systems in the Katanga Copperbelt, Democratic Republic of Congo. *Ore Geology Reviews* 36, 315-332.
- Engel, A.E.J., Engel, C.G., Havens, R.G. 1965: Chemical characteristics of oceanic basalts and the upper mantle. *Geological Society of America Bulletin* 76, 719-734.
- Eriksson, P.G. & Cheney, E.S. 1992: Evidence for the transition to an oxygen-rich atmosphere during the evolution of red beds in the Lower Proterozoic sequences of southern Africa. *Precambrian Research* 54, 257-269.
- Fabricius, J. 1979: Kobberforekomsten på Ulveryggen, Finnmark, Norge. *Dansk Geologisk Forening. Årsskrift for 1979*, 107-110.

- Gablina, I.F. 1990: Mineralogical-geochemical criteria for identifying red-bed formations in metamorphic strata of the Precambrian in connection with copper content. *Lithology and Mineral Resources* 3, 95-109 (*in Russian*).
- Gale, A., Dalton, C.A., Langmuir, C.H., Su, Y., Schilling, J.G. 2013: The mean composition of ocean ridge basalts. *Geochemistry, Geophysics, Geosystems* 14: doi:10.1029/2012GC004334
- Garven, G., Raffensperger, J.P. 1997: Hydrology and geochemistry of ore genesis in sedimentary basins. *In: Barnes, H.L. (ed): Geochemistry of ore deposits*. John Wiley & Sons, New York, pp. 146-165.
- Gee, D.G., Fossen, H., Henriksen, N., Higgins, A.K. 2008: From the early Paleozoic platforms of Baltica and Laurentia to the Caledonide orogen of Scandinavia and Greenland. *Episodes* 31, 44-51.
- Grant, J.A. 1986: The isocon diagram; a simple solution to Gresens' equation for metasomatic alteration. *Economic Geology* 81, 1976-1982.
- Grant, J.A. 2005 Isocon analysis: A brief review of the method and applications. *Physics and Chemistry of the Earth* 30, 997-1004.
- Hanor, J.S. 1979: The sedimentary genesis of hydrothermal fluids. *In: Barnes, H.L. (ed.) Geochemistry of Hydrothermal ore deposits*. John Wiley & Sons, New York, 137-172.
- Heijlen, W., Banks, D.A., Muchez, Ph., Stensgard, B.M., Yardley, B.W.D. 2008: The nature of mineralizing fluids of the Kipushi Zn-Co-Cu deposit, Katanga, Democratic Republic of Congo: quantitative fluid inclusion analysis using lasera ablation ICP-MS and bulk crush-leach methods. *Economic Geology* 103, 1459-1482.
- Hitzman, M., Kirkham, R., Broughton, D., Thorson, J., Selley, D. 2005: The sediment-hosted stratiform copper ore system. *Economic Geology 100th Anniversary Vol.*, 609–642.
- Hitzman, M.W., Selley, D., Bull, S. 2010: Formation of sedimentary rock-hosted stratiform copper deposits through Earth history. *Economic Geology* 105, 627-639.

Hutchison, M.N., Scott, S.D. 1981: Sphalerite geobarometry in the Cu-Fe-Zn-S system. *Economic Geology* 76, 143-153.

Jensen, P.A. 1996: *The Altenes and Repparfjord tectonic windows, Finnmark, northern Norway: Remnants of a Palaeoproterozoic Andean-type plate margin at the rim of the Baltic Shield*. PhD thesis, University of Tromsø, 120 pp.

Jiang, Yu., Niu, H., Bao, Zh., Shan, Q., Yang, W., Yan, Sh. 2014: Fluid evolution of the Paleoproterozoic Hujiayu copper deposit in the Zhongtiaoshan region: evidence from fluid inclusions and carbon-oxygen isotopes. *Precambrian Research* 255, 734-747.

Keith, J.D., Whitney, J.A., Hattori, K., Ballantyne, G.H., Christiansen, E.H., Barr, D.L., Cannan, T.M., Hook, C.J. 1997: The role of magmatic sulphides and mafic alkaline magmas in the Bingham and Tintic Mining Districts, Utah. *Journal of Petrology* 38, 1679-1690.

Kirkham, R.V. 1989: Distribution, settings, and genesis of sediment-hosted stratiform copper deposits. *In*: Boyle, R.W., Brown, A.C., Jefferson, C.W., Jowett, E.C., Kirkham, R.V. (eds.): *Sediment-hosted stratiform copper deposits*. Geological Association of Canada Special Paper 36, 3-38.

Kirkland, C.L., Daly, J.S., Whitehouse, M.J. 2006: Granitic magmatism of Grenvillian and late Neoproterozoic age in Finnmark, Arctic Norway—Constraining pre-Scandian deformation in the Kalak Nappe Complex. *Precambrian Research* 145, 24-52.

Kontak, D.J. 2004: Analysis of evaporate mounds as a complement to fluid-inclusion thermometric data: case studies from granitic environments in Nova Scotia and Peru. *Canadian Mineralogist* 42, 1315-1329.

Matthews, A. 1976: Magnetite formation by the reduction of hematite with iron under hydrothermal conditions. *American Mineralogist* 61, 927-932.

Melezhik, V.A. & Fallick, A.E. 1996: A widespread positive $\delta^{13}\text{C}_{\text{carb}}$ anomaly at around 2.33-2.06 Ga on the Fennoscandian Shield: a paradox? *Terra Nova* 8, 141-157.

Melezhik, V.A., Bingen, B., Sandstad, J.S., Pokrovsky, B.G., Solli, A., Fallick, A.E. 2015: Sedimentary-volcanic successions of the Alta–Kvænangen Tectonic Window in the northern Norwegian Caledonides: Multiple constraints on deposition and correlation with complexes on the Fennoscandian Shield. *Norwegian Journal of Geology* 95, 245-284.

Mun, Y. 2013: *The Nussir copper deposit: petrology, mineralogy, geochemistry and distribution of ore mineralization*. Master thesis. University of Tromsø, 54pp.

Nasuti, A., Roberts, D., Dumais, M.-A., Ofstad, F., Hyvönen, E., Stampolidis, A., Rodionov, A. 2015: New high-resolution aeromagnetic and radiometric surveys in Finnmark and North Troms: linking anomaly patterns to bedrock geology and structure. *Norwegian Journal of Geology* 95, 217-243.

Nordgulen, Ø. & Andresen, A. 2008: The Precambrian. *In*: Ramberg, I.B., Bryhni, I., Nøttvedt, A., Rangnes, K. (eds.): *The making of land – geology of Norway*. Norsk Geologisk Forening. Trondheim, 58-119.

Nussir ASA 2019: Official grades from Nussir ASA. http://www.nussir.no/en_projec_nussir.php (accessed 20.06.2019).

Perelló, J., Clifford, J.A., Creaser, R.A., Valencia, V.A. 2015: An example of synorogenic sediment-hosted copper Mineralization: geologic and geochronologic evidence from the Paleoproterozoic Nussir deposit, Finnmark, Arctic Norway. *Economic Geology* 110, 677–689.

Pharaoh, T.C., MacIntyre, R.M., Ramsay, D.M. 1982: K-Ar age determination on the Raipas suite in the Komagfjord Window, northern Norway. *Norsk Geologisk Tidsskrift* 62, 51-57.

Pharaoh, T.C., Ramsey, D., Jansen, Ø. 1983: Stratigraphy and structure of the northern part of the Repparfjord - Komagfjord window, Finnmark, Northern Norway. *Norges Geologiske Undersøkelse* 377, 1-45.

Pharaoh, T.C. & Pearce, J.A. 1984: Geochemical evidence for the geotectonic setting of early Proterozoic metavolcanic sequences in Lapland. *Precambrian Research* 25, 283-308.

- Pharaoh, T.C. 1985: Volcanic and Geochemical Stratigraphy of the Nussir Group of Arctic Norway – an Early Proterozoic Greenstone Suite. *Journal of Geological Society* 142, 259-278.
- Pharaoh, T.C. & Brewer, T.S. 1990: Spatial and temporal diversity of early Proterozoic volcanic sequences – comparison between the Baltic and Laurentian shields. *Precambrian Research* 47, 169-189.
- Pirajno, F. 2009: Hydrothermal processes and mineral systems. Springer Science, Business Media B.V., 1249 pp.
- Reitan, P.H. 1963: The geology of the Komagfjord tectonic window of the Raipas suite, Finnmark, Norway. *Norges Geologiske Undersøkelse* 221, 1-71.
- Ripley, E.M., Lambert, M.W., Berendsen, P. 1980: Mineralogy and paragenesis of Red-Bed copper mineralization in the Lower Permian of South Central Kansas. *Economic Geology* 75, 722-729.
- Roedder, E. 1984: Fluid inclusion. *Reviews in mineralogy* 12: 646 pp.
- Rose, A.W. 1976: The effect of cuprous chloride complexes in the origin of red-bed copper and related deposits. *Economic Geology* 71, 1036-1048.
- Sandstad, J.S., Viola, G., Nilsson, L.P. 2007: Reconnaissance structural geological mapping and field XRF-analyses of the Ulveryggen copper deposit, Finnmark, Norway. *NGU Report 2007.064*, 16 pp.
- Sandstad, J.S. 2010: Microscope and SEM (scanning electron microscope) investigations of thin sections from the Nussir copper deposit. *NGU. Report 2010.025*, 55pp.
- Schröder, S., Bekker, A., Beukes, N.J., Strauss, H., Van Niekerk, H.S. 2008: Rise in seawater sulphate concentration associated with the Paleoproterozoic positive carbon isotope excursion: evidence from sulphate evaporites in the ~2.2-2.1 Gyr shallow-marine Lucknow Formation, South Africa. *Terra Nova* 20, 108-117.

Selley, D., Broughton, D., Scott, R., Hitzman, M., Bull, S., Large, R., McGoldrick, P., Croaker, M., Pollington, N., Barra, F. 2005: A new look at the Geology of the Zambian Copperbelt. *Economic Geology* 100th Anniversary Volume, 965-1000.

Seward, T.M., Williams-Jones, A., Migdisov, A. 2013: The chemistry of metal transport and deposition by ore-forming hydrothermal fluids. *In*: Holland, H.D. & Turekian K.K. (eds.): *Treatise on Geochemistry*. 2nd Edition. 13, 29-57.

Siedliecka, A., Krill, A.G., Often, M., Sandstad, J.S., Solli, A., Iversen, E., Lieungh, B. 1985: Lithostratigraphy and correlation of the Archaean and Early Proterozoic rocks of Finnmarksvidda and the Sørvaranger district. *Norges Geologiske Undersøkelse Bulletin* 403, 7–36.

Sillitoe, R.H., Perelló, J., Carcía, A. 2010: Sulfide-bearing veinlets throughout the stratiform mineralization of the Central African Copperbelt: temporal and genetic implications. *Economic Geology* 105, 1361-1368.

Singer, D.A. 1995: World class base and precious metal deposits – a quantitative analysis. *Economic Geology* 90, 88-104.

Stakes, D.S., O'Neil, J.R. 1982: Mineralogy and stable isotope geochemistry of hydrothermally altered oceanic rocks. *Earth and Planetary Science Letters* 57, 285–304.

Stribny, B. 1985: The conglomerate-hosted Repparfjord copper ore deposit, Finnmark, Norway: *Monograph Series on Mineral Deposits* 24. Gebrüder Borntraeger, Berlin, Stuttgart, 75 pp.

Torgersen, E., Viola, G. 2014: Structural and temporal evolution of a reactivated brittle–ductile fault – Part I: Fault architecture, strain localization mechanisms and deformation history. *Earth and Planetary Science Letters* 407, 205-220.

Torgersen, E., Viola, G., Zwingmann, H., Harris, C. 2014: Structural and temporal evolution of a reactivated brittle–ductile fault – Part II: Timing of fault initiation and reactivation by K–Ar dating of synkinematic illite/muscovite. *Earth and Planetary Science Letters* 407, 221-233.

Torgersen, E., Viola, G., Sandstad, J.S. 2015a: Revised structure and stratigraphy of the northwestern Repparfjord Tectonic Window, Northern Norway. *Norwegian Journal of Geology* 95, 397-421.

Torgersen, E., Viola, G., Sandstad, J.S., Stein, H., Zwingmann, H., Hannah, J. 2015b: Effects of frictional–viscous oscillations and fluid flow events on the structural evolution and Re–Os pyrite–chalcopyrite systematics of Cu-rich carbonate veins in northern Norway. *Tectonophysics* 659, 70-90.

Torske, T., Bergh, S.G. 2004: The Caravari Formation of the Kautokeino Greenstone Belt, Finnmark, North Norway Palaeoproterozoic foreland basin succession. *Norges Geologiske Undersøkelse Bulletin* 442, 5-22.

Viola, G., Sandstad, J.S., Nilsson, L.P., Heincke, B. 2008: Structural and ore geological studies in the northwestern part of the Repparfjord Window, Kvalsund, Finnmark, Norway. *NGU Report 2008.029*. 93 pp.

Warren, J. 1999: *Evaporites: their evolution and economics*. Blackwell Science, 438 pp.

Zhang, Y.-G. & Frantz, J.D. 1987: Determination of the homogenization temperatures and densities of supercritical fluids in the system NaCl-KCl-CaCl₂-H₂O using synthetic fluid inclusions. *Chemical Geology* 64, 335-350.

Figure and Table captions

Figure. 1 *Simplified geological map of the Repparfjord Tectonic Window (modified after Torgersen et al., 2015a).*

Figure. 2 *Schematic diagram illustrating the modal distribution of ore minerals at the Nussir and Ulveryggen deposits. The figure is compiled from Stribrny (1985), Sandstad (2010), Mun (2013), and results of this study. HCVR – highly carbonated volcanic rocks; *Ag – different Ag-bearing minerals including hessite, naumannite, bohdanowiczite, amalgam, undifferentiated phases, Au – different Au-bearing minerals including electrum, bogdanovite, sylvanite, Bi – native bismuth, Bn – bornite, Cb – cobaltite, Ccp – chalcopyrite, Cct – chalcocite, Crl – carolyte, Cst – clausthalite, Cu ox – Cu oxides, Cv –*

covellite, Dg – digenite, FeOx – iron oxides, Gdf – gersdorffite, Gn – galena, Hs – hessite, Idt – idaite, Mb – molybdenite, Ndg – neodigenite, *Pd – undifferentiated Pd phases including isomertierite, Po – pyrrhotite, Py – pyrite, Sph – sphalerite, *Te – Te-bearing phases with Pd and Ag.

Figure 3. Lithological section for the drill hole NS-DD-08-006. The colours correspond to the legend on Fig. 1. Ore mineral abbreviations are given in Fig. 3.

Figure 4 Photographs of core samples from (A-C) the Nussir deposit (drill hole NUS-DD-06-007, 20-30 m interval) (Ns): Cu-bearing dolomitic marble (Dol). The dolomitic marble is hydrothermally reworked with quartz (Qz) – carbonate (Cb) veins enriched in bornite (Bn) and chalcopyrite (Ccp); (D, E) mineralized arkosic metasandstone from Ulveryggen deposit (Ulv) (drill hole US-004-10/ intervals (D) 45.16 m, (E) 48.5 m). The mineralization is disseminated and fill the space between Qz and feldspar (Fsp) aggregates, white mica (Mc) is also observed between Qz grains.

Figure 5. Microphotographs taken in crossed-polarized light of typical host rocks and veining at the Nussir and Ulveryggen deposits: A) dolostone (Dol) with rip-up clast of metapelite (Pel) and quartz vein (Qz); NS-16 sample; B) metavolcanics with actinolite (Act) and feldspar (Fsp) crystals; NS-10 sample; C) quartz-carbonate vein in metavolcanics; NS-10 sample; D) deformed carbonate vein in carbonaceous metasandstone; NS-14 sample; E) sigmoidally shaped quartz-carbonate aggregate with ore minerals (black) in metapelite; sample NS-1a; F) carbonate vein cross-cutting metapelite (Pel), quartz, carbonate, and ore minerals (black). Secondary muscovite (Ms) developed in the host metasilstone; sample NS-1a; G) metasandstone with clasts of quartz and feldspar and with muscovite and sericite (Ser) along grain boundaries; sample Ulv-2; H) cluster of recrystallized quartz from the vein in the host metasandstone; sample Ulv-4.

Figure 6. Backscatter electron images of mineralized samples from the Nussir and Ulveryggen deposits: A) bornite (Bn), chalcopyrite (Ccp), and galena (Gn); sample NS-27, drill hole NUS-DD-14-001, 730 m depth; B) bornite partially replaced by chalcocite (Cct) with inclusions of clausthalite (Cst), galena, and sphalerite (Sp); sample NS-40, drill hole NUS-DD-11-004, 459.8 m depth; C) chalcocite intergrown with

bornite having small inclusions of clausthalite; sample NS-32, drill hole NUS-DD-90-002, 53 m depth; D) native bismuth (Bi) in chalcocite-bornite aggregate; sample NS-32, drill hole NUS-DD-90-002, 53 m depth; E) cobaltite (Cbt) inclusion in chalcopyrite; sample NS-44, drill hole NUS-06-005, 232.2 m depth; F) stromeyerite (Stm) and AgBiS phase in bornite; sample NS-32, drill hole NUS-DD-90-002, 53 m depth; G) inclusions of hessite (Hs) and clausthalite in chalcopyrite; sample NS-42, drill hole NUS-DD-13-020, 366 m depth; H) chalcopyrite overgrown with pyrite (Py) crystals having small inclusions of AgSe phase; sample NS-44, drill hole NUS-DD-06-005, 232.2 m depth; I) inclusions of sphalerite and galena in chalcopyrite; sample NS-34, drill hole NUS-DD-11-004, 33 m depth; J) chalcopyrite with bornite inclusions; sample Ulv-1, drill hole US-003-10, 39.1 m depth; K) microinclusion of Bi-bearing mineral phase in chalcocite. Chalcocite is partly replaced by bornite; sample Ulv-12, drill hole US-015-10, 3.4 m depth; L) vermicular intergrowth of bornite and chalcocite. Note tiny inclusion of hessite in bornite; sample Ulv-14, drill hole US-020-10, 50.1 m depth.

Figure 7. A) the photograph of sample NS-45, metatuffite from HCVR crosscut by quartz-carbonate vein; B) the photograph of sample NS-39 metasiltstone crosscut by quartz vein; C)) the photograph of sample NS-52: quartz double-side polished wafter from sample NS-45; D) the photograph of double-side polished wafter (sample NS-51A-J) from sample NS-39; E-H) microphotographs illustrating FIs in quartz: S-type – secondary inclusions; L+V+S – liquid + vapour + salt; L+S – liquid + salt; L+V – liquid + vapour; i, j) backscattered electron image of decrepitated evaporate mounds formed by overheating of FIs.

Figure 8. Histograms illustrating ranges of variation in homogenization temperature and salinity obtained from FIs. Note that different colours are assigned to different types of FIs (see the text for further details) for the Nussir and Ulveryggen deposits.

Figure 9. Element mapping of a decrepitated fluid inclusion in vein quartz from the Nussir deposit (sample NS-51). LI – layered image.

Figure 10. Images illustrating element distribution in decrepitated secondary fluid inclusion in vein quartz from the Nussir deposit. Brightness illustrates the intensity of the signal (sample NS-51).

Figure 11. Scatter diagram of $\delta^{13}\text{C}$ (V-PDB) versus $\delta^{18}\text{O}$ (V-PDB) illustrating the source of carbon and oxygen for the studied carbonate samples and the data obtained in the previous studies (Stakes & O'Neil (1982); Torgersen et al. (2014); Melezhik et al. (2015)).

Figure 12. Isocon diagrams illustrating the element mass change in mineralized rocks with respect to non-mineralized rock (see the text for explanation) in A) volcanic rocks from the Nussir deposit; B) carbonate-siliciclastic rocks from the Nussir deposit; C) host rocks from the Ulveryggen deposit.

Figure 13. The graph illustrates the relationship between the homogenization temperature and salinity of analysed FIs. Thin lines demonstrate isopleths of equal density (in g/cm^3). Isothermal mixing trend implies mixing of two fluids with different salinities but similar temperatures. Only few inclusions show this trend. Types 2b and 3 FIs plot along the $1.10 \text{ g}/\text{cm}^3$ isopleth, just at the border of NaCl saturation area and demonstrate a trend of gradual cooling.

Figure 14. Isochoric curves showing minimum homogenization temperature of selected fluid inclusions in quartz combined with sphalerite geothermometer (Hutchison and Scott 1981).

Figure 15. Proposed model for the evolution of the basin and metal-bearing fluids. See the text for further details. Modified from Sandstad et al. (2007) and Torgersen et al. (2015a).

Table 1. Whole-rock data for basaltic andesites and tuffs from the Nussir deposit.

Table 2. Whole-rock data for carbonate-siliciclastic rocks from the Nussir deposit.

Table 3. Whole-rock data for siliciclastic rocks from the Ulveryggen deposit.

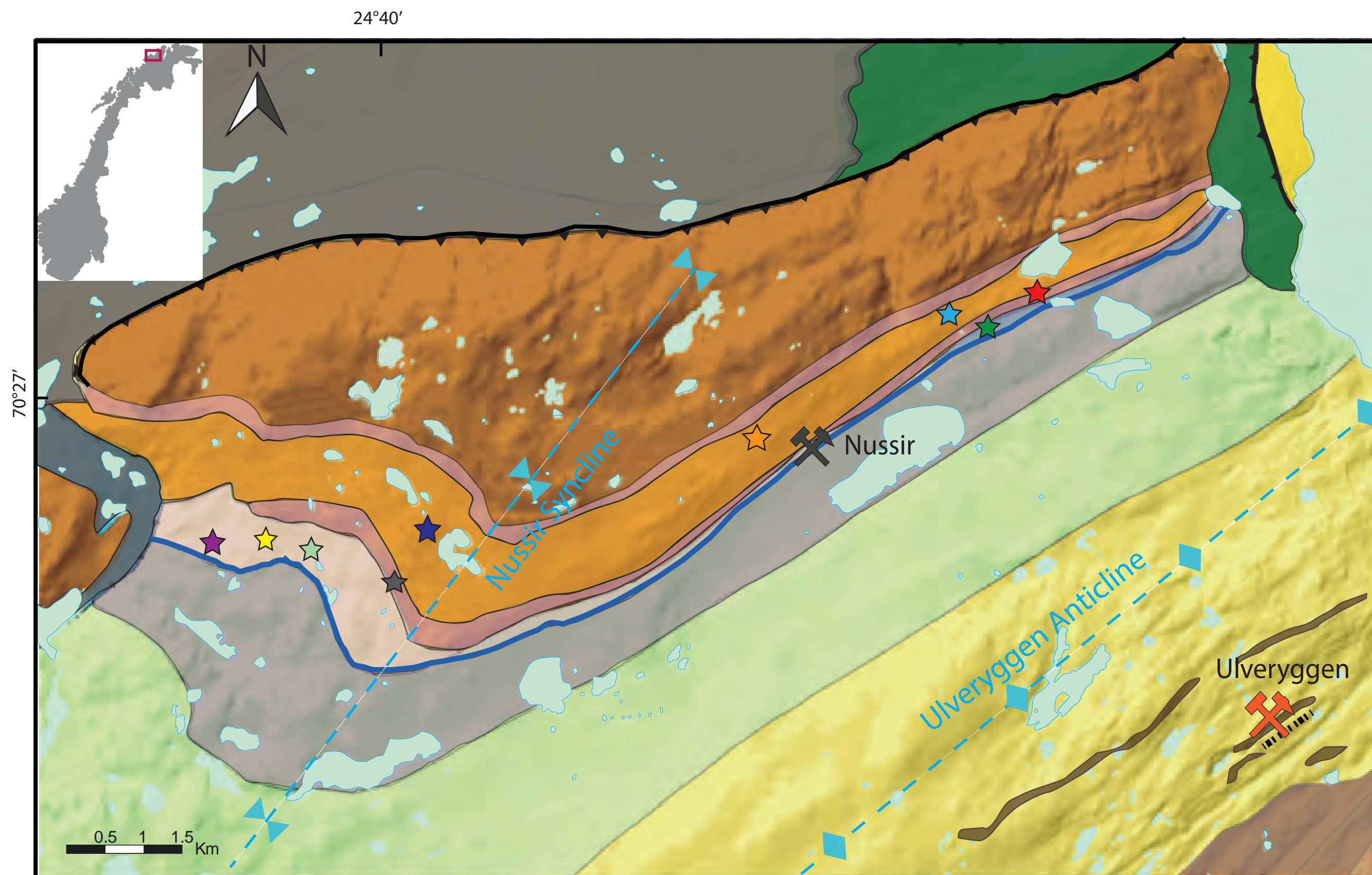
Table 4. Mineral chemistry of the selected ore minerals from the Nussir and Ulveryggen deposits. Am – amalgam, Arg – argentite, Bn – bornite, Brt – barite, Cbt – cobaltite, Ccp – chalcopyrite, Cct – chalcocite, Clag – chlorargente (Cl is not precisely measured), Cst – clausthalite, Cv – covellite, Dg – digenite, Ga –

galena, Hs – hessite, Gf – gersdorfite; Stm – stromeyerite, Laboratories: UiO – University of Oslo; IGG – Institute on Geology and Geophysics, Republic of Uzbekistan; UCR – University of California, Riverside.

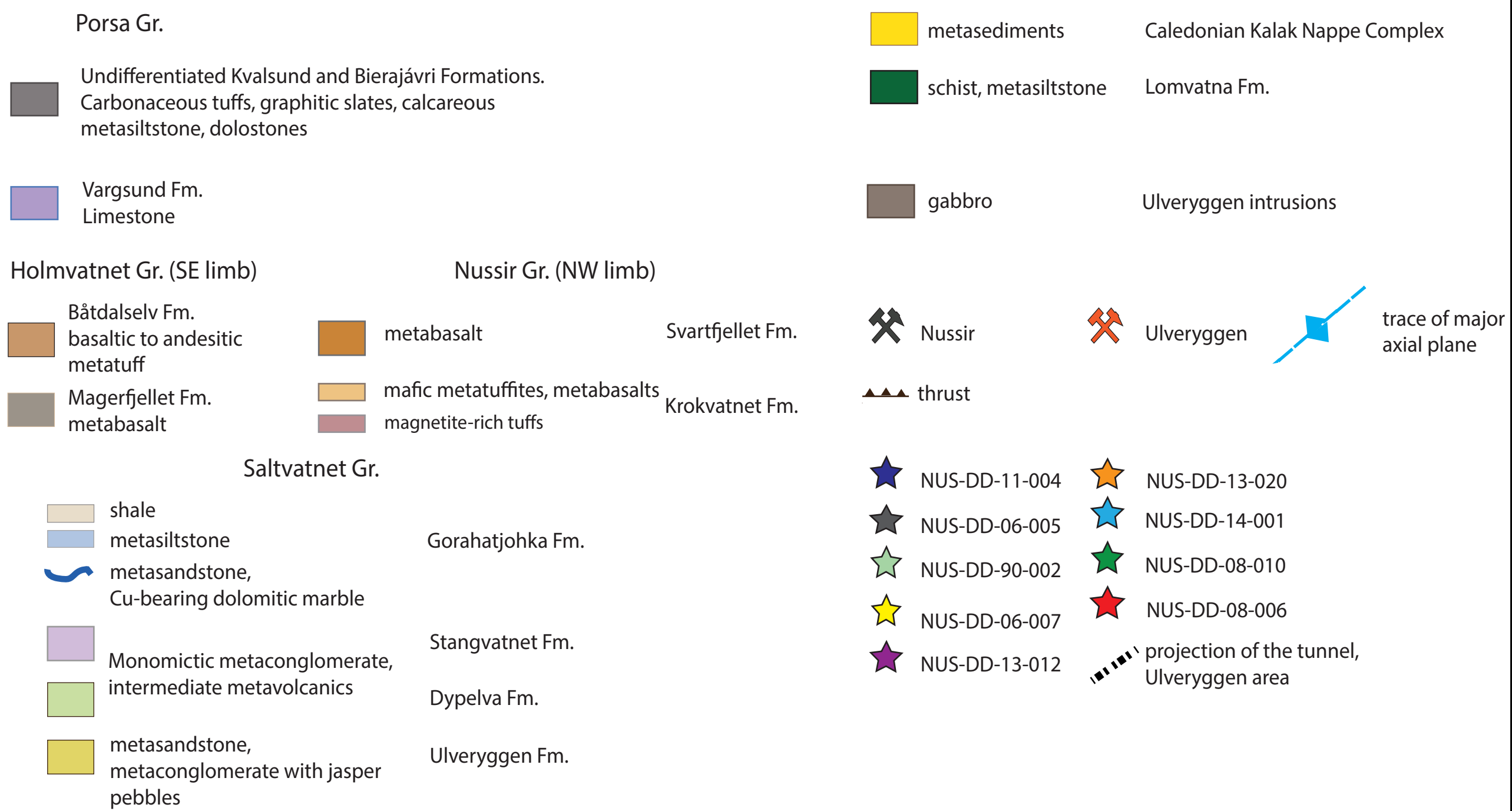
Table 5. *Chemical data for selected decrepitated evaporate mounds obtained with EDS detector (wt%).*

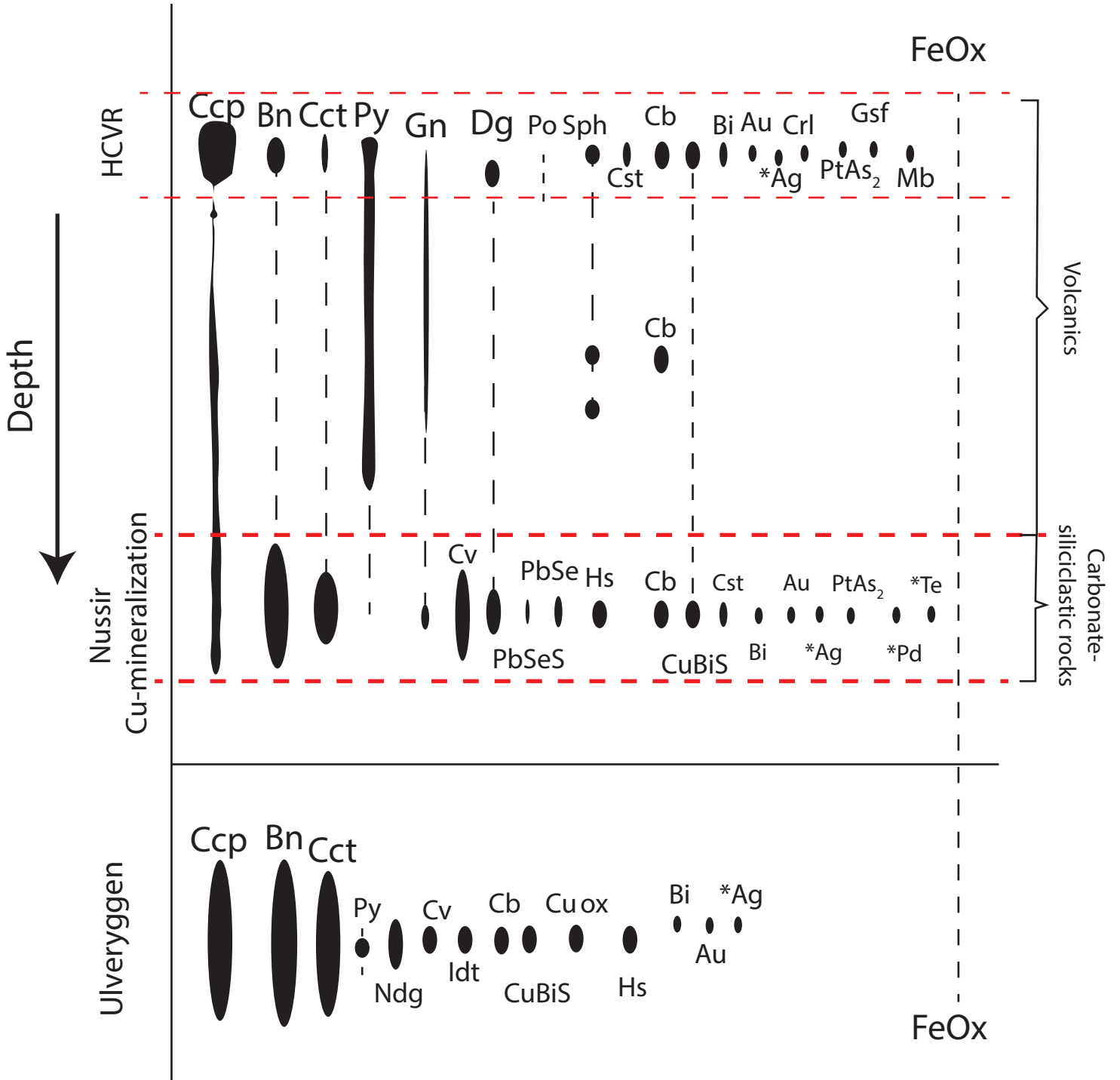
Table 6. *Carbon and oxygen isotope composition of host dolomitic marble and ore-bearing carbonate veins. V-PDB – Vienna Pee Dee Belemnite.*

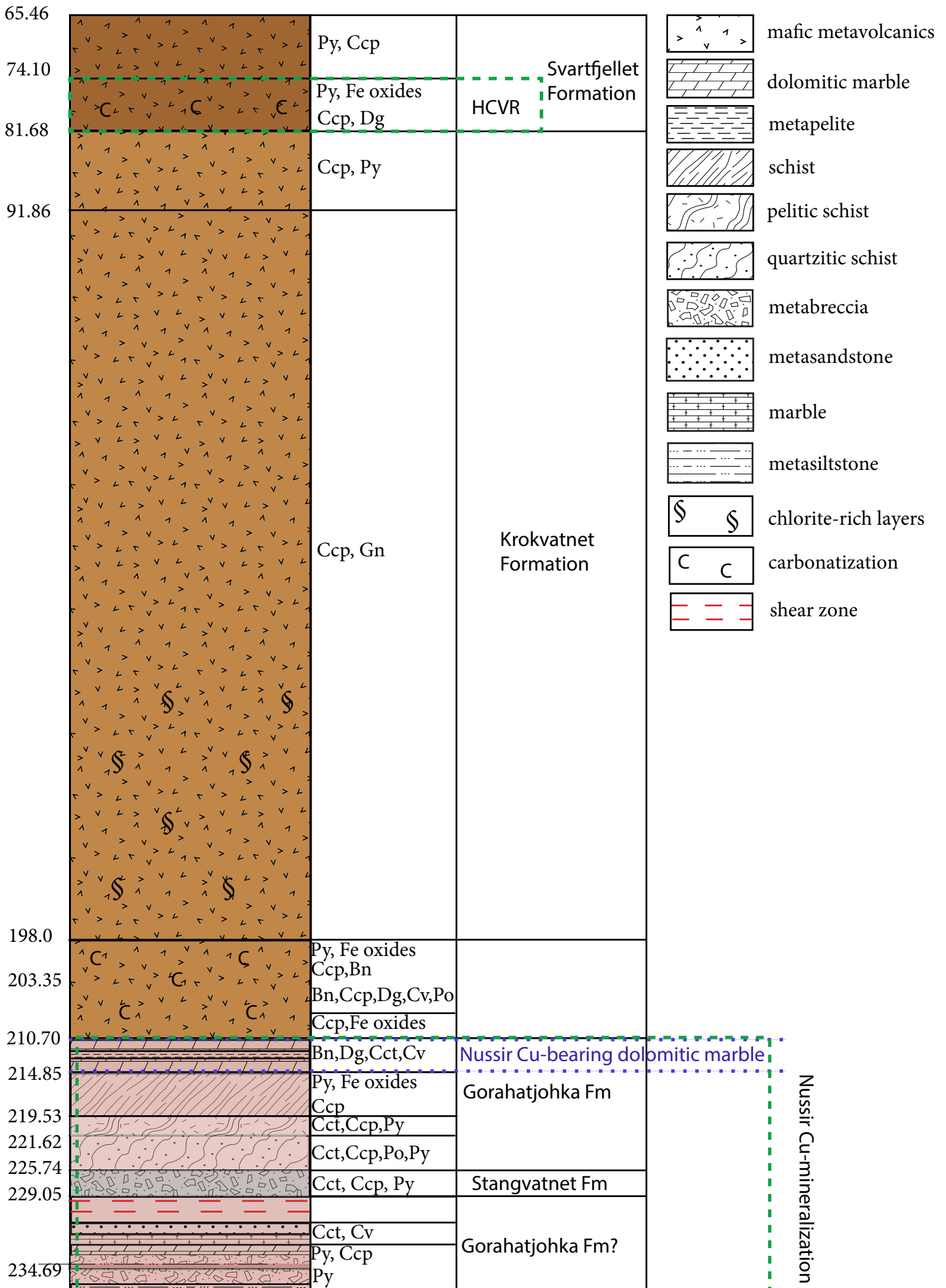
Supplementary Table 1. *The list of samples with studied drill cores, depth and lithology.*

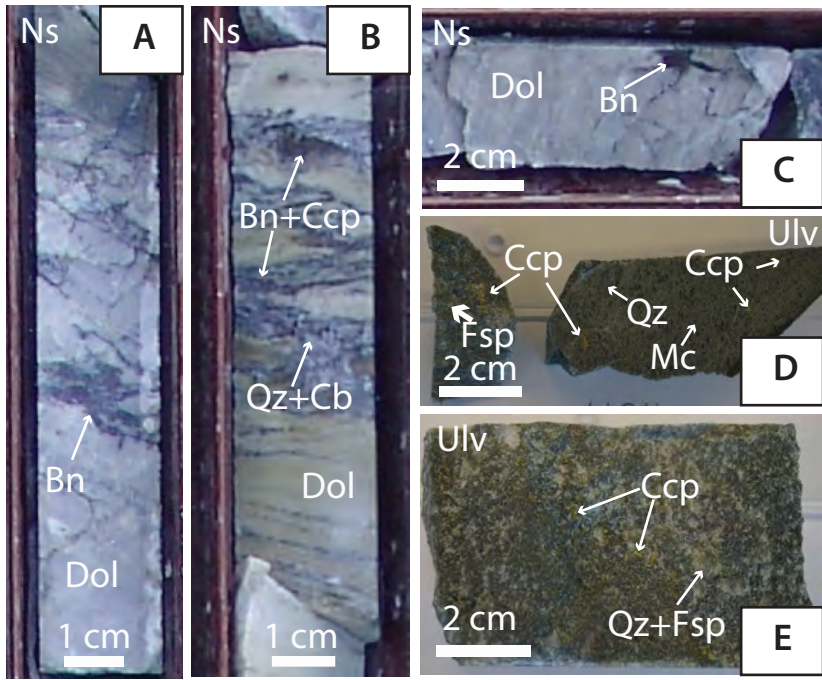


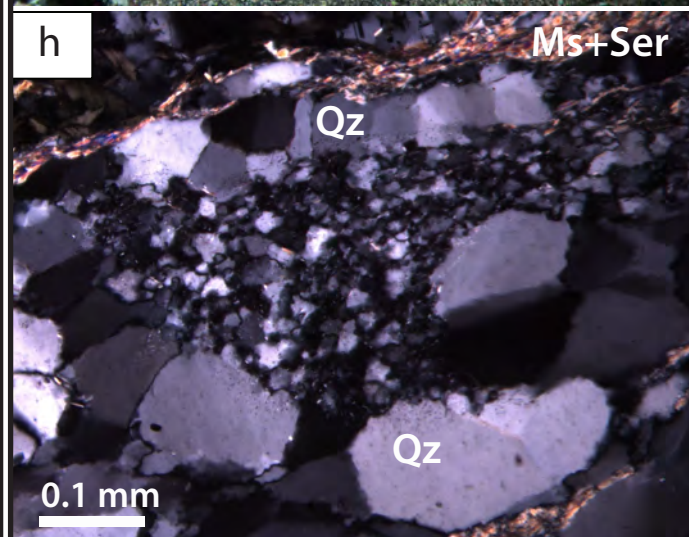
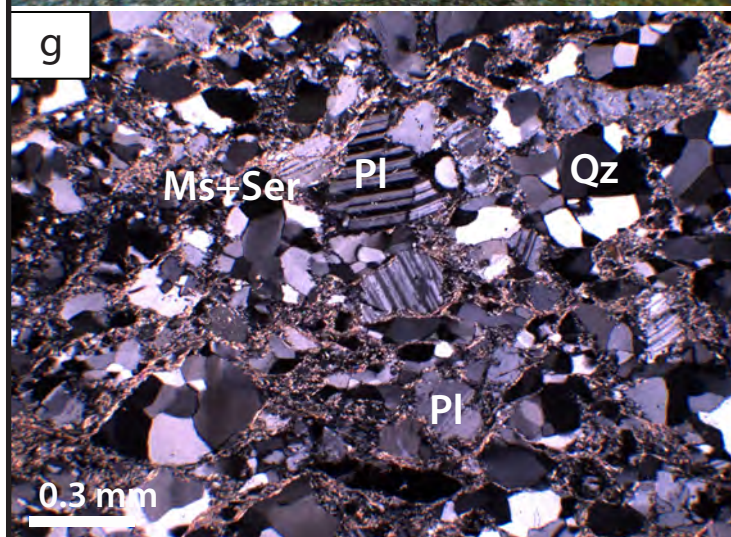
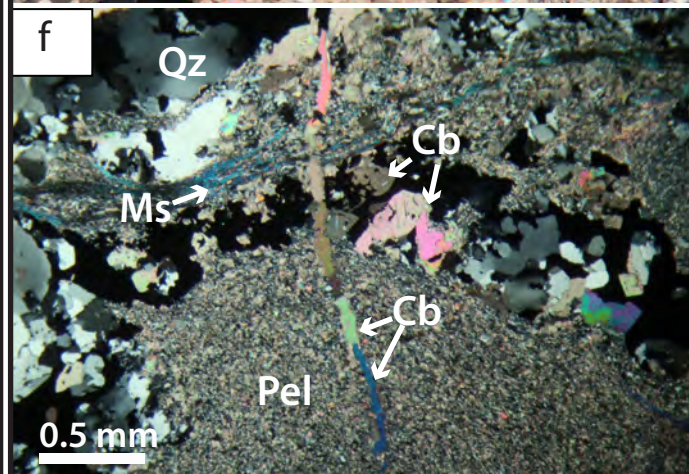
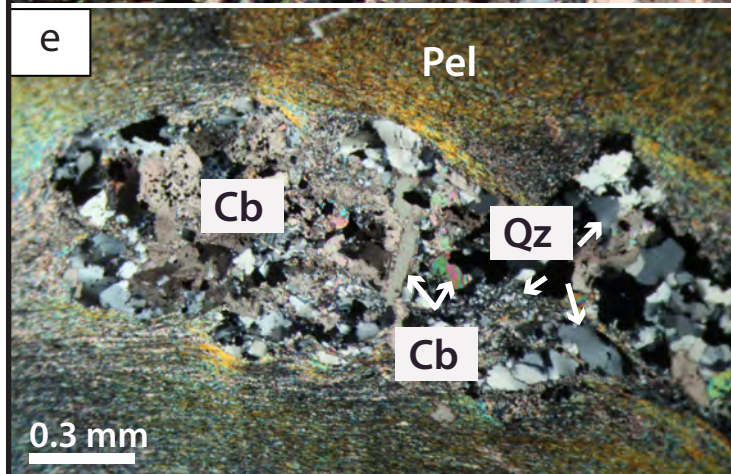
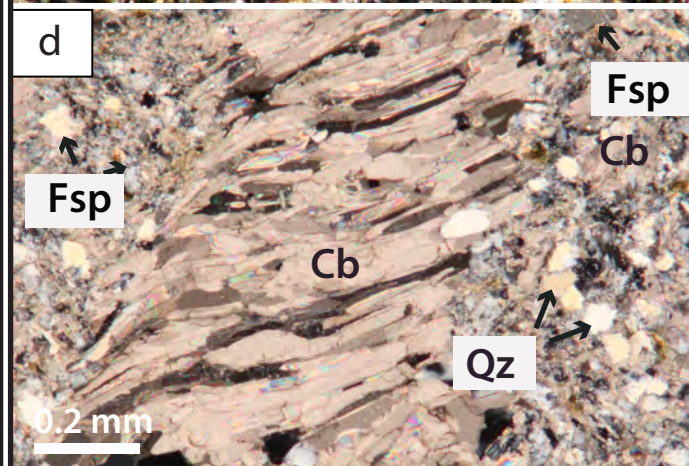
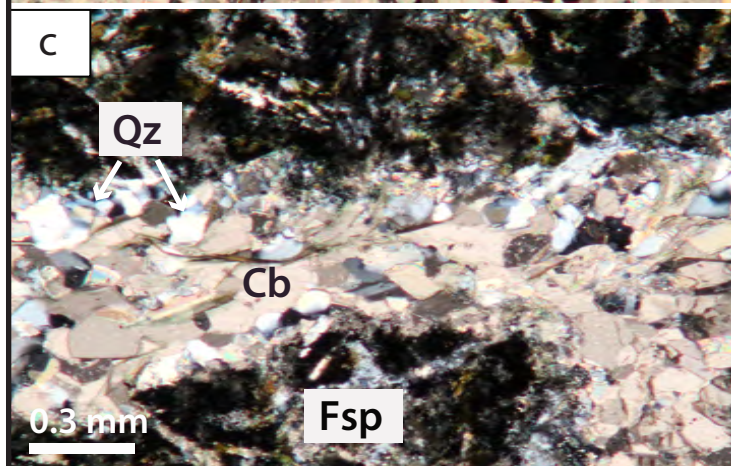
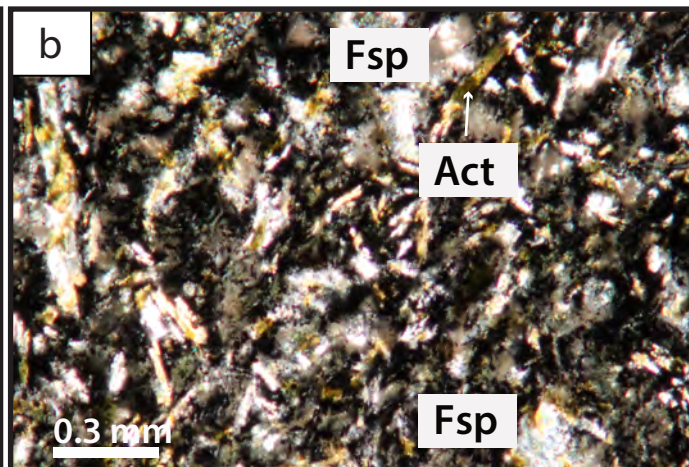
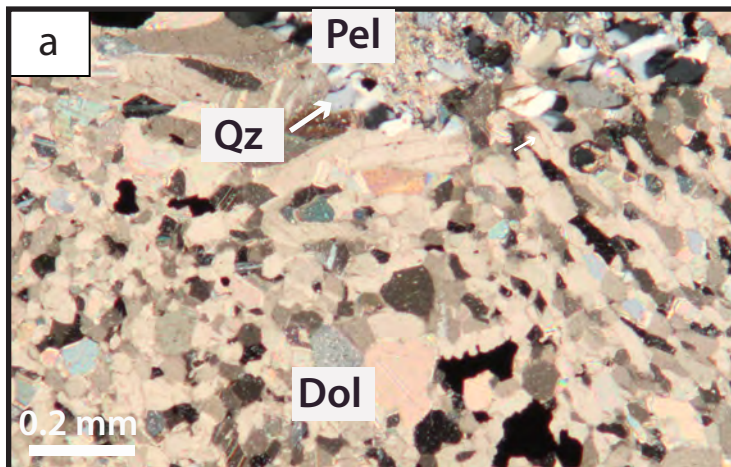
Raipas Supergroup (Pharaoh et al. 1983, Torgersen et al. 2015a)

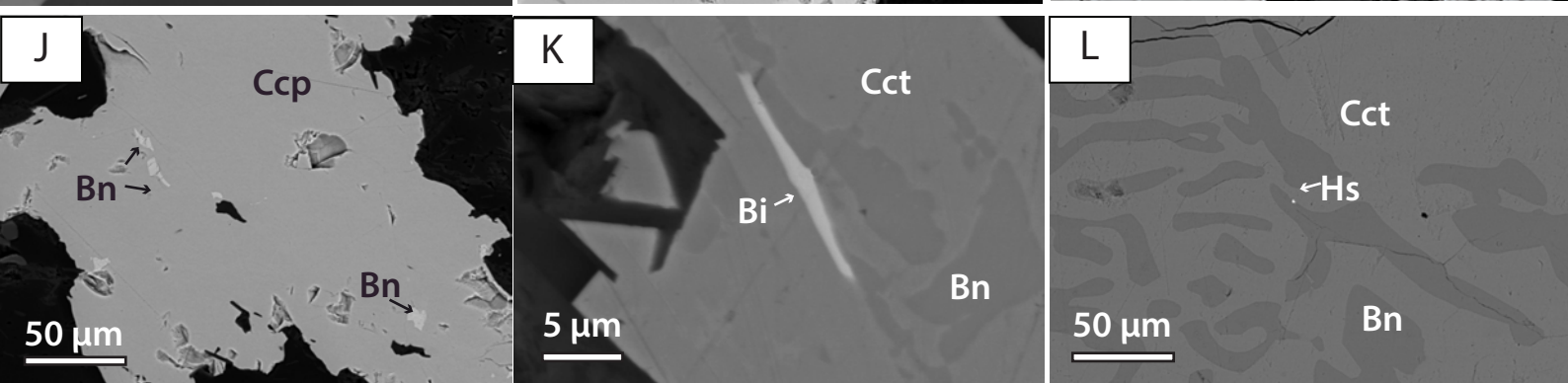
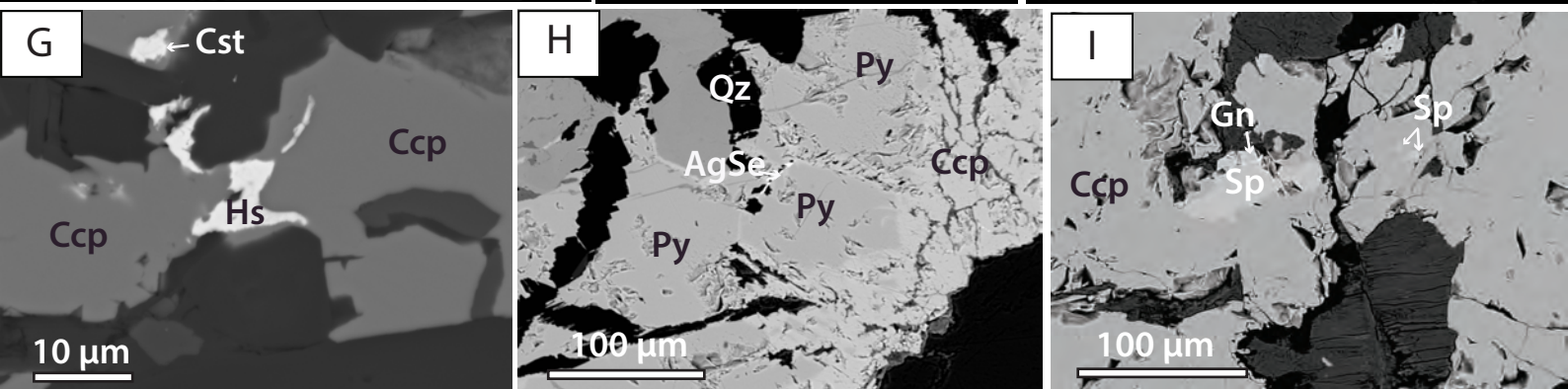
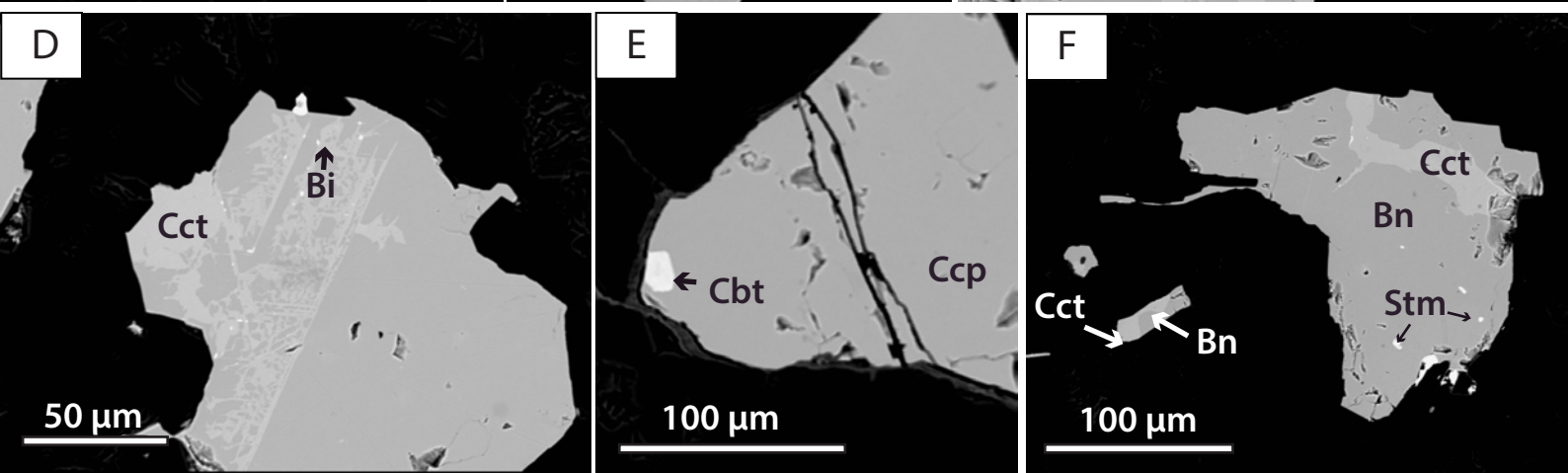
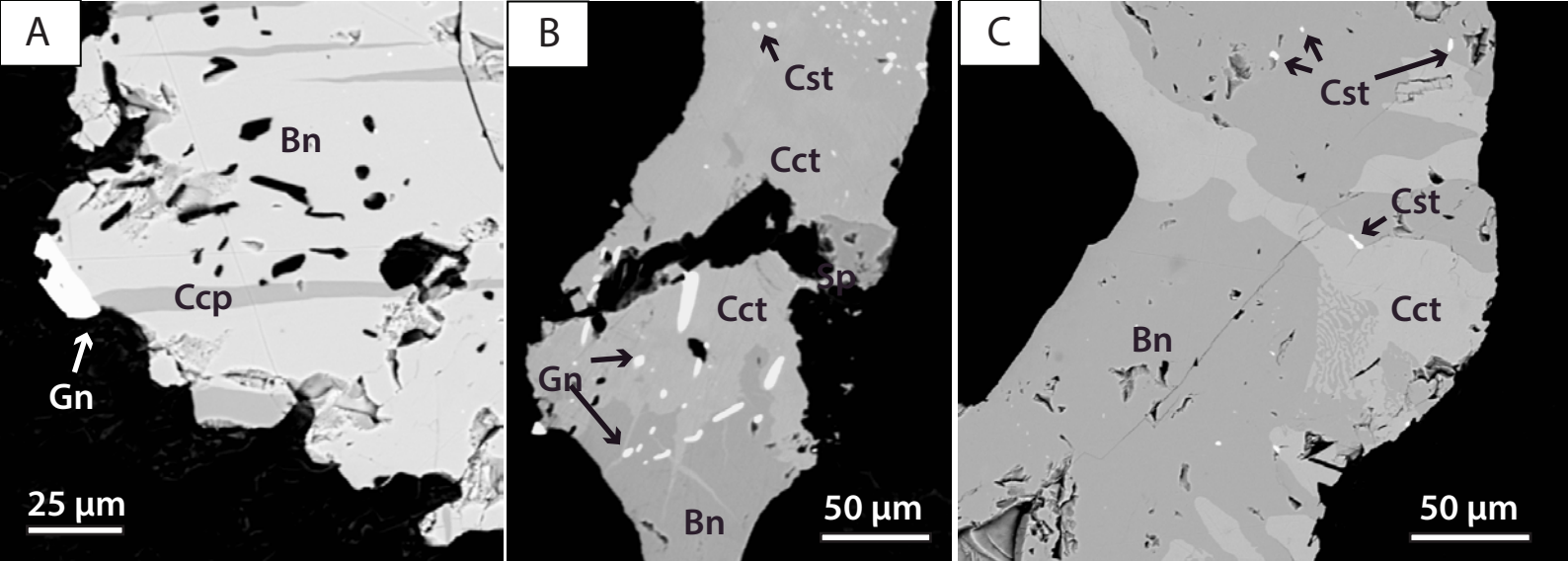


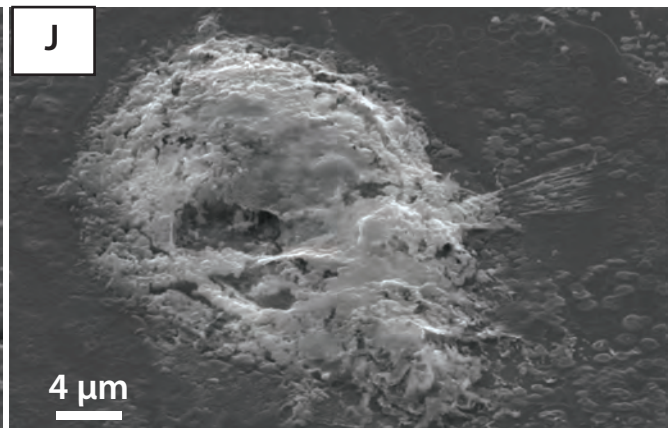
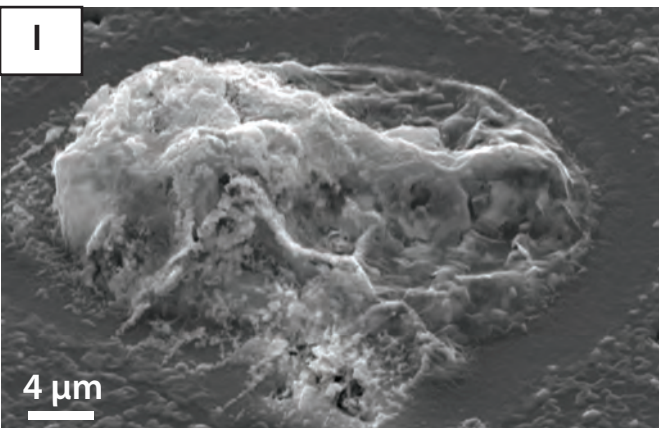
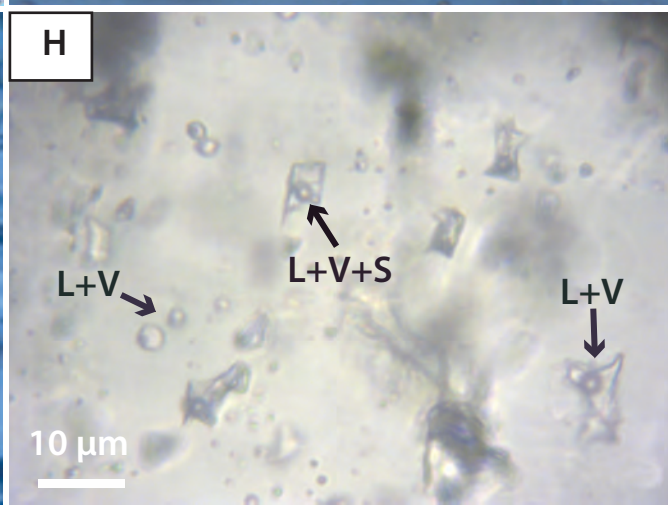
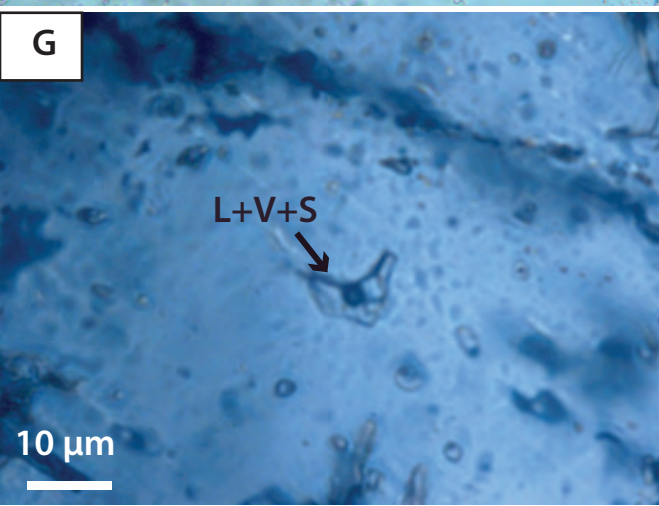
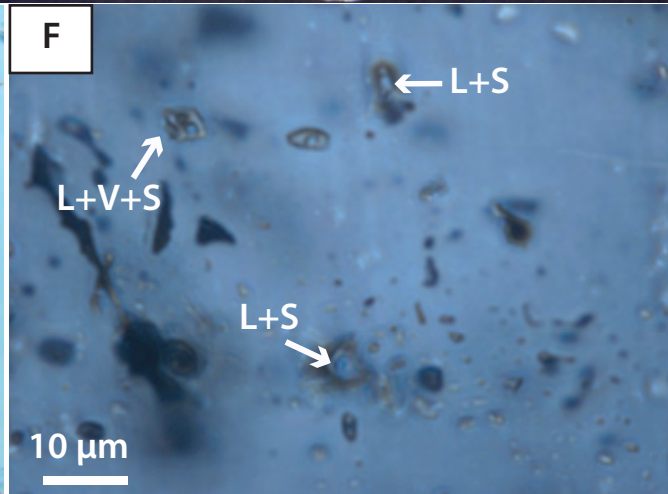
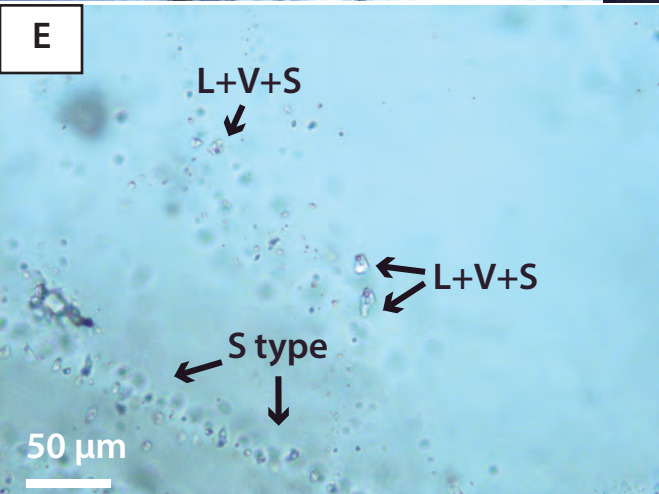
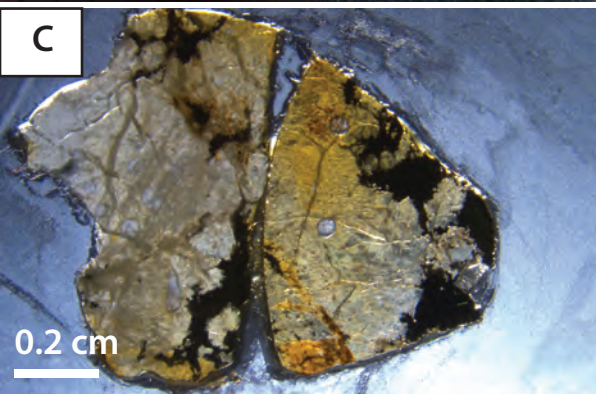
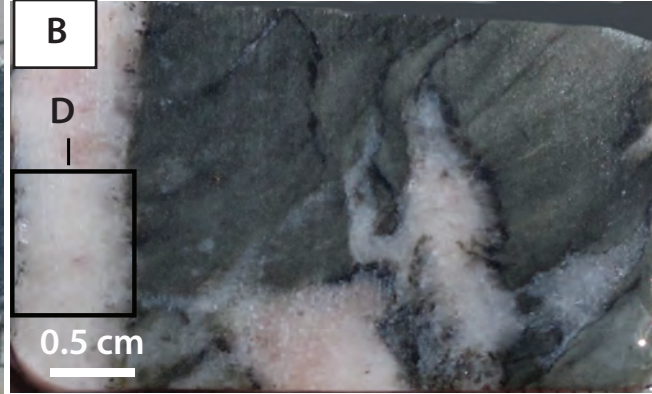
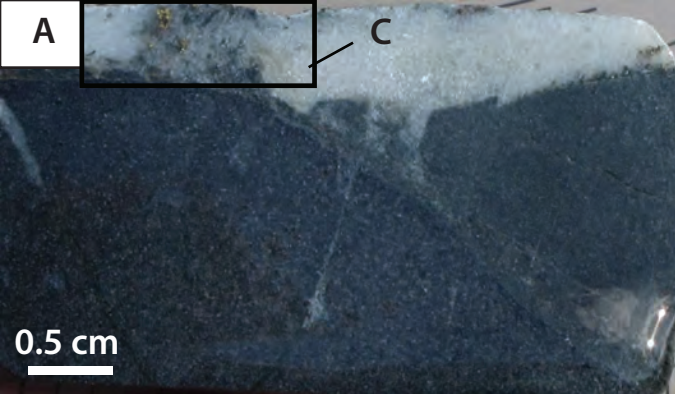


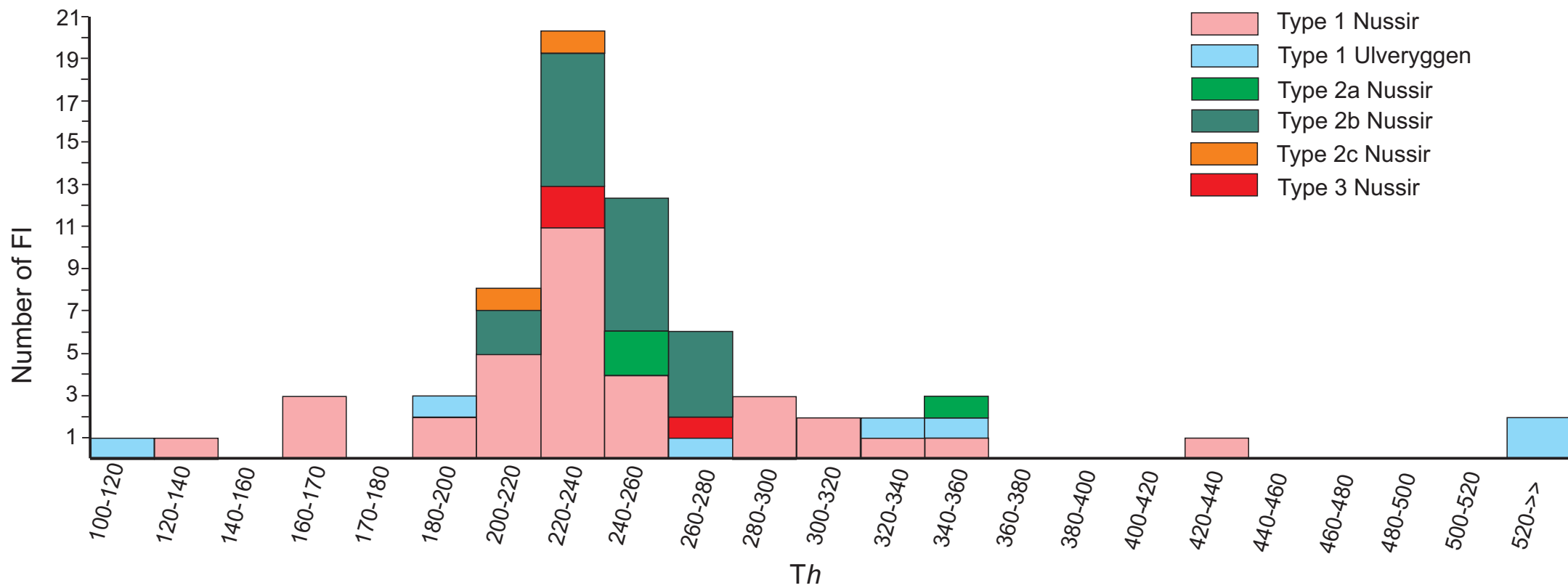
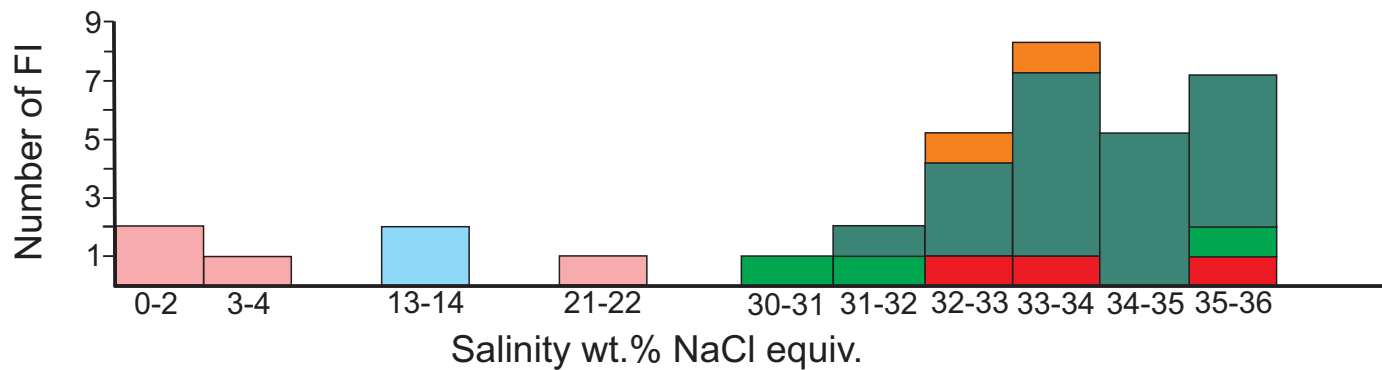


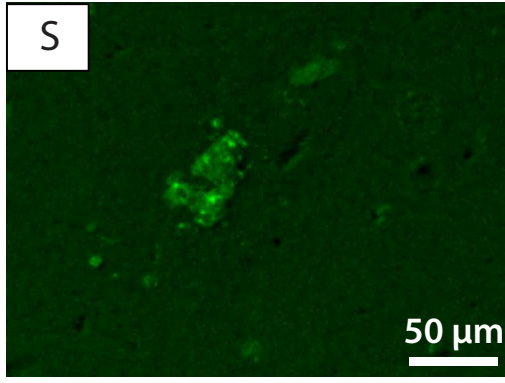
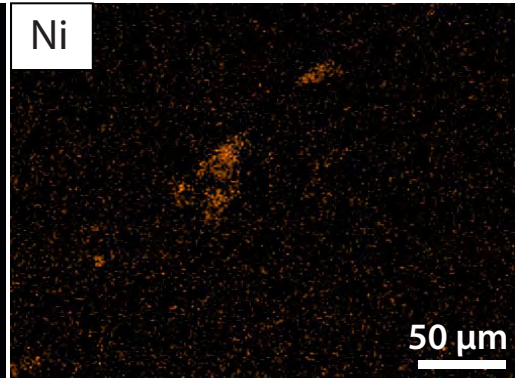
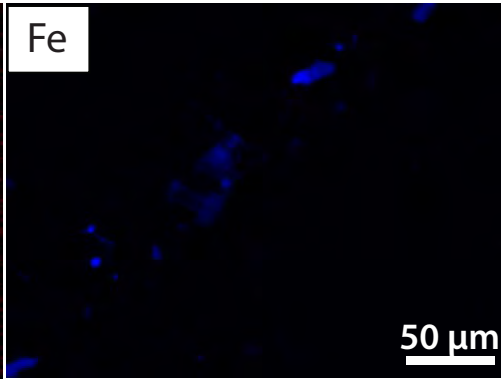
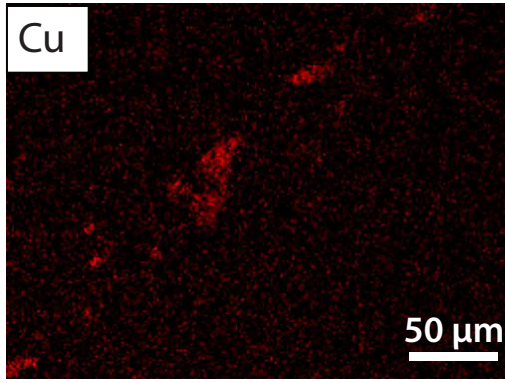
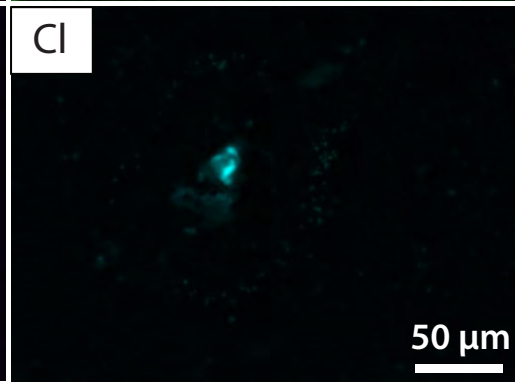
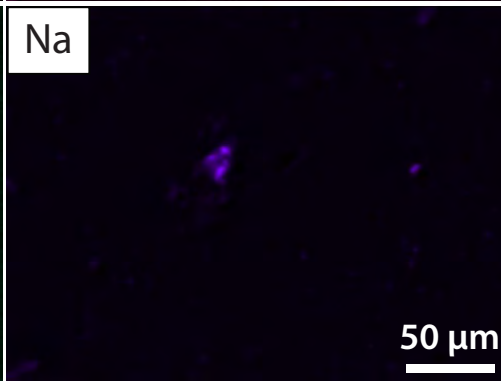
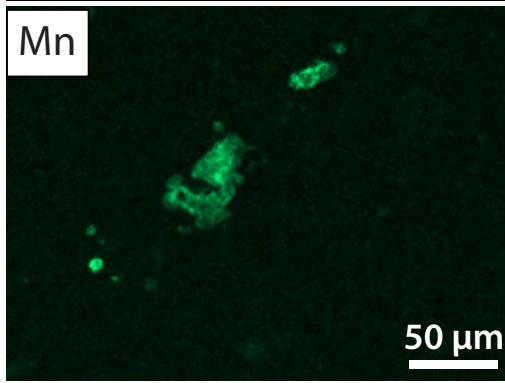
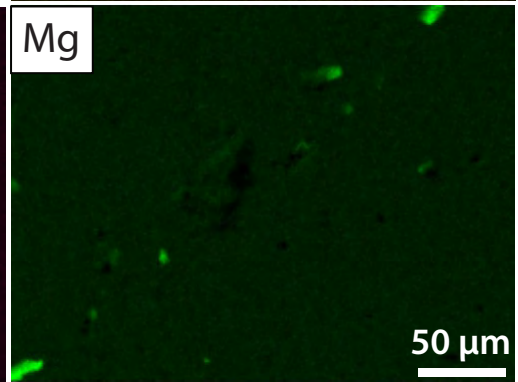
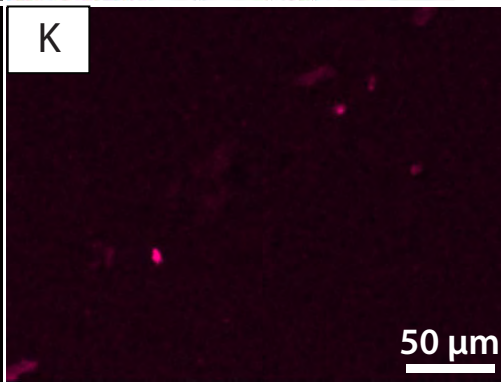
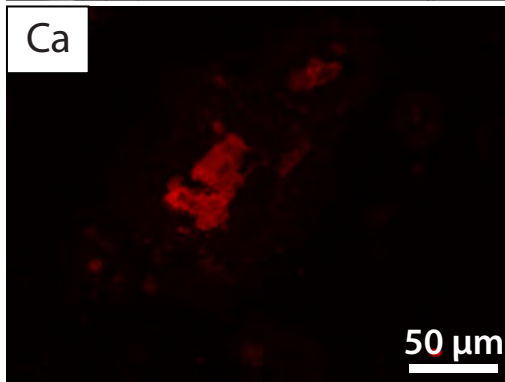
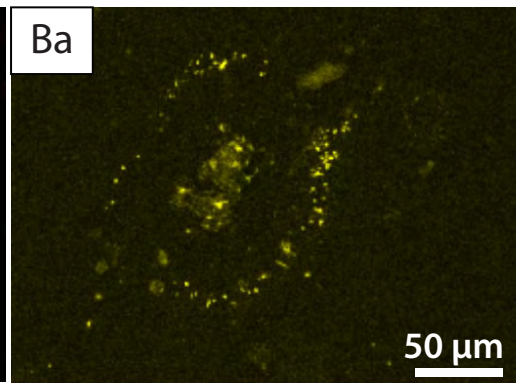
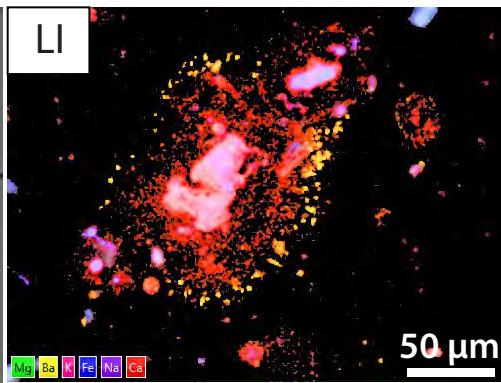
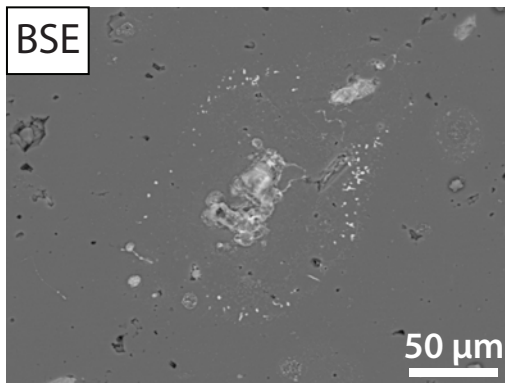


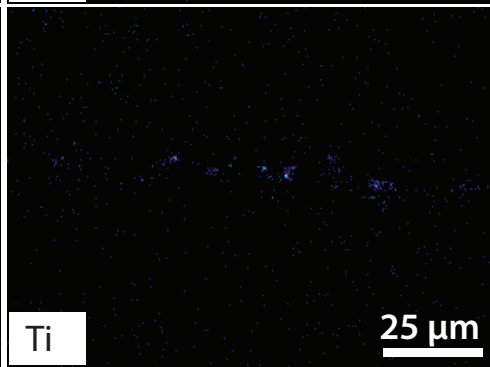
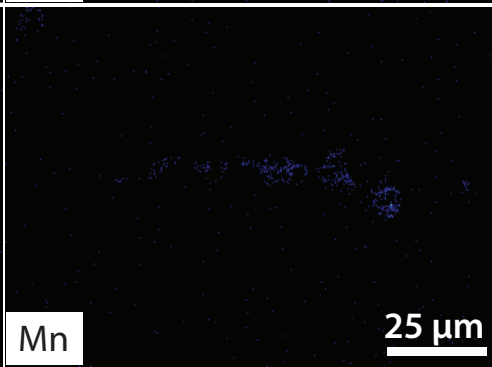
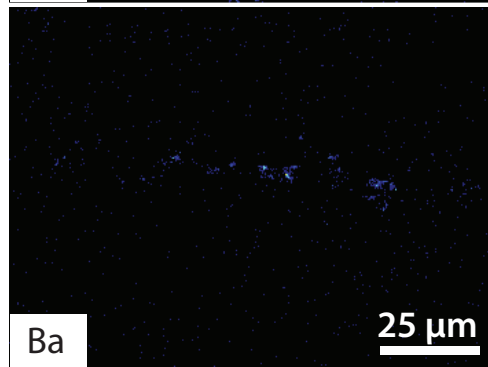
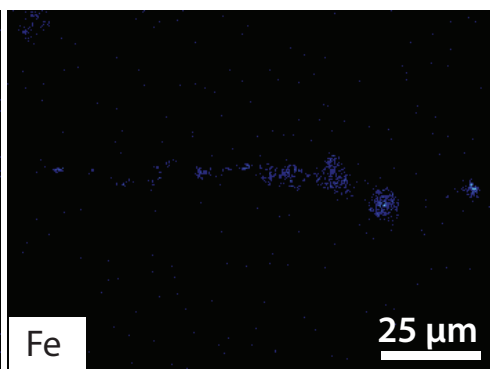
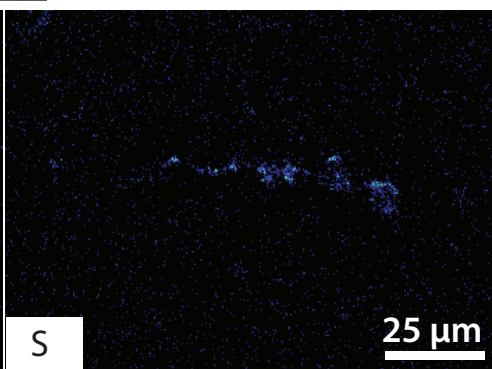
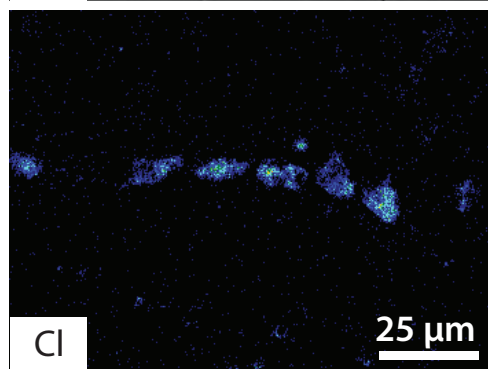
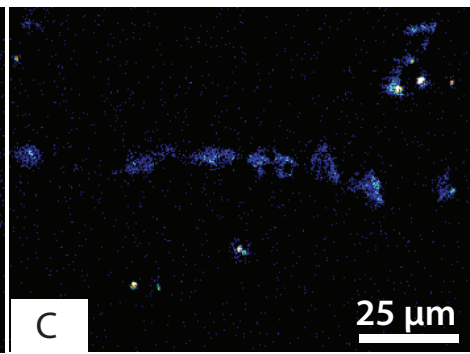
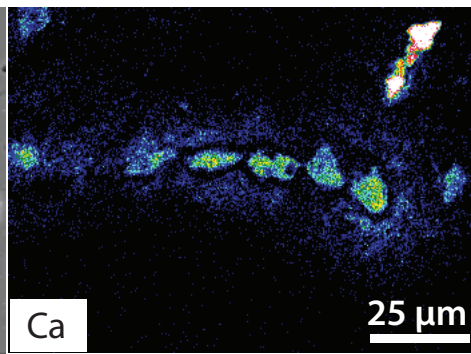
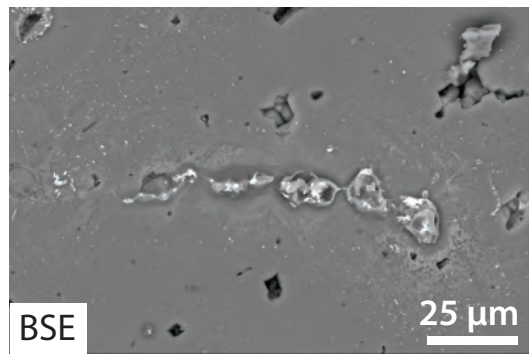


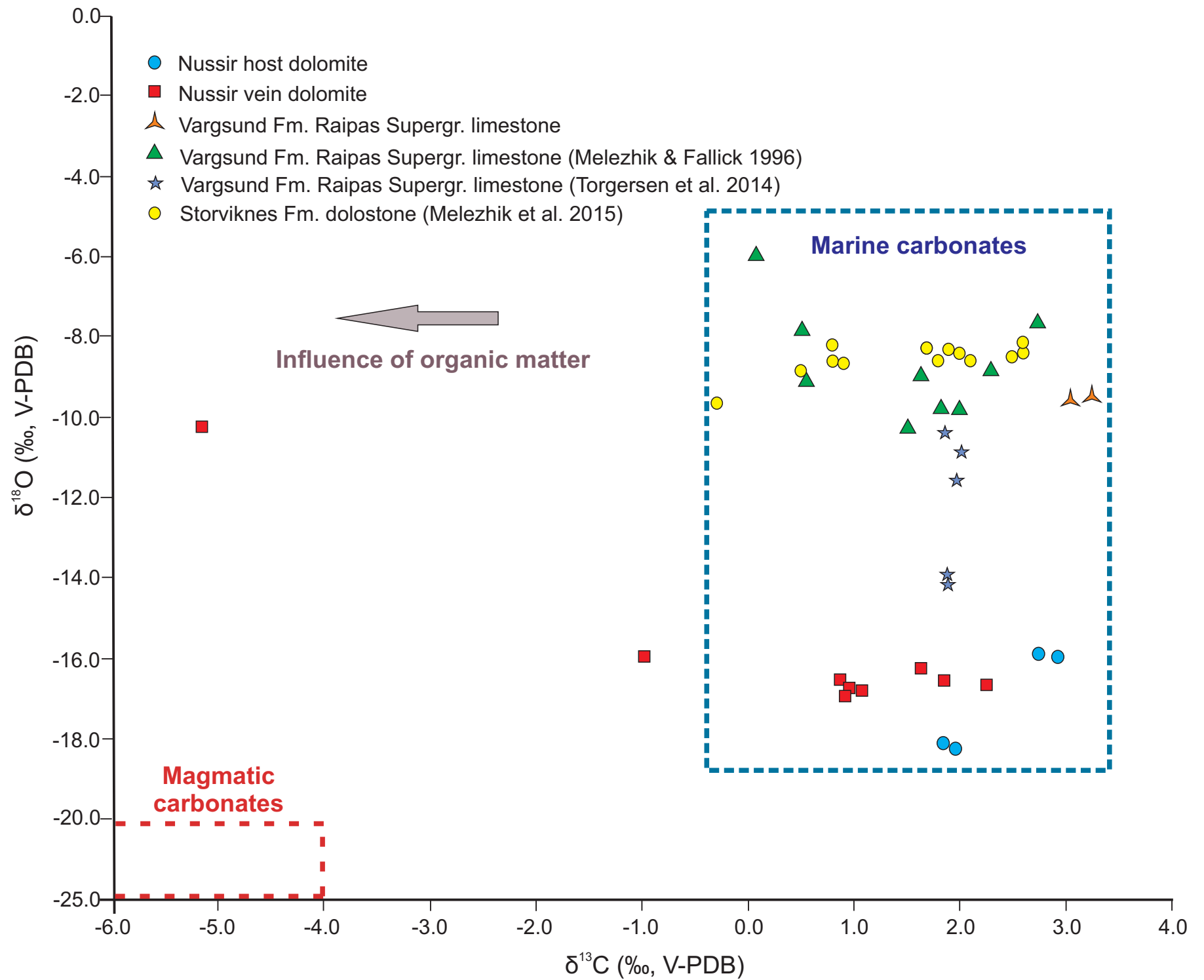


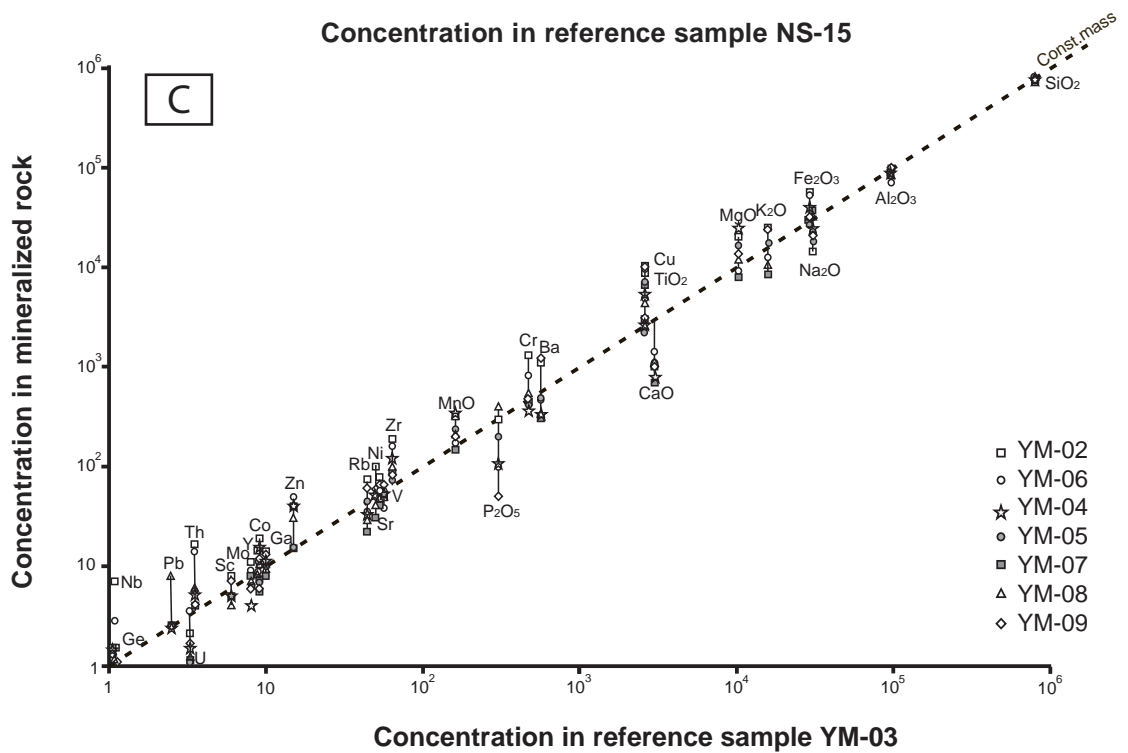
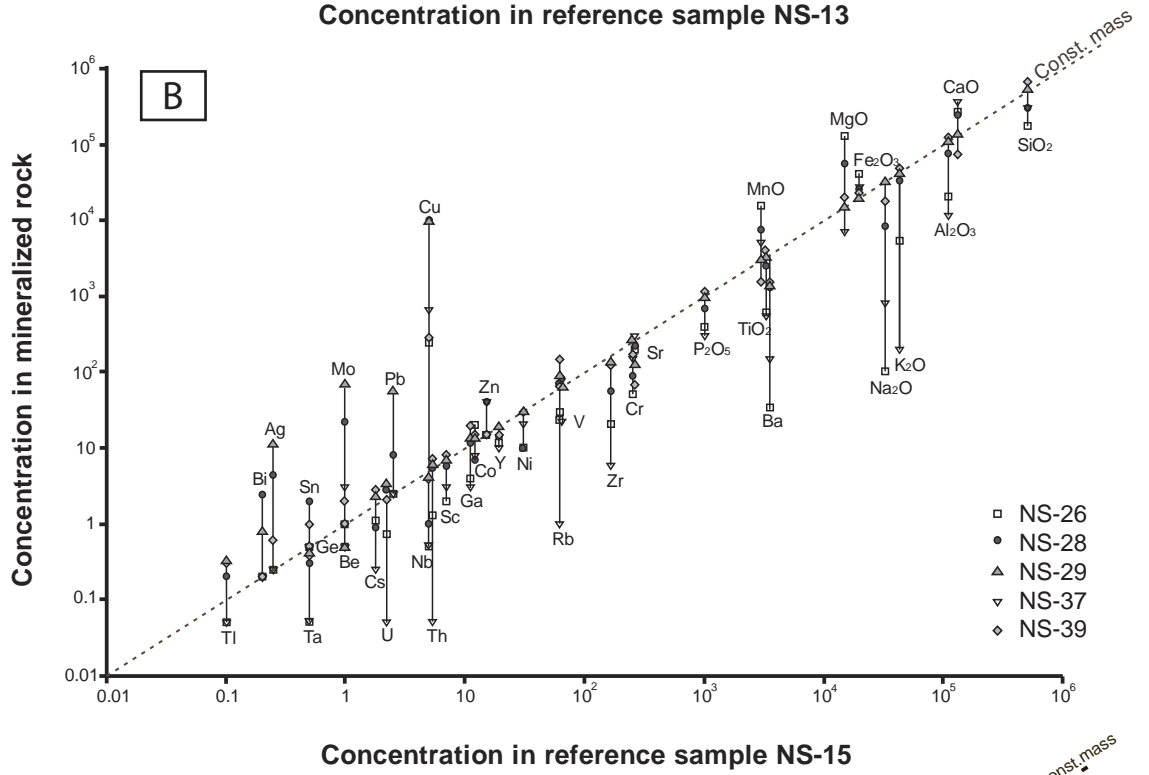
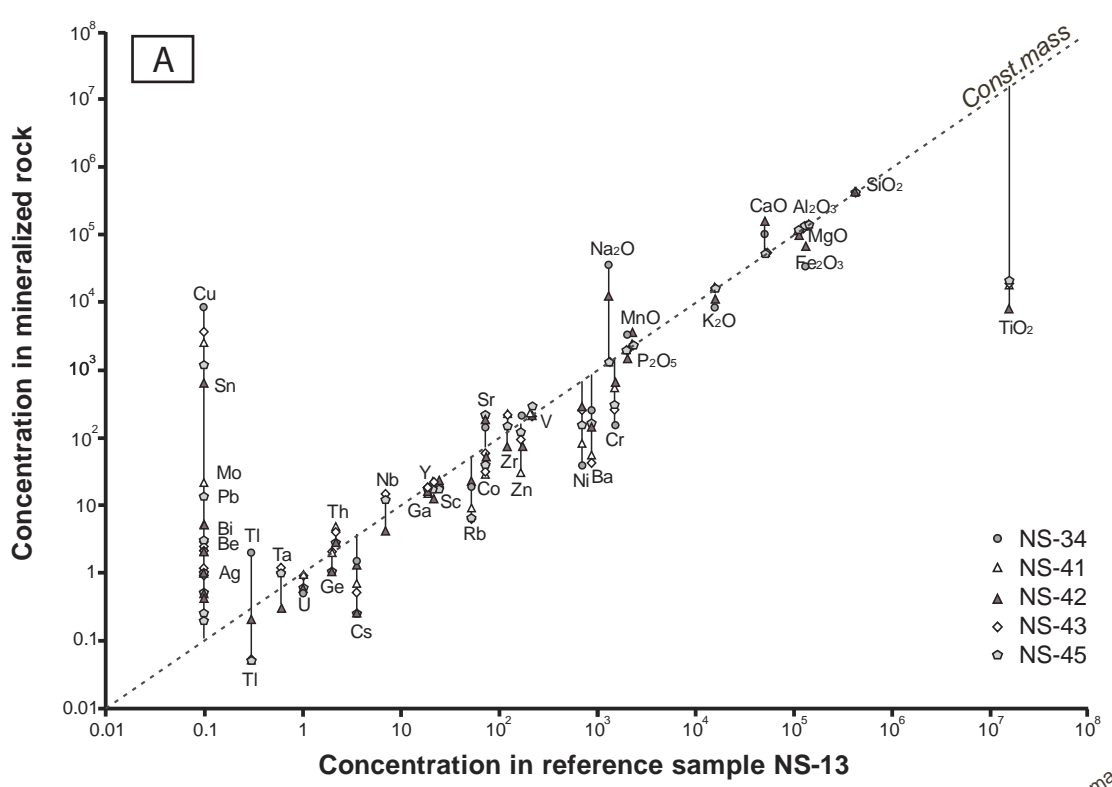


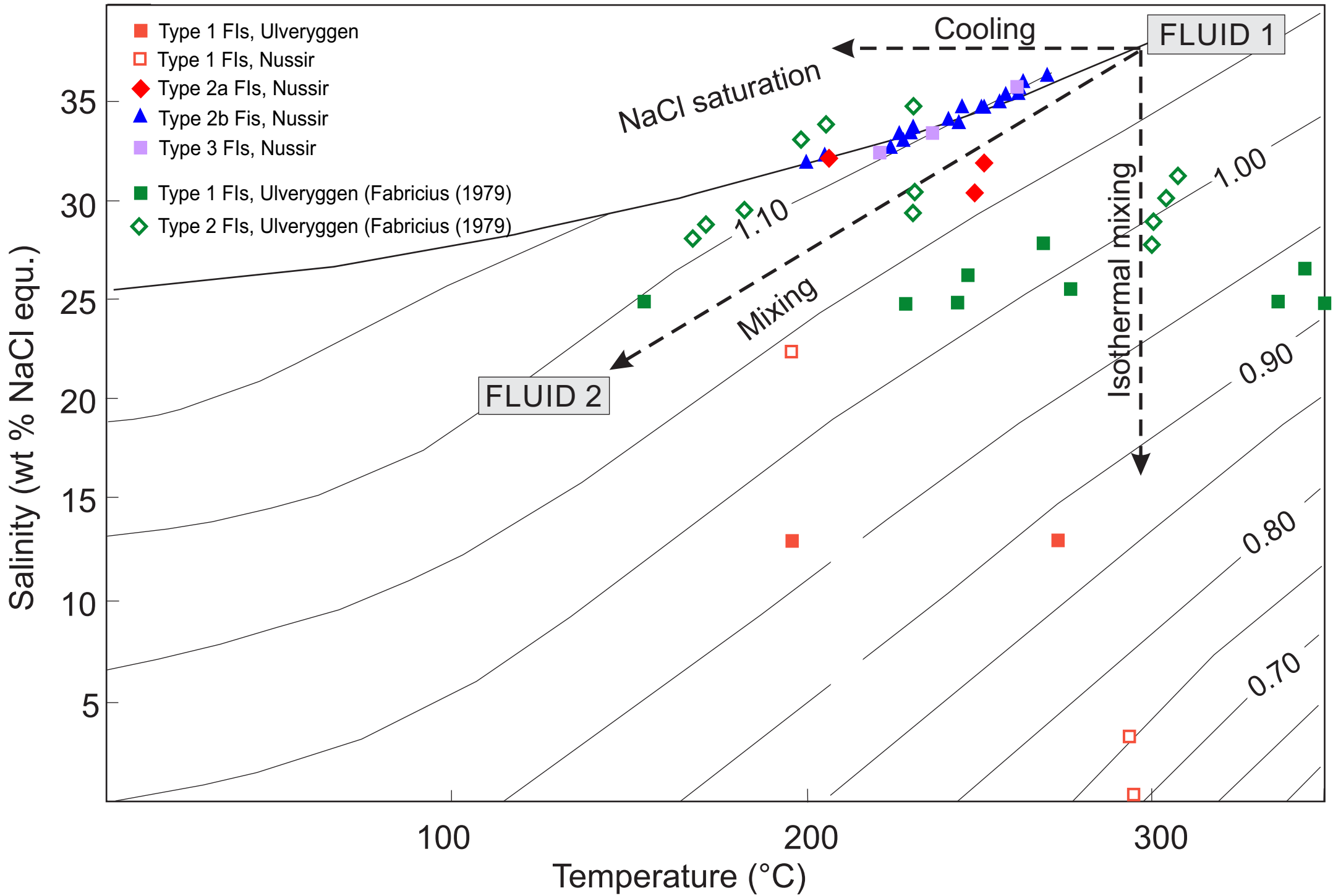


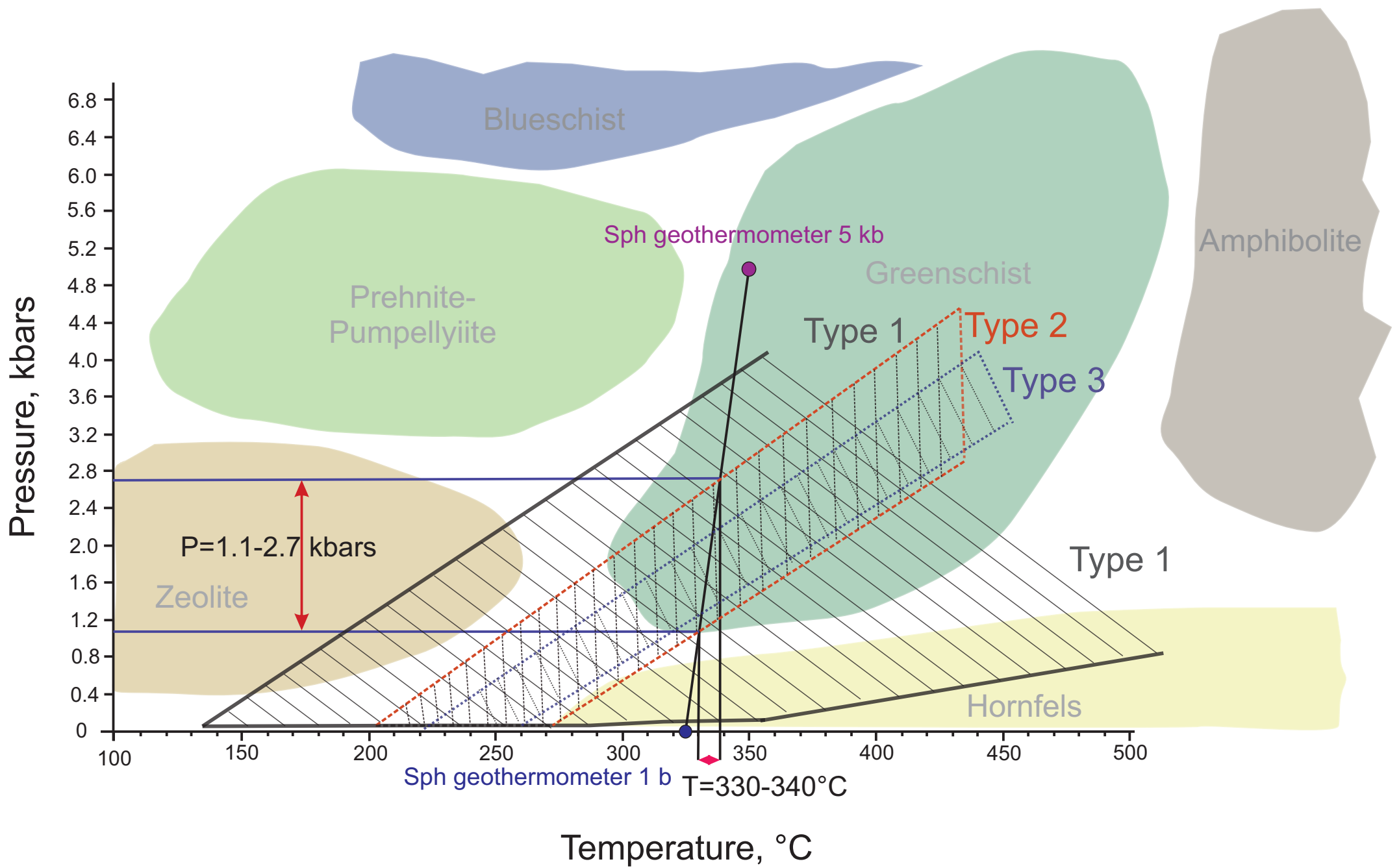


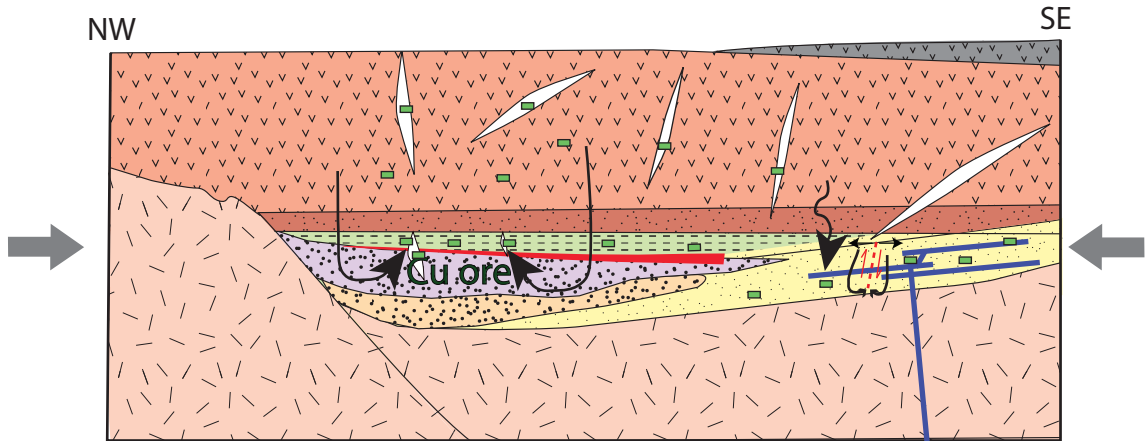












- | | | | |
|------------------|------------------|-----------------------|------------------------|
| andesite | Stangevatnet Fm. | disseminated Cu ore | shear zones |
| basalt | Dypelva Fm. | evaporite | quartz-carbonate veins |
| mafic tuff | Ulveryggen Fm. | Ulveryggen intrusions | |
| Gorahatjohka Fm. | basement | | |

Table 1

Sample number	Nussir Volcanics non-mineralized							Nussir Volcanics mineralized											
	NS-6	NS-13	NS-36	NS-14				NS-10	NS-44	NS-33	NS-8	NS-12	NS-42	NS-45	NS-41	NS-43	NS-34		
Major oxides, %	LD	non-min	non-min	non-min	non-min	MV	SD	low min	low-min	low-min	min	min	min	min	min	min	min	MV	SD
SiO ₂	0.01	54.69	42.60	44.82	59.11	50.31	6.82	45.04	51.41	47.45	52.53	53.01	44.72	45.33	56.32	54.02	41.01	49.08	4.76
Al ₂ O ₃	0.01	14.65	11.45	15.88	10.91	13.22	2.10	12.50	13.59	14.32	13.99	14.45	9.11	11.41	13.46	12.68	11.20	12.67	1.60
Fe ₂ O ₃ (T)	0.01	13.71	13.60	18.38	4.97	12.67	4.84	16.85	15.13	15.30	13.80	15.66	7.05	12.42	16.54	13.27	14.86	14.09	2.69
MnO	0.001	0.171	0.231	0.260	0.212	0.219	0.032	0.196	0.192	0.222	0.131	0.111	0.332	0.301	0.067	0.155	0.244	0.195	0.079
MgO	0.01	6.20	13.17	5.10	1.55	6.51	4.21	3.68	4.69	4.65	2.87	4.36	6.37	3.96	2.30	7.71	3.51	4.41	1.52
CaO	0.01	1.77	5.10	4.30	8.62	4.95	2.45	7.06	4.56	5.58	4.26	2.01	15.17	11.22	2.08	2.61	10.39	6.49	4.21
Na ₂ O	0.01	2.91	0.13	3.88	3.53	2.61	1.47	4.29	5.41	4.34	5.61	3.87	1.18	4.58	6.26	3.14	3.60	4.23	1.36
K ₂ O	0.01	1.53	1.59	1.49	2.05	1.67	0.23	0.83	0.45	1.01	0.73	1.81	1.08	0.44	0.36	0.25	0.87	0.78	0.44
TiO ₂	0.001	1.457	1.576	3.196	0.656	1.721	0.922	1.918	2.350	3.091	1.834	2.023	0.791	2.095	1.434	1.568	2.107	1.921	0.572
P ₂ O ₅	0.01	0.15	0.20	0.24	0.15	0.19	0.04	0.15	0.30	0.34	0.24	0.22	0.14	0.26	0.11	0.16	0.32	0.22	0.08
LOI		3.75	8.98	3.33	7.76			5.97	2.37	2.53	3.70	2.84	14.34	7.33	1.62	5.11	9.36		
Total		101.00	98.63	100.90	99.52			98.50	100.50	98.82	99.69	100.40	100.30	99.36	100.60	100.70	97.47		
Trace elements, ppm																			
Sc	1	31	25	23	9	22	8	21	22	28	20	27	22	17	21	19	18	22	3
Be	1	2	LLD	2	LLD	1	1	1	2	2	1	2	LLD	1	1	1	2	1	1
V	5	226	219	327	83	214	87	411	319	332	213	245	193	268	246	208	225	266	65
Ba	3	328	865	409	1126	682	328	185	137	295	207	381	140	167	53	43	256	186	99
Sr	2	63	73	123	154	103	37	68	159	129	58	30	171	216	42	31	141	105	63
Y	2	24	22	35	19	25	6	17	23	25	19	22	12	18	22	22	16	20	4
Zr	4	196	125	238	225	196	44	100	163	229	148	173	72	142	222	215	159	162	49
Cr	20	760	1540	150	250	675	550	70	160	150	540	720	630	250	520	240	160	344	222
Co	1	72	74	49	14	52	24	36	48	41	40	48	51	39	29	61	52	45	9
Ni	20	360	700	110	30	300	261	50	110	90	180	250	280	160	80	250	40	149	84
Cu	10	10	LLD	10	50	18	19	80	110	120	230	280	620	1190	2520	3700	8610	1746	2562
Zn	30	110	170	200	LLD	120	76	60	140	160	50	60	70	120	30	90	210	99	54
Ga	1	23	19	27	11	20	6	20	21	22	20	25	15	17	15	19	16	19	3
Ge	1	3	2	LLD	1	2	1	2	1	1	2	3	1	1	2	2	LLD	2	1
As	5	LLD	LLD	LLD	LLD			LLD	LLD	LLD	LLD	LLD	LLD	LLD	LLD	LLD	LLD	24	7
Rb	2	50	53	36	58	49	8	27	8	22	21	58	22	6	9	6	18	20	15
Nb	1	11	7	19	6	11	5	6	13	19	11	12	4	12	13	14	15	12	4
Mo	2	LLD	LLD	LLD	LLD			LLD	LLD	LLD	LLD	LLD	LLD	3	22	LLD	LLD	3	7
Ag	0.5	0.8	LLD	1.5	0.5	0.7	0.5	LLD	LLD	1.7	LLD	0.7	LLD	LLD	1.0	1.1	1.1	0.6	0.6
In	0.2	0.2	LLD	LLD	LLD	0.1	0.1	LLD	LLD	LLD	LLD	LLD	LLD	LLD	LLD	LLD	0.2	0.0	0.1
Sn	1	2	LLD	2	LLD	1	1	LLD	1	2	2	2	LLD	LLD	2	2	1	1	1
Sb	0.5	LLD	LLD	LLD	LLD			LLD	LLD	LLD	LLD	LLD	LLD	LLD	LLD	LLD	LLD		
Cs	0.5	1.6	3.5	3.3	2.0	2.6	0.8	1.7	LLD	1.9	1.0	1.6	1.3	LLD	0.7	0.5	1.5	1.0	0.7
Hf	0.2	4.8	3.2	6.2	5.4	4.9	1.1	2.7	3.9	6.2	3.7	4.4	2.0	3.3	5.7	5.1	3.8	4.1	1.2
Ta	0.1	1.0	0.6	1.5	0.6	0.9	0.4	0.5	1.1	1.6	0.8	1.0	0.3	1.0	1.1	1.1	1.0	1.0	0.3
W	1	LLD	LLD	LLD	LLD			LLD	LLD	LLD	LLD	LLD	LLD	LLD	LLD	LLD	2	0	1
Tl	0.1	0.2	0.3	0.3	0.2	0.3	0.1	LLD	LLD	LLD	LLD	LLD	0.2	0.2	LLD	LLD	2.0	0.2	0.6
Pb	5	LLD	LLD	LLD	LLD			LLD	7	LLD	LLD	LLD	LLD	13	LLD	LLD	LLD	2	4
Bi	0.4	LLD	LLD	LLD	LLD			LLD	0.0	LLD	LLD	LLD	LLD	LLD	4.9	2.7	LLD	0.8	1.6
Th	0.1	4.7	2.2	4.0	5.7	4.2	1.3	2.3	3.2	3.8	2.6	3.2	2.8	2.8	4.8	4.2	2.8	3.3	0.7
U	0.1	1.1	1.0	0.9	2.1	1.3	0.5	0.6	0.8	0.9	0.5	0.7	0.6	0.6	0.9	0.9	0.5	0.7	0.2
REE, ppm																			
La	0.1	23.2	13.6	31.7	16.2	21.2	7.0	9.6	36.0	25.0	20.3	21.1	11.5	32.2	25.2	17.6	12.3	21.1	8.3
Ce	0.1	51.2	28.9	75.1	35.3	47.6	17.8	23.2	75.3	60.8	46.4	46.3	23.8	70.1	53.2	40.6	28.5	46.8	17.5
Pr	0.05	6.84	4.00	10.50	4.35	6.42	2.60	3.12	9.37	8.24	5.98	5.99	3.04	8.67	7.18	5.55	3.79	6.09	2.17
Nd	0.1	29.7	18.4	45.9	17.0	27.8	11.6	14.3	38.4	34.6	25.5	26.7	12.8	35.7	30.2	24.3	16.1	25.9	8.7
Sm	0.1	6.9	5.1	9.9	4.1	6.5	2.2	3.5	7.4	7.7	5.5	5.9	2.9	7.0	6.3	5.5	3.4	5.5	1.6
Eu	0.05	1.86	1.60	2.48	0.88	1.71	0.57	1.20	2.31	1.87	1.65	1.79	0.75	1.89	1.67	1.51	0.86	1.55	0.46
Gd	0.1	6.1	4.8	8.9	3.6	5.9	2.0	3.7	6.0	5.8	4.5	5.1	2.6	5.1	5.0	4.9	3.1	4.6	1.1
Tb	0.1	0.9	0.8	1.4	0.6	0.9	0.3	0.6	0.9	0.9	0.7	0.8	0.4	0.7	0.8	0.8	0.5	0.7	0.2
Dy	0.1	5.1	4.6	8.2	3.4	5.3	1.8	3.7	4.8	5.6	4.2	4.8	2.6	3.7	4.8	4.6	3.0	4.2	0.9
Ho	0.1	1.0	0.9	1.5	0.7	1.0	0.3	0.7	0.9	1.1	0.8	0.9	0.5	0.7	0.9	0.9	0.6	0.8	0.2
Er	0.1	2.8	2.3	4.1	2.0	2.8	0.8	1.9	2.5	3.1	2.1	2.6	1.4	2.0	2.7	2.4	1.8	2.3	0.5
Tm	0.05	0.38	0.31	0.56	0.28	0.38	0.11	0.26	0.34	0.43	0.29	0.37	0.21	0.29	0.36	0.33	0.26	0.31	0.06
Yb	0.1	2.3	1.8	3.1	1.9	2.3	0.5	1.6	2.1	2.7	1.8	2.3	1.3	1.8	2.2	2.2	1.7	2.0	0.4
Lu	0.04	0.33	0.25	0.39	0.29	0.32	0.05	0.24	0.30	0.39	0.26	0.32	0.18	0.25	0.35	0.31	0.24	0.28	0.06

Note: LD - limit of detection; LLD - lower than limit of detection; MV - mean value; SD - standard deviation; min - mineralized

Table 2

Nussir

Carbonate-siliciclastic rocks

Sample number		NS-15	NS-18	NS-20	NS-38	NS-24	NS-32	NS-26	NS-39	NS-37	NS-40	NS-27	NS-28	NS-29		
Major oxides, %	LD	non-min	non-min	non-min	low-min	low-min	low-min	min	min	min	min	min	min	min	MV	SD
SiO ₂	0.01	61.20	63.33	68.60	51.90	33.09	60.51	17.34	60.04	28.95	65.55	58.75	31.86	50.91	50.16	15.95
Al ₂ O ₃	0.01	10.50	15.08	9.88	8.84	4.21	14.12	2.02	11.94	1.16	11.43	17.26	7.83	11.13	9.65	4.66
Fe ₂ O ₃ (T)	0.01	2.17	5.97	4.04	2.58	3.31	3.38	4.00	2.22	2.69	0.81	9.62	2.58	1.97	3.49	2.14
MnO	0.001	0.216	0.054	0.123	0.316	0.754	0.190	1.567	0.153	0.495	0.156	0.022	0.740	0.308	0.392	0.408
MgO	0.01	1.30	2.25	0.92	1.85	1.43	3.80	12.89	1.98	0.68	0.38	1.92	5.58	1.50	2.81	3.20
CaO	0.01	8.98	1.62	4.89	16.04	30.15	4.32	26.46	7.54	35.48	7.52	0.75	23.14	13.18	13.85	11.02
Na ₂ O	0.01	3.25	0.99	1.34	0.95	0.03	1.02	0.01	1.78	0.08	2.84	0.54	0.86	3.26	1.30	1.11
K ₂ O	0.01	2.02	7.59	5.66	3.62	2.31	6.26	0.53	4.82	0.02	5.42	6.70	3.47	4.31	4.06	2.25
TiO ₂	0.001	0.468	0.529	0.421	0.276	0.213	0.496	0.060	0.385	0.054	0.229	1.030	0.256	0.326	0.365	0.241
P ₂ O ₅	0.01	0.15	0.13	0.12	0.09	0.07	0.13	0.04	0.11	0.03	0.10	0.12	0.07	0.10	0.10	0.03
LOI		8.76	3.25	4.73	14.09	24.41	6.46	34.60	7.52	29.04	6.43	3.26	20.10	10.12	13.29	10.02
Total		99.02	100.80	100.70	100.60	99.97	100.70	99.52	98.49	98.68	100.90	99.99	96.48	97.10	99.46	1.39
Trace elements, ppm																
Sc	1	7	12	5	6	4	11	2	8	3	4	10	6	7	7	3
Be	1	1	2	LLD	1	LLD	2	LLD	2	LLD	LLD	4	1	LLD	1	1
V	5	64	146	72	48	60	82	30	65	22	27	113	77	67	67	33
Ba	3	3512	1898	3597	1067	620	1462	34	1549	146	1974	1635	1333	1418	1557	1030
Sr	2	262	39	112	140	112	54	194	69	297	71	44	232	130	135	83
Y	2	19	14	16	13	16	10	12	15	10	7	42	14	19	16	8
Zr	4	167	153	273	108	93	199	21	128	6	121	435	56	134	146	108
Cr	20	250	230	330	240	150	210	50	170	150	240	90	90	270	190	78
Co	1	12	20	8	15	7	15	20	15	8	3	30	7	13	13	7
Ni	20	30	50	20	40	LLD	50	LLD	30	20	LLD	30	LLD	30	23	18
Cu	10	LLD	LLD	LLD	20	30	110	250	280	650	1500	4970	>10000	>10000	2139	3595
Zn	30	LLD	LLD	LLD	LLD	LLD	90	LLD	LLD	40	LLD	LLD	40	LLD	13	26
Ga	1	11	24	11	11	8	19	4	18	3	11	30	12	13	13	7
Ge	1	LLD	1	LLD	LLD	LLD	LLD	LLD	LLD	LLD	LLD	1	LLD	0	0	0
As	5	LLD	LLD	LLD	LLD	LLD	LLD	LLD	LLD	LLD	LLD	LLD	LLD	LLD	LLD	LLD
Rb	2	62	253	124	133	60	224	24	147	LLD	81	208	70	89	113	75
Nb	1	5	4	5	3	2	5	LLD	4	LLD	2	25	1	4	5	6
Mo	2	LLD	LLD	3	3	LLD	6	LLD	LLD	3	10	7	22	68	9	18
Ag	0.5	LLD	LLD	0.9	0.6	LLD	3.0	LLD	0.6	LLD	0.5	2.5	4.4	11.3	1.8	3.0
In	0.2	LLD	LLD	LLD	LLD	LLD	LLD	LLD	LLD	LLD	LLD	LLD	LLD	LLD	LLD	LLD
Sn	1	LLD	1	LLD	LLD	LLD	1	LLD	1	LLD	LLD	4	2	0	1	1
Sb	0.5	LLD	LLD	LLD	LLD	LLD	LLD	LLD	LLD	LLD	LLD	LLD	LLD	LLD	LLD	LLD
Cs	0.5	1.8	4.3	1.6	2.8	1.1	7.2	1.1	2.9	LLD	0.5	4.2	0.9	2.3	2.4	1.9
Hf	0.2	4.4	3.9	6.7	2.7	2.3	5.1	0.6	3.2	LLD	2.8	10.5	1.5	3.6	3.6	2.6
Ta	0.1	0.5	0.5	0.5	0.4	0.2	0.6	LLD	0.4	LLD	0.2	2.3	0.3	0.4	0.5	0.6
W	1	LLD	LLD	LLD	LLD	LLD	LLD	LLD	LLD	LLD	LLD	LLD	LLD	1	LLD	0
Tl	0.1	0.1	0.6	0.3	0.3	0.2	0.8	0.0	0.3	LLD	0.1	0.6	0.2	0.3	0.3	0.2
Pb	5	LLD	LLD	LLD	LLD	5	LLD	LLD	LLD	LLD	11	7	8	57	7	15
Bi	0.4	LLD	LLD	LLD	LLD	LLD	LLD	LLD	LLD	LLD	0.9	1.8	2.4	0.8	0.5	0.8
Th	0.1	5.3	7.6	6.8	4.3	3.2	7.4	1.3	7.2	LLD	1.1	10.5	5.3	6.1	5.1	2.9
U	0.1	2.2	3.8	2.8	1.8	2.7	2.3	0.7	2.1	LLD	1.8	2.7	2.7	3.4	2.2	1.0
REE, ppm																
La	0.1	15.1	26.0	21.4	22.3	18.3	22.7	48.0	18.1	0.6	24.3	54.3	30.0	23.4	25.0	13.1
Ce	0.1	32.4	53.0	45.0	42.9	41.1	45.5	94.8	31.6	1.2	46.3	115.0	56.8	46.5	50.2	27.1
Pr	0.05	3.96	6.09	5.5	5.31	4.6	5.43	11	4.34	0.14	5.41	13.5	6.57	5.48	5.95	3.12
Nd	0.1	16.6	22.7	21.4	20.5	17.4	20.4	40.5	16.5	0.7	20.6	55.2	23.4	22.0	22.9	12.3
Sm	0.1	3.9	4.1	4.3	3.7	3.5	3.8	7.0	3.0	0.2	3.5	11.9	4.1	4.1	4.4	2.6
Eu	0.05	1.1	1	1.02	0.75	0.86	0.91	1.19	0.59	0.09	0.56	2.32	0.82	0.74	0.92	0.49
Gd	0.1	3.7	2.8	3.3	2.4	3.1	2.6	4.1	2.4	0.3	1.9	9.7	3.1	3.6	3.3	2.1
Tb	0.1	0.6	0.5	0.5	0.4	0.5	0.4	0.5	0.4	<0.1	0.3	1.6	0.4	0.6	0.5	0.3
Dy	0.1	3.5	2.7	3.1	2.3	2.9	2.2	2.2	2.6	0.9	1.3	9.2	2.1	3.5	3.0	1.9
Ho	0.1	0.7	0.5	0.6	0.6	0.6	0.4	0.4	0.5	0.3	0.3	1.7	0.4	0.7	0.6	0.3
Er	0.1	1.9	1.4	1.8	2.1	1.9	1.3	1.0	1.8	1.7	0.8	4.6	1.2	1.9	1.8	0.9
Tm	0.05	0.25	0.21	0.28	0.37	0.27	0.2	0.12	0.27	0.29	0.13	0.68	0.16	0.28	0.27	0.14
Yb	0.1	1.5	1.3	1.8	3.0	1.8	1.5	0.7	1.8	2.6	0.9	4.5	1.0	1.6	1.8	1.0
Lu	0.04	0.22	0.2	0.28	0.56	0.29	0.25	0.11	0.27	0.52	0.13	0.66	0.13	0.24	0.30	0.17

Note: LD - limit of detection; LLD - lower than limit of detection; MV - mean value; SD - standard deviation; min - mineralized

Table 3 Ulveryggen

Sample number		YM-03	YM-08	YM-04	YM-07	YM-05	YM-02	YM-06	YM-09		
Major oxides, %	LD	min	min	min	min	min	min	min	min	MV	SD
SiO2	0.01	79.03	80.30	77.16	79.11	81.22	71.73	78.52	76.60	77.96	2.74
Al2O3	0.01	9.68	8.40	9.04	8.82	8.41	9.67	7.11	9.89	8.88	0.86
Fe2O3(T)	0.01	2.92	3.15	4.02	3.05	2.75	5.65	5.32	3.22	3.76	1.06
MnO	0.001	0.016	0.021	0.034	0.015	0.023	0.032	0.017	0.020	0.022	0.007
MgO	0.01	1.03	1.17	2.56	0.82	1.66	2.07	0.92	1.36	1.45	0.57
CaO	0.01	0.30	0.11	0.08	0.07	0.11	0.10	0.14	0.10	0.13	0.07
Na2O	0.01	3.08	3.25	2.41	3.73	1.82	1.44	2.27	2.11	2.51	0.73
K2O	0.01	1.59	1.03	1.25	0.88	1.76	2.54	1.26	2.38	1.59	0.57
TiO2	0.001	0.258	0.256	0.266	0.304	0.225	0.863	0.488	0.308	0.371	0.201
P2O5	0.01	0.03	0.04	0.01	LLD	0.02	0.03	0.01	LLD	0.02	0.01
LOI		1.46	1.04	1.96	1.12	1.42	2.37	0.85	1.58		
Total		99.40	98.78	98.79	97.92	99.41	96.49	96.92	97.56		
Trace elements, ppm											
Sc	1	6	4	5	5	5	8	5	7	6	1
Be	1	LLD	LLD	LLD	LLD	LLD	LLD	LLD	LLD		
V	5	53	48	48	41	53	78	57	66	56	11
Cr	20	470	540	360	440	420	1310	820	480	605	296
Co	1	9	10	15	7	11	19	10	12	12	4
Ni	20	50	40	50	30	50	100	50	60	54	19
Cu	10	2610	4300	5470	6910	7070	>10000	>10000	>10000	7045	2643
Zn	30	LLD	30	40	LLD	LLD	40	50	40	25	20
Ga	1	10	9	11	8	10	14	8	13	10	2
Ge	0.5	1.1	0.8	0.8	0.8	0.8	1.5	0.8	1.0	1.0	0.2
As	5	LLD	LLD	LLD	LLD	LLD	LLD	LLD	LLD		
Rb	1	44	28	33	22	45	74	35	61	43	16
Sr	2	56	57	52	52	53	50	38	66	53	7
Y	0.5	8.9	8.5	9.6	5.6	6.8	14.5	8.9	5.9	8.6	2.6
Zr	1	64	98	120	86	73	188	159	81	109	41
Nb	0.2	1.0	1.1	1.4	1.5	0.8	6.9	2.8	1.2	2.1	1.9
Mo	2	8	7	4	8	6	11	9	6	7	2
Ag	0.5	LLD	LLD	LLD	LLD	LLD	LLD	0.6	LLD	0.1	0.2
In	0.1	LLD	LLD	LLD	LLD	LLD	LLD	LLD	LLD		
Sn	1	LLD	LLD	LLD	LLD	LLD	LLD	LLD	LLD		
Sb	0.2	0.4	0.4	0.3	0.5	0.4	1.2	0.3	0.6	0.5	0.3
Cs	0.1	0.5	0.7	0.4	0.3	0.5	0.9	0.7	0.8	0.6	0.2
Ba	2	562	334	338	304	485	1091	468	1207	599	330
Hf	0.1	1.6	2.6	3.1	2.2	1.9	4.8	4.0	2.2	2.8	1.0
Ta	0.01	0.22	0.21	0.28	0.19	0.23	0.75	0.42	0.24	0.32	0.18
W	0.5	0.6	LLD	0.7	0.9	2.8	4.1	LLD	LLD	1.1	1.4
Tl	0.05	0.43	0.17	0.19	0.16	0.23	0.55	0.44	0.39	0.32	0.14
Pb	5	LLD	8	LLD	LLD	LLD	LLD	LLD	LLD	1	3
Bi	0.1	LLD	LLD	LLD	LLD	LLD	LLD	LLD	3.1	0.4	1.0
Th	0.05	3.54	5.95	5.11	4.00	5.66	16.90	14.20	4.07	7.43	4.80
U	0.01	3.24	1.25	1.47	1.13	1.00	2.10	3.53	1.67	1.92	0.90
REE, ppm											
La	0.05	6.97	17.10	23.00	9.19	12.80	21.10	12.90	12.60	14.46	5.20
Ce	0.05	12.10	36.00	47.20	19.60	25.80	44.20	26.90	22.20	29.25	11.43
Pr	0.01	1.71	3.95	5.22	2.18	2.83	5.00	2.90	2.70	3.31	1.20
Nd	0.05	7.02	13.70	18.50	8.17	10.10	19.60	10.60	9.48	12.15	4.39
Sm	0.01	1.81	2.42	2.99	1.52	1.93	3.86	2.00	1.67	2.28	0.74
Eu	0.01	0.52	0.56	0.80	0.44	0.49	1.04	0.52	0.43	0.60	0.20
Gd	0.01	1.79	1.79	2.29	1.21	1.62	2.91	1.57	1.31	1.81	0.52
Tb	0.01	0.29	0.27	0.33	0.18	0.22	0.50	0.25	0.19	0.28	0.10
Dy	0.01	1.72	1.52	1.77	1.04	1.24	2.99	1.51	1.12	1.61	0.58
Ho	0.01	0.33	0.30	0.34	0.21	0.25	0.55	0.29	0.22	0.31	0.10
Er	0.01	0.91	0.83	0.98	0.63	0.73	1.56	0.90	0.65	0.90	0.28
Tm	0.01	0.13	0.13	0.15	0.10	0.11	0.25	0.14	0.11	0.14	0.05
Yb	0.01	0.83	0.86	0.96	0.73	0.70	1.57	1.00	0.76	0.93	0.26
Lu	0.002	0.133	0.140	0.154	0.116	0.127	0.242	0.162	0.120	0.149	0.038

Note: LD - limit of detection; LLD - lower than limit of detection; MV - mean value; SD - standard deviation; min - mineralized

Wt%	Lab	Mineral	Sample	S	Pb	Fe	Co	Ni	Cu	Zn	As	Se	Mo	Ag	Te	Hg	Bi	Au	Ba	O	Cl	Total
	UIO	Ccp	NS-9	35.33	-	30.53	-	-	33.63	0.12	0.04	-	-	0.05	-	-	0.09	-	-	-	-	99.74
	UIO	Ccp	NS-12	35.95	-	30.94	-	-	-	0.05	-	-	-	-	-	-	0.09	-	-	-	-	100.92
	UIO	Ccp	NS-42	34.7	-	29.77	-	-	33.29	0.07	0.01	0.03	2.86	0.03	-	-	-	-	-	-	-	100.76
	UIO	Bn	NS-4	24.97	-	10.69	-	-	58.74	0.08	0.02	-	-	3.7	-	-	-	-	-	-	-	98.2
	UIO	Bn	NS-26	25.34	-	11.01	-	-	62.8	-	0.04	-	-	0.5	-	-	0.04	-	-	-	-	99.75
	UIO	Bn	NS-27	26.11	-	14.26	-	-	60.5	0.08	-	0.06	-	-	0.07	0.05	-	-	-	-	-	101.13
	UIO	Bn	NS-32	25.2	-	10.93	-	0.02	62.42	0.04	-	0.12	1.92	0.15	0.03	0.06	-	-	-	-	-	100.92
	UIO	Bn	NS-40	24.95	-	10.72	-	0.04	62.83	0.11	-	0.42	2.18	-	-	-	-	-	-	-	-	101.26
	UIO	Cct	NS-14	23.11	-	0.83	0.04	-	75.24	0.06	0.02	-	-	0.38	-	-	-	-	-	-	-	99.57
	UIO	Cct	NS-32	20.5	-	0.19	0.01	0.01	78	0.14	-	0.17	1.59	0.22	-	-	-	-	-	-	-	100.83
	UIO	Cct	NS-40	20.63	-	0.03	0.01	-	78.05	0.17	-	0.31	1.54	0.01	-	0.1	-	-	-	-	-	100.85
	UIO	Dg	NS-16	20.9	-	0.12	-	-	79.21	0.11	-	-	-	0.17	-	-	-	-	-	-	-	100.38
	UIO	Dg	NS-26	22.81	-	0.73	-	-	75.09	0.07	-	-	-	0.6	-	-	-	-	-	-	-	99.19
	UIO	Cv	NS-14	25.98	-	11.5	-	-	62.53	0.07	0.06	-	-	0.29	-	-	-	-	-	-	-	100.36
	UIO	Cv	NS-26	25.45	-	11.36	-	-	62.37	0.11	0.05	-	-	0.14	-	-	-	-	-	-	-	99.44
	UIO	Py	NS-10	52.7	-	46.84	-	-	-	-	0.03	-	-	0.04	-	-	0.16	-	-	-	-	99.77
	UIO	Py	NS-44	39.68	-	52.08	0.22	0.46	4.58	0.06	-	0.11	3.19	0.44	-	0.05	-	-	-	-	-	100.91
	UIO	Ga	NS-4	13.29	86.55	0.25	-	-	0.04	-	-	-	-	0.02	-	-	0.01	-	-	-	-	100.1
	UIO	Ga	NS-27	11.96	84.73	0.43	0.01	0.01	1.73	-	-	1.94	-	0.09	0.01	-	-	-	-	-	-	100.93
	UIO	Cst	NS-32	0.55	68.98	0.42	-	-	1.28	-	-	25.74	0.07	3.99	-	-	-	-	-	-	-	101.08
	UIO	Cst	NS-32	1.61	73.62	0.23	-	-	1.79	-	-	24.17	0.11	0.41	-	-	-	-	-	-	-	101.94
	IGG	Mol	NS-1a	41.04	-	-	-	-	-	-	-	-	58.96	-	-	-	-	-	-	-	-	100
	IGG	Gf	NS-1a	18.03	-	1.55	0.64	31.69	1.49	-	46.49	-	-	-	-	-	-	-	-	-	-	100
	UIO	Cbt	NS-44	22.21	-	5.02	31.44	0.74	-	-	41.25	0.42	-	0.04	-	-	0.07	-	-	-	-	101.0
	UIO	Cbt	NS-44	21.6	-	4.4	30.97	0.68	-	-	41.18	0.33	1.43	0.09	-	0.03	0.01	-	-	-	-	100.79
	UIT	Sph	NS-34	33.33	-	7.63	-	-	0.72	57.54	-	-	-	-	-	-	-	-	-	-	-	Cd=0.71 99.93
	UIT	Sph	NS-34	32.93	-	6.81	-	-	0.6	58.74	-	-	-	-	-	-	-	-	-	-	-	Cd=1.18 100.26
	UIT	Sph	NS-34	33.47	-	7.78	-	-	0.73	59.26	-	-	-	-	-	-	-	-	-	-	-	Cd=0.88 102.12
	UIO	Sph	NS-44	32.32	-	7.05	0.17	0.08	0.73	60.20	0.02	0.02	-	-	-	0.07	-	-	-	-	-	100.66
	UIT	Am	NS-27	-	-	-	-	-	-	-	-	-	-	88.2	-	11.8	-	-	-	-	-	100
	UIT	Am	NS-27	-	-	-	-	-	-	-	-	-	-	86.56	-	13.44	-	-	-	-	-	100
	UIT	Am	NS-4	0.02	-	0.11	-	-	0.283	-	0.03	-	-	99.3	-	-	-	-	-	-	-	99.72
	IGG	Arg	NS-1a	12.36	-	-	-	-	0.31	-	-	-	-	87.33	-	-	-	-	-	-	-	100
	IGG	Arg	NS-1a	12.98	-	-	-	-	-	-	-	-	-	87.02	-	-	-	-	-	-	-	100
	IGG	Stm	NS-1a	15.12	-	0.41	-	-	29.33	-	-	-	-	55.14	-	-	-	-	-	-	-	100
	IGG	Stm	NS-1a	15.35	-	-	-	-	33.39	-	-	-	-	51.26	-	-	-	-	-	-	-	100
	IGG	Clag*	NS-1a	0.81	-	-	-	-	0.28	-	-	-	-	76.37	-	-	-	-	-	-	8.97	86.42
	UIT	Hs	NS-43	-	-	-	-	-	1.8	-	-	-	-	62.57	35.63	-	-	-	-	-	-	100
	UIT	Hs	NS-43	-	-	-	-	-	3.19	-	-	-	-	65.35	31.46	-	-	-	-	-	-	100
	UIT	Hs	NS-43	-	-	-	-	-	1.95	-	-	-	-	58.46	39.59	-	-	-	-	-	-	100
	UIT	Hs	NS-43	-	-	-	-	-	3.58	-	-	-	-	60.09	36.33	-	-	-	-	-	-	100
	UIT	Hs	NS-43	-	-	-	-	-	3.18	-	-	-	-	61.1	35.72	-	-	-	-	-	-	100
	UCR	FeO	Ulv-5	-	-	71.3	-	-	-	-	-	-	-	-	-	-	-	-	-	27.73	-	99.03
	UCR	FeO	Ulv-5	0.39	-	69.23	-	-	1.95	-	-	-	-	-	-	-	-	-	-	27.54	-	99.11
	UCR	Bn	Ulv-5	24.3	-	10.05	-	-	63.26	-	-	-	-	-	-	-	-	-	-	-	-	97.6
	UCR	Bn	Ulv-5	24.79	-	12.6	-	-	60.72	-	-	-	-	-	-	-	-	-	-	-	-	98.11
	UCR	Cct	Ulv-5	20.07	-	1.87	-	-	75.76	-	-	-	-	-	-	-	-	-	-	-	-	97.7
	UCR	Cct	Ulv-5	20.65	-	1.02	-	-	77.96	-	-	-	-	-	-	-	-	-	-	-	-	99.63
	UCR	Brt	Ulv-14	14.39	-	-	-	-	-	-	-	-	-	-	-	-	-	-	-	-	26.12	98.97
	UCR	Cct	Ulv-14	21.51	-	0.36	-	-	77.54	-	-	-	-	-	-	-	-	-	-	-	-	99.42
	UCR	Cv	Ulv-14	20.8	-	-	-	-	80.62	-	-	-	-	-	-	-	-	-	-	-	-	101.42
	UCR	FeO	Ulv-14	-	-	0.71	-	-	-	-	-	-	-	-	-	-	-	-	-	-	-	100
	UCR	FeO	Ulv-14	-	-	67.8	-	-	-	-	-	-	-	-	-	-	-	-	-	29.56	Ti: 2,64	100
	UCR	FeO	Ulv-14	-	-	73.61	-	-	-	-	-	-	-	-	-	-	-	-	-	-	-	100

Atoms per formula unit

S	Pb	Fe	Co	Ni	Cu	Zn	As	Se	Mo	Ag	Te	Hg	Bi	Au	Ba	O	Cl	Total			
2.021	-	1.003	-	-	0.970	0.003	0.001	-	-	0.001	-	-	-	0.001	-	-	-	-	-	-	4
2.675	-	1.322	-	-	-	0.002	-	-	-	-	-	-	-	0.001	-	-	-	-	-	-	4
1.994	-	0.982	-	-	0.965	0.002	-	0.001	0.055	0.001	-	-	-	-	-	-	-	-	-	-	4
4.035	-	0.992	-	-	4.788	0.006	0.001	-	-	0.178	-	-	-	-	-	-	-	-	-	-	10
3.990	-	0.995	-	-	4.988	-	0.003	-	-	0.023	-	-	-	0.001	-	-	-	-	-	-	10
4.023	-	1.261	-	-	4.702	0.006	-	0.004	-	-	0.003	0.001	-	-	-	-	-	-	-	-	10
3.953	-	0.984	-	0.002	4.940	0.003	-	0.008	0.101	0.007	0.001	0.002	-	-	-	-	-	-	-	-	10
3.912	-	0.965	-	0.003	4.970	0.008	-	0.027	0.114	-	-	-	-	-	-	-	-	-	-	-	10
1.123	-	0.023	0.001	-	1.845	0.001	-	0.000	0.000	0.005	-	-	-	-	-	-	-	-	-	-	3
1.013	-	0.005	-	-	1.945	0.003	-	0.003	0.026	0.003	-	-	-	-	-	-	-	-	-	-	3
1.018	-	0.001	-	-	1.944	0.004	-	0.006	0.025	0.000	-	0.001	-	-	-	-	-	-	-	-	3
4.794	-	0.016	-	-	9.166	0.012	-	-	-	0.012	-	-	-	-	-	-	-	-	-	-	14
5.207	-	0.096	-	-	8.648	0.008	-	-	-	0.041	-	-	-	-	-	-	-	-	-	-	14
0.808	-	0.205	-	-	0.982	0.001	0.001	-	-	0.003	-	-	-	-	-	-	-	-	-	-	2
0.801	-	0.205	-	-	0.990	0.002	0.001	-	-	0.001	-	-	-	-	-	-	-	-	-	-	2
1.985	-	1.013	-	-	-	-	-	-	-	-	-	-	-	0.001	-	-	-	-	-	-	3
1.619	-	1.220	0.005	0.010	0.094	0.001	-	0.002	0.043	0.005	-	-	-	-	-	-	-	-	-	-	3
0.990	0.997	0.011	-	-	0.002	-	-	-	-	-	-	-	-	-	-	-	-	-	-	-	2
0.885	0.970	0.018	-	-	0.065	-	-	0.058	-	0.002	-	-	0.000	-	-	-	-	-	-	-	2
0.046	0.898	0.020	-	-	0.054	-	-	0.879	0.002	0.100	-	-	0.000	-	-	-	-	-	-	-	2
0.134	0.949	0.011	-	-	0.075	-	-	0.817	0.003	0.010	-	-	0.000	-	-	-	-	-	-	-	2
2.703	-	0.000	-	-	-	-	-	1.297	-	-	-	-	0.000	-	-	-	-	-	-	-	4
0.945	-	0.047	0.018	0.908	0.039	-	1.043	-	-	-	-	-	-	-	-	-	-	-	-	-	3
1.102	-	0.143	0.849	0.020	-	-	0.876	0.008	-	0.001	-	-	0.001	-	-	-	-	-	-	-	3
1.087	-	0.127	0.848	0.019	-	-	0.887	0.007	0.024	0.001	-	-	0.000	-	-	-	-	-			

Table 5

	O	Na	Si	S	Cl	K	Ca	Mn	Fe	Ba	Al	Cu	Br	Total
NS-51-d-36	44.8	0.56	29.95	2.89	0.17	-	5.96	3.98	4.86	7.3	0.41	-	-	100.9
NS-51-d-37	45.06	1.49	30.82	1.41	0.27	0.17	9.43	4.56	6.22	0.95	0.27	0.25	-	100.89
NS-51-d-38	46.83	0.43	34.25	2.04	0.45	-	7.95	1.59	1.37	4.98	-	-	-	99.89
NS-51-d-39	48.77	0.46	37.4	1.1	0.45	-	7.61	1.69	2.75	0.35	-	-	-	100.57
NS-51-d-40	48.06	0.63	34.76	1.87	0.53	-	10.96	1.37	1.27	0.39	0.29	-	-	100.14
NS-51-d-41	47.01	0.82	34.52	0.94	0.29	0.13	7.94	3.63	4.92	0.65	0.28	-	-	101.14
NS-51-d-42	46.66	0.64	32.76	3.14	0.18	-	5.55	1.74	2.08	9.48	-	-	-	102.23
NS-51-d-43	46.19	1.15	32.83	1.69	0.49	0.13	9.42	2.37	4.34	0.7	-	0.22	0.36	99.9
NS-51-d-44	42.9	0.61	28.51	2.96	0.23	0.11	5.36	3.14	5.02	8.28	0.34	-	-	97.45

Table 6

Sample #	Sample description	$\delta^{13}\text{C}$ (‰, VPDB)	$\delta^{18}\text{O}$ (‰, VPDB)
Gorahatjohka Formation, Saltvatn Group, Nussir Deposit, Repparfjord			
*NS-31A	host dolomite	2.7	-15.9
*NS-31B	host dolomite	2.9	-16.0
*NS-16	host dolomite	2.0	-18.3
*NS-17	host dolomite	1.8	-18.2
★NS-24 4	vein dolomite	1.6	-16.3
★NS-24 3	vein dolomite	1.9	-16.6
★NS-24 2	vein dolomite	2.3	-16.7
★NS-24 1	vein dolomite	-1.0	-16.0
★NS-32 4	vein dolomite	0.9	-17.0
★NS-32 3	vein dolomite	1.1	-16.8
★NS-32 2	vein dolomite	0.9	-16.6
★NS-32 1	vein dolomite	1.0	-16.8
Vargsung Formation, Raipas Group, Repparfjord			
*PO-14-1	calcite	3.1	-9.6
*PO-14-2	calcite	3.2	-9.5
Vargsund Formation, Raipas Group, Repparfjord (Melezhik & Fallick, 1996)			
RF-2	dolostone	1.5	-10.2
RF-3	dolostone	1.8	-9.8
RF-7	dolostone	2.0	-9.8
RF-8	dolostone	2.7	-7.6
RF-9	dolostone	-5.2	-10.3
RF-13	dolostone	0.6	-9.1
RF-14	dolostone	1.6	-9.0
RF-16	dolostone	0.1	-6.0
RF-17	dolostone	0.5	-7.9
RF-18	dolostone	2.3	-8.8
Vargsund Formation, Raipas Group, Kvenklubben Fault, Repparfjord (Torgersen et al. 2014)			
ETO 113	dolostone	1.9	-14.0
ETO 114	dolostone	1.9	-14.1
ETO 115	dolostone	2.0	-11.6
ETO 116	dolostone	2.0	-10.9
ETO 119	dolostone	1.9	-10.4
Storviknes Formation, Raipas Group, Alta-Kvænangen Window (Melezhik et al., 2015)			
RP_14	dolostone	-0.3	-9.7
RP_1	dolostone	1.9	-8.3
RP_2	dolostone	2.1	-8.6
RP_3	dolostone	2.0	-8.4
RP_4	dolostone	1.8	-8.6
RP_5	dolostone	1.7	-8.3
RP_6	dolostone	2.6	-8.4
RP_7	dolostone	2.3	-8.9
RP_8	dolostone	2.6	-8.2
RP_9	dolostone	2.5	-8.5
RP_10	dolostone	0.8	-8.6
RP_11	dolostone	0.9	-8.7

RP_12	dolostone	0.5	-8.9
RP_13	dolostone	0.8	-8.2

* UCR

★UiT

Supplementary table 1

# Sample #	Drill hole	Coordinates		Total length (m)	Sample Depth (m)	Description
		NORTH	EAST			
1 NS-1a	NUS-DD-06-007	7819199.887	389972.34	120	28.45-28.50	Pelitic metasiltstone
2 NS-1b	-	-	-	-	-	metasiltstone
3 NS-2a	-	-	-	-	28.52-28.56	sericitic siltstone
4 NS-2b	-	-	-	-	-	metasiltstone
5 NS-3a	-	-	-	-	28.60-28.65	metasiltstone
6 NS-3b	-	-	-	-	-	metasiltstone
7 NS-4	-	-	-	-	28.75-28.80	metapelite
8 NS-5a	-	-	-	-	28.80-28.92	dolomitic marble
9 NS-5b	-	-	-	-	-	metapelite
10 NS-6	NUS-DD-08-006	7819891.786	395912.563	236.6	65.46-65.51	metatuffite
11 NS-7	-	-	-	-	67.20-67.33	mafic metavolcanite
12 NS-8	-	-	-	-	74.10-74.14	metatuffite
13 NS-9	-	-	-	-	75.35-75.40	metavolcanics
14 NS-10	-	-	-	-	79.11-79.26	metabasalt
15 NS-11	-	-	-	-	81.68-81.70	metavolcanics
16 NS-12	-	-	-	-	91.86-91.89	metatuffite
17 NS-13	-	-	-	-	198	metatuffite
18 NS-14	-	-	-	-	203.35-203.40	metatuffite
19 NS-15	-	-	-	-	206.84-206.9	metatuffite
20 NS-16	-	-	-	-	210.70-210.80	metapelite
21 NS-17	-	-	-	-	214.85-214.9	pelitic schist
22 NS-18	-	-	-	-	219.53-219.63	metasandstone
23 NS-19	-	-	-	-	221.62-221.66	quartzitic schist
24 NS-20	-	-	-	-	225.74-225.79	metaconglomerate
25 NS-21	-	-	-	-	227.05-227.10	metasiltstone
26 NS-22	-	-	-	-	229.64	shear zone
27 NS-23	-	-	-	-	231.74-231.76	metasandstone
28 NS-24	-	-	-	-	231.90-231.92	dolomitic marble
29 NS-25	-	-	-	-	234.69	metasiltstone
30 NS-26	NUS-DD-08-010	7819755.794	395569.327	163.5	132.8-133.0	dolomitic marble
31 NS-27	NUS-DD-14-001	-	-	-	730	mica schist
32 NS-28	NUS-DD-13-020	-	-	-	580	dolomitic marble
33 NS-29	-	-	-	-	594	quartzitic schist
34 NS-30	NUS-DD-13-012	-	-	-	11.9	dolomitic marble
35 NS-31	NUS-DD-90-002	7819047.28	390231.564	99.1	45.3	dolomitic marble
36 NS-32	-	-	-	-	53	schist
37 NS-33	NUS-DD-11-004	7819853.504	395411.609	461.9	32.9	metatuffite
38 NS-34	-	-	-	-	33	metatuffite
39 NS-35	-	-	-	-	33.05	metatuffite-breccia
40 NS-36	-	-	-	-	33.17	metatuffite
41 NS-37	-	-	-	-	34.3	dolomitic marble
42 NS-38	-	-	-	-	448	carbonate schist
43 NS-39	-	-	-	-	452	metagraywacke
44 NS-40	-	-	-	-	459.8	metagraywacke
45 NS-41	NS-DD-13-020	-	-	-	365.8	metatuffite
46 NS-42	-	-	-	-	366	metatuffite
47 NS-43	-	-	-	-	367.15	metatuffite
48 NS-44	NUS-06-005	7818485.14	390827.138	306	223.2	metatuffite
49 NS-45	-	-	-	-	225.9	metatuffite
50 NS-46	-	-	-	-	245.9	dolomitic marble
51 Ulv-1	US-003-10	-	-	-	31.9	arkosic metasandstone
52 Ulv-2	-	-	-	-	40.3	arkosic metasandstone
53 Ulv-3	-	-	-	-	47.2	arkosic metasandstone
54 Ulv-4	-	-	-	-	51.5	arkosic metasandstone
55 Ulv-5	US-004-10	-	-	-	31.4	arkosic metasandstone
56 Ulv-6	-	-	-	-	32.3	arkosic metasandstone
57 Ulv-7	-	-	-	-	45.16	arkosic metasandstone
58 Ulv-8	-	-	-	-	48.7	arkosic metasandstone
59 Ulv-9	US-008-10	-	-	-	13.45	arkosic metasandstone
60 Ulv-10	-	-	-	-	14.45	arkosic metasandstone
61 Ulv-11	US-015-10	-	-	-	17	arkosic metasandstone
62 Ulv-12	US-020-10	-	-	-	3.4	arkosic metasandstone
63 Ulv-13	-	-	-	-	49.1	arkosic metasandstone
64 Ulv-14	-	-	-	-	50.1	arkosic metasandstone
64 Ulv-15	-	-	-	-	51.9	arkosic metasandstone

Paper 2

**Stability of Cu-sulphides in submarine tailing disposals: A case study from
Repparfjorden, northern Norway,**

Mun Y., Strmić Palinkaš S., Forwick M., Junttila J., Pedersen K.B., Sternal B.,
Neufeld K., Tibljaš D., Kullerud K.

*to be submitted to a special issue of Minerals "Environmental Geochemistry of Mineral
Deposits", deadline for manuscript submissions: 30 November 2019.*

Paper 3

The role of ore-forming processes and tailing disposal site conditions on a contrasting environmental impact of Cu-sulphide deposits in Norway

Mun Y., Strmić Palinkaš S., Kullerud K.

to be submitted to Journal of Geochemical Exploration